

NISTIR 88-3808



Narrow-Angle Laser Scanning Microscope System for Linewidth Measurements on Wafers

D. Nyyssonen

CD Metrology, Inc.
Germantown, MD 20874

June 1988

Issued April 1989

Prepared for:
U.S. DEPARTMENT OF COMMERCE
National Institute of Standards and Technology
(Formerly National Bureau of Standards)
National Engineering Laboratory
Center for Manufacturing Engineering
Precision Engineering Division
Gaithersburg, MD 20899

NISTIR 88-3808

Narrow-Angle Laser Scanning Microscope System for Linewidth Measurements on Wafers

D. Nyysönen

CD Metrology, Inc.
Germantown, MD 20874

June 1988

Issued April 1989



National Bureau of Standards became the National Institute of Standards and Technology on August 23, 1988, when the Omnibus Trade and Competitiveness Act was signed. NIST retains all NBS functions. Its new programs will encourage improved use of technology by U.S. industry.

Prepared for:
U.S. DEPARTMENT OF COMMERCE
National Institute of Standards and Technology
(Formerly National Bureau of Standards)
National Engineering Laboratory
Center for Manufacturing Engineering
Precision Engineering Division
Gaithersburg, MD 20899

U.S. DEPARTMENT OF COMMERCE
Robert Mosbacher, Secretary
NATIONAL INSTITUTE OF STANDARDS
AND TECHNOLOGY
Raymond G. Kammer, Acting Director

Table of Contents

	Page
Abstract	1
Introduction	1
Characteristics of Patterned Thin Films	2
Optical Design of a Metrological Microscope	6
Spatial Coherence and Angle of Incidence	7
Aberrations	11
Alignment	11
Alignment Procedure	13
Measurement of Linewidth	15
Radiometric Signal/Noise Ratio	17
Scalar Theory for Thin-Layer Imaging	17
Vector Theory for Thick-Layer Imaging	20
Accuracy and Precision	24
Design of Linewidth Calibration Standards	26
Summary	27
Acknowledgments	28
References	28
Figures	31
Appendix I	46
Appendix II	55

NARROW-ANGLE LASER SCANNING MICROSCOPE SYSTEM
FOR LINEWIDTH MEASUREMENT ON WAFERS*

Diana Nyyssonen**
CD Metrology, Inc.
Germantown, MD 20874

ABSTRACT: The integrated-circuit industry in its push to finer and finer line geometries approaching submicrometer dimensions has created a need for ever more accurate and precise feature-size measurements to establish tighter control of fabrication processes. Under the auspices of the NBS Semiconductor Line-width Metrology Program, a unique narrow-angle laser measurement system was developed. This report describes the theory, optical design, and operation of this system and includes computer software useful for characterizing the pertinent optical parameters and images for patterned thin layers. For thick layers, the physics is more complex, and only elements of the theory are included here. However, for more detail the reader is referred to several related reports listed in the references.

KEY WORDS: metrology, coherence, critical dimensions, linewidth measurements, micrometrology, scanning microscopy

INTRODUCTION

The push to submicrometer feature sizes on integrated-circuit (IC) wafers has resulted in a need for more accurate and precise dimensional measurements in order to establish tighter control of fabrication processes, improve yield, and ensure that lithographic

* Contribution of the National Bureau of Standards; not subject to copyright.

** Formerly with the National Bureau of Standards; collaboration continues under a Guest Worker Agreement.

and linewidth measurement systems meet specifications. Measurement systems used in the fabrication process must have accuracy and precision much better than the variation in the parts being measured and, in turn, the accuracy and precision of calibration standards must be still better than the instruments being calibrated.

Under the Semiconductor Metrology Program within the Center for Electronics and Electrical Engineering at NBS a project was initiated to develop improved instrumentation, calibration procedures and standard reference materials for linewidth measurement on IC wafers. The result was the development of the NBS narrow-angle laser linewidth measurement system. This system was first described in 1978 [1] and discussions of various aspects of this system have appeared in the literature since then [2-7]. However, there is no single report which adequately describes the details of its theory, design and operation. This report attempts to rectify this situation. In order to understand the motivation behind the development of this system, it is necessary to understand the optical characteristics of the patterned features on integrated circuits which this system was designed to measure.

CHARACTERISTICS OF PATTERNED THIN FILMS

The optical properties of patterned integrated circuit wafers are best described using the language of ellipsometry. Wafers are typically made up of layers of insulators and conductors with one or more of these layers patterned. These layers may vary in thickness from approximately $0.1\ \mu\text{m}$ to $0.5\ \mu\text{m}$ or more. In this report discussion is limited to thin layers, those less than one-quarter of the illuminating wavelength. Thicker layers cannot be described by scalar theory and a vector treatment must be used. See ref. 19. For the moment consider a region on the wafer where only the top layer is patterned as shown in Fig. 1. A single

plane wave of wavelength λ is incident at an angle θ . This plane wave is refracted and reflected at each interface. To determine the complex reflectance, that is, both the amplitude and phase of the reflected wave, the Fresnel equations [8] are used. In matrix form [9], each layer is characterized by a matrix of the form

$$M_j = \begin{pmatrix} \cos v_j & \frac{-i}{u_j} \sin v_j \\ -i u_j \sin v_j & \cos v_j \end{pmatrix} \quad (1)$$

$$\text{where } u_j = \begin{cases} \frac{\hat{n}_j}{\cos \theta_j} & \text{parallel polarization} \\ \hat{n}_j \cos \theta_j & \text{perpendicular polarization} \end{cases}$$

and $\hat{n} = n_j + iK_j$ is the complex index of refraction of the j th layer. θ_j is found from Snell's law:

$$\hat{n}_0 \sin \theta_0 = \hat{n}_j \sin \theta_j = \text{a constant for all } j$$

and v_j , the effective optical thickness, is given by

$$v_j = \frac{2\pi}{\lambda} (\hat{n}_j t_j \cos \theta_j)$$

A. UNPATTERNED LAYERS

The characteristic matrix for the composite of N unpatterned layers is then given by the product of the characteristic matrices of the individual layers

$$M_{1,N} = M_1 \cdot M_2 \cdot \dots \cdot M_j \cdot \dots \cdot M_N \quad (2)$$

with

$$M_{1,N} = \begin{pmatrix} m_{11} & m_{12} \\ m_{21} & m_{22} \end{pmatrix}$$

The amplitude and phase of the reflected and transmitted waves are found from the characteristic matrix M. Let

$$X = m_{11} + \hat{n}_s m_{12}$$

$$Y = m_{21} + \hat{n}_s m_{22}$$

then the complex reflectance is given by

$$r = \frac{X-Y}{X+Y} \quad (3)$$

If $r = x+iy$, then the phase of the reflected wave is given by

$$\psi = \tan^{-1} \left(\frac{y}{x} \right) \quad (4)$$

and

$$R = |r|^2$$

B. PATTERNED LAYERS

For the case of a patterned wafer (Fig. 1) where the relative reflectance and phase difference at an edge are needed, first the characteristic matrix $M_{1,N}$ for layers 1 through N is calculated and then the matrix $M_{2,N}$ for layers 2 through N. A relative reflectance, R, to be used later, is then defined by

$$R = \begin{cases} \frac{R_{1,N}}{R_{2,N}} & R_{1,N} < R_{2,N} \\ \frac{R_{2,N}}{R_{1,N}} & R_{2,N} < R_{1,N} \end{cases} \quad (5)$$

where the convention is chosen so that $R \leq 1$. The corresponding relative phase difference is defined by

$$\phi = \psi_{2,N} - \psi_{1,N} + 2k_0 t_1 \cos \theta \quad (6)$$

where $k_0 = \frac{2\pi}{\lambda}$ and t_1 is the thickness of the top layer. At normal incidence, there is no difference between incident waves with parallel or perpendicular polarization and these equations simplify. Appendix I includes a short computer program written in FORTRAN 77 which calculates R and ϕ at normal incidence. The calculation of R and ϕ represents the first step in modeling the image of a patterned wafer.

C. BEHAVIOR OF R AND ϕ

R and ϕ vary with index and thickness of the layers, angle of incidence, polarization and wavelength. In addition, dielectrics behave differently from metals. Figures 2-5 illustrate variations of R and ϕ as a function of these parameters. In Figs. 2(a) and (b), the curves for R and ϕ as a function of t_1 are relatively simple for a single patterned layer on a silicon substrate. These same curves may also be plotted parametrically as $R(t_1)$ vs $\phi(t_1)$ as shown in Figs. 2(c) and 2(d).

In Fig. 3, the situation is more complex. With an oxide layer under the metal, one has the option of varying either the thickness of the metal layer or the thickness of the oxide layer

underneath. If the metal layer is held constant and the oxide is varied, the resulting curve is an ellipse.

Figures 2 and 3 are for the case of normal incidence and a single wavelength. Figures 4 and 5 illustrate the variations with wavelength and angle of incidence for a silicon dioxide layer on silicon. In real cases, the index of refraction also varies with wavelength, changing the behavior of the curves for silicon dioxide shown in Fig. 4.

For accurate linewidth measurements, R and \emptyset must be constant over the solid angle of illumination. It is possible to determine the maximum allowable angle for a given material (or combination of materials) using eqs. (1)-(6). For example, for SiO_2 on Si, if a 2% variation in R with θ is allowed, θ_{max} can be determined as a function of thickness of the oxide. See Fig. 5. θ_{max} is then the maximum allowable illumination angle for the measurement system. For thick layers, this requirement rather than the coherence requirement will determine the illumination cone angle for the system.

OPTICAL DESIGN OF A METROLOGICAL MICROSCOPE

The variations in R and \emptyset with wavelength and angle of incidence are the driving force behind the design of the narrow-angle, laser linewidth microscope. As in ellipsometry, accurate dimensional measurements become exceedingly difficult and the data analysis time consuming if all of the experimental parameters are allowed to vary. Ideally then, the optimal solution to dimensional metrology would be a single wavelength, single-angle-of-incidence system analogous to that used in ellipsometry [10]. Single wavelength is readily achieved using a laser source. However, in optical microscopy, it is neither desirable nor necessary to use a single angle of incidence; a narrow illuminating cone angle over which the resulting R and \emptyset of the specimen are essentially

constant is sufficient. The cone angle numerical aperture (N.A.), however, must be chosen with care for the particular index of refraction and thickness of the material to be measured.

A schematic of the layout of such a system built at NBS is shown in Fig. 6. The combination of the rotating ground glass disc and the illumination optics is used to control the illumination cone angle and the coherence at the back focal plane of the objective. With these parameters very tightly prescribed the microscope behaves like a modified bright-field microscope, that is, it operates as an effectively coherent imaging system. Although the system uses a one-dimensional piezo electric scanning stage [11] with interferometric readout of distance and a stationary slit in the image plane, it is also possible to scan the image plane with a moving slit arrangement. However, the system requirements for these two modes of operation are different.

The chief disadvantage of the single wavelength, narrow angle system is the low throughput. A 1-W laser is used on the NBS system and approximately 1 nW reaches the detector. The principal losses come from use of the rotating ground glass disc, overfilling of apertures to get uniform illumination, the small aperture limiting the illumination cone angle, the oversize illuminated area at the wafer, and the small slit in the image plane. The requirement on this slit width is that it be $1/6$ or less of the Airy disc diameter of the objective when projected back to the wafer in order not to degrade the image waveform [12].

SPATIAL COHERENCE AND ANGLE OF INCIDENCE

In order to discuss the coherence aspects of the system, it is necessary to introduce some concepts related to coherence. It is conventional in microscopy to describe spatial coherence in a bright-field microscope in terms of a coherence parameter defined by the ratio of the numerical aperture of the condenser with respect to the N.A. of the imaging objective:

$$S_B = \frac{\text{N.A. condenser}}{\text{N.A. objective}} \quad (7)$$

The limit $S \rightarrow 0$ is associated with coherent illumination as in the case of a collimated laser beam and the limit $S \rightarrow \infty$ with incoherent illumination. In conventional imaging in a microscope, neither of these limits is ever realized. However, it is useful to introduce the ideas of effective coherence and incoherence here. Effective coherence or incoherence means that the images of lines on wafers would be essentially the same as that seen in a fully coherent or a fully incoherent system.

For effective coherence:

$S_B < 2/3$, for thin, high contrast objects such as opaque photomasks, and

$S_B < 1/5$, for thick, low contrast objects with phase variations such as most wafer features.

For effective incoherence:

S_B may have any value for thin low contrast objects with no phase variations present (rare), and

$S_B > 2$, for all other cases.

For practical purposes, the images formed for these values of S_B would be indistinguishable from those corresponding to completely coherent or incoherent images as illustrated in Fig. 7. One consequence of these considerations is that a high numerical aperture conventional bright-field imaging system with 0.9-N.A. dry microscope objective can never be effectively incoherent since S_B can never exceed 2; one must therefore deal with partially coherent or effectively coherent imaging with such a microscope.

For focused-beam scanning systems with the roles of the illumination and detection systems interchanged, the coherence parameter is defined analogously as the inverse of that given above, i.e.,

$$S_F = \frac{N.A._{collector}}{N.A._{focused\ beam}} \quad (8)$$

(See Ref. 13). For such systems, effective coherence and incoherence are similarly defined for this S_F . Therefore, it is possible to produce a system with an effectively coherent or incoherent response using either a laser or thermal source such as a tungsten-halogen lamp. By analogy, the narrow-angle, effectively-coherent NBS system could have been configured with a focused laser beam and narrow angle collector. However, because of the response of thin films to angle of incidence, these two configurations would not have produced the same response.

One major difference between coherent and incoherent imaging is sensitivity to phase changes in the object or feature being measured. This aspect will be discussed further with respect to the imaging characteristics of the system. The concepts of effective coherence and incoherence discussed here refer to the plane of the wafer and assume that the back focal plane of the objective is incoherently illuminated (which is not fully realizable in practice).

It is useful, therefore to discuss here the reciprocal relationship between coherence and size of the illuminated area at the back focal plane with respect to the same parameters at the wafer. This relationship has not yet made its way into textbooks but was introduced by Wolf [14]. As applied to the microscope, it states that the coherence at the back focal plane of the objective determines the illuminated area (and intensity distribution) at the wafer, while the size and distribution of the illuminated area at the back focal plane determines the coherence at the wafer, providing that: 1) the illuminated area is large

compared to the coherence area, 2) the intensity is constant or slowly varying across the back focal plane, and 3) the region near the edges of the illuminated area is not being considered.

Because of throughput it is not desirable to require a high degree of incoherence at the back focal plane of the objective. In fact, if only small line objects are viewed a relatively small circular field of view is required and the diameter D_C^{BF} of the coherence area at the back focal plane can be found from

$$D_C^{BF} \leq \frac{0.6\lambda f}{D_I^W} \quad (9)$$

where D_I^W is the desired diameter of the illuminated area on the wafer, λ the wavelength, and f the focal length of the objective. It is also required that

$$D_C^{BF} \ll D_I^{BF} \quad (10)$$

where $D_I^{BF} = 2(N.A._{condenser})f$. Therefore, for a 4 mm focal length objective at a wavelength of 0.5 μm and $D_I^W = 50 \mu m$ these parameters would be $D_I^{BF} \approx 1 \text{ mm}$ and $D_C^{BF} > 25 \mu m$ for an effectively coherent system. If the coherence area at the back focal plane is reduced, a larger area on the sample will be illuminated and lower throughput will result. On the other hand, if the coherence area is increased, a smaller area will be illuminated at the sample making it difficult to find the patterns which need to be measured and possibly violating the requirement that $D_C^W \gg D_I^W$.

Only spatial coherence, that is, coherence in the plane of the wafer or lens aperture, has been discussed. The concept of

coherence volume (coherence area times coherence length) is useful here as well. Because there are no differences in optical path length in an ideal imaging system, coherence length is not usually of concern. However, in coherent imaging systems, coherent noise or speckle becomes a problem due to the extremely long coherence length of the laser source. Normally, dust particles and scratches on optical surfaces produce diffraction patterns which may be observed in the image plane due to the long coherence length. As shown in Fig. 8(a), a system using unfiltered tungsten illumination (white light) has a very short coherence length and small volume compared to a laser source (Fig. 8(b)) and therefore will not exhibit these effects. The present narrow-angle laser system has a peculiar pencil-shaped coherence volume as shown in Fig. 8(c), which eliminates most of the coherence effects normally associated with coherent imaging.

ABERRATIONS

In a system with a stationary slit and moving wafer where only the axial image is used, only spherical aberration is of concern. When the image is scanned with a moving slit, the off-axis aberrations are also of concern. Because it is desirable to eliminate as many variables which effect the measurement as possible, diffraction-limited performance and aberration tolerances of $\lambda/4$ or less are desirable. The ultimate test, however, is whether the system produces a diffraction-limited image waveform. Although aberrations may be taken into account in edge detection formulas [4], this approach is not recommended.

ALIGNMENT

A bright-field microscope operating in an effectively coherent mode has much more severe requirements on alignment than a conventional microscope. Because of sensitivity to phase variation, the illumination must be not only uniform in intensity across the line pattern but also uniform in phase across the illuminated

area. If this requirement is not met, the resulting nonsymmetric images invalidate the algorithms used for accurate edge detection. Because poor quality lines will also produce nonsymmetric images, it is necessary to distinguish between these two sources of nonsymmetry. One method is to rotate the specimen 180° and compare image waveforms. System asymmetry will stay the same while line irregularity will rotate. However, this test is difficult to interpret when both sources of nonsymmetry are present.

A special test wafer is therefore used for testing system performance. The ideal wafer is a patterned layer with $R = 1$, $\phi \approx \pi$. The waveform for a 180 nm thick layer of SiO_2 ($R = 1$, $\phi = 0.6\pi$) is shown in Fig. 9. This line pattern is ideal because of the symmetric waveform produced at each edge. Three sources of error readily show up in the image waveform: 1) misalignment of the illumination system including decentering of the aperture stop and tilt errors in the optical elements, 2) tilt of the wafer with respect to the focal plane of the objective and 3) tilt of the scanning plane with respect to the image plane when a moving slit is used.

In order to interpret the waveforms, it is necessary to understand the diffraction-limited behavior of this waveform with defocus. Figure 10(a) illustrates the nonsymmetry produced with defocus. On one side of focus, one of the maxima at the image edge is enhanced while the other is reduced. On the other side of focus, the opposite occurs. In addition, as defocus increases, the distance between these peaks increases as shown in Fig. 10(b).

When the only error is the tilt of the wafer with respect to the focal plane, one edge of the line will lead (or lag) the changing image waveform as a series of scans are made through focus. A similar effect occurs when the image plane is tilted with respect to the scanning plane. This effect is illustrated in Fig. 11.

Misalignment can produce a large variation in waveforms. An example is illustrated in Fig. 12(a). In general, nonsymmetry is present as focus is varied but is different from that shown in Fig. 10(a). There is also a loss in resolution, so that the distance between peaks is larger than that shown in Fig. 10(b). With both wafer tilt and misalignment present, it is possible to get waveforms like that shown in Fig. 13 where there is symmetry, but of the wrong kind.

Given the difficulty of determining and correcting these errors when all of these effects (misalignment, wafer tilt, poor line edge quality) are present, a procedure which will now be discussed has been worked out for laser alignment of the microscope.

ALIGNMENT PROCEDURE

We have found that in a high quality microscope the individual microscope optics are usually aligned adequately in their own mounts. However, these components when assembled to form the microscope are generally improperly aligned. This is probably because manufacturing tolerances of conventional microscopes are not adequate for this highly demanding mode of operation. It is common practice, for example, to correct errors in one component by an offsetting adjustment in another. One can expect, therefore, to have to shim and in some cases redesign mounts and adjustments to achieve the desired alignment accuracy.

The required tools for this job are a small HeNe laser (1 mW or less), neutral density filters to reduce the power to a comfortable level for visual viewing through the microscope, a laser beam steerer or other method for controlling the position and tilt of the laser beam, a polished silicon wafer or other highly reflective, flat surface, and a wafer holder with tilt adjustment.

The first step is to disassemble the microscope. If possible, remove all optics except the beam splitter in the head and the wafer on the stage. Then select a small aperture on the illumination side and one on the viewing side for reference. The center of these apertures together with the requirement that the return beam fall on the exit aperture of the laser determines the optical axis of the system. All components will be aligned to this axis as illustrated in Fig. 14.

The principle of this procedure is to add components one at a time and make sure that each is aligned to this axis. This is achieved by making sure that the return beam goes back to the laser aperture and the forward beam remains centered on the chosen reference aperture for each added optical element. In general, centering is done first and if the forward and return beams cannot both be returned to their reference points, then tilt must be adjusted by shimming or other means. In general, the tilt must be under- or over-corrected and the element re-centered and these steps repeated until the desired alignment accuracy is achieved.

One difficulty with this method is that the laser beam changes diameter at the reference aperture as elements are added. In some cases, it may be necessary to temporarily remove an element already aligned if it can be replaced exactly in order to keep the beam size small and maintain the desired accuracy. No rule of thumb can be given for "tolerable errors." Because of the large number of components (9 lenses, a beam splitter and 2 apertures in the NBS system) and the variations in microscope design, it is best to align every element as accurately as possible, that is, within a small fraction of the laser beam diameter. Because of its high magnification, the microscope objective is left for last. The aperture pinhole, which determines the illumination cone angle, will be next to last. The ultimate test of the accuracy achieved is the symmetry of the resulting waveform in a series of profiles with increasing amounts of defocus.

When all of the microscope optics have been aligned adequately, the argon or other high-power laser source is brought into coincidence with the alignment laser as shown in Fig. 15 and the beam expander and ground glass are aligned. Through these last steps, the aperture pinhole as viewed through the microscope with an auxiliary alignment telescope (such as used for centering the disc in phase contrast microscopy) or other device must remain stationary and uniformly illuminated.

One element that needs special attention is the rotating ground glass disc. If the normal to the surface precesses about the optical axis, fluctuations in intensity in the image plane will be observed. For this reason, a flexible coupling and a precision bearing at the drive motor are recommended.

After the alignment is completed, the alignment wafer is replaced with the SiO_2 test wafer. A scan of a line is made and the tilt of the wafer adjusted if indicated. If nonsymmetry due to misalignment is detectable, the alignment procedure was not performed accurately enough. Once alignment is deemed satisfactory, other adjustments of optical elements should be required or made thereafter. With each new wafer, only wafer tilt and focus are adjusted.

MEASUREMENT OF LINEWIDTH

The system must produce and maintain an ideal image waveform for the test line object because of the demands of accurate edge detection. An equally important requirement is the accurate measurement of distance (i.e. linewidth). To scan the image, the NBS laser system moves the wafer and measures the motion with a laser interferometer, thus providing traceability to fundamental standards of length. Aside from the usual demands of accurate laser interferometry, this system has some unique aspects principally involving alignment of the elements of the scanning system including scanning slit, line object, axis of stage motion and interferometer axis. The principal difficulty stems from the

extremely short distance of motion of the piezo electric stage, typically less than 50 μm .

The easiest method of alignment is to use the crosshair in the viewing eyepiece as a fiducial mark. The slit and line object can be centered and aligned to the vertical axis visually. In addition, the axis of stage motion can be aligned to the horizontal axis visually by inspecting the motion of a horizontal line object as it traverses the field of view. In order to align the interferometer axis parallel to the piezo electric stage axis, an auxiliary mirror has been used. This mirror has a mount that fits into the holes at the pivot points on the stage (See Ref. 11.) and is constructed so that the mirror face is accurately perpendicular to the direction of motion. Without this auxiliary mirror, the method is one of trial and error; minimizing a measured linespacing to eliminate the possible cosine error. Fortunately, because of the short distances scanned, the angle accuracy required for a given tolerance on a one micrometer linewidth is not very demanding. The final check, however, is measurement of a known linespacing traceable to national standards of length.

The major sources of distance measurement errors are vibration (the system should be mounted on a massive vibration isolation system), the least count of the interferometer, and temperature effects on the system. Because of the short distances, temperature effects on the wafers being measured are negligible.

In the NBS system, the precision of the interferometry is a fundamental limit on the precision of linewidth measurements. One cannot measure the size of an object to better precision than that of the distance measurement. This limitation is to some extent due to the basic design of the microscope, which is sensitive to both acoustic and mechanical sources of vibration and temperature.

RADIOMETRIC SIGNAL/NOISE RATIO

In most microscope linewidth measurement systems employing tungsten sources, the radiometric precision is limited by photon noise. Here the laser power has been increased in order to maintain the single wavelength, narrow angle mode of operation. Thus photon noise has been traded for laser output fluctuations. However, the specifications on the laser (< 0.5% variation) are adequate in this case. In addition to increasing the power, the system uses a variable speed chopper and lock-in amplifier operating at approximately 350 Hz with high and low-pass filters. The resulting signal/noise ratio is better than 200/1.

SCALAR THEORY FOR THIN-LAYER IMAGING

Scalar theory of partially coherent imaging has been developed using several different approaches including convolution integrals and Fourier analysis. The most efficient approach for computer calculations is the use of the transmission crosscoefficient of the optical system [15] as applied to the imaging of line objects by Kintner [16]. Based on the methods of Fourier analysis, the complex amplitude transmittance of the patterned line object is described by

$$t(x) = \begin{cases} 1 & 0 < x < W/2 \\ \sqrt{R}\exp(i\phi) & W/2 < x < P \end{cases} \quad (11)$$

which is expanded in the Fourier series

$$t(x) = \sum_m A_m \cos \left(\frac{2\pi m x}{P} \right) \quad (12)$$

where the line object is repeated at a period P which may be chosen arbitrarily large to describe isolated line objects. R and ϕ are the relative reflectance and phase difference at the line edge as introduced earlier. (See Eqs. 5 and 6.) The image is calculated from the Fourier series equation

$$I(y) = \sum_{n=-\infty}^{\infty} b_n \cos \left(\frac{2\pi ny}{P} \right) \quad (13)$$

where, for a symmetric line object,

$$b_n = \left\{ A_n A_0 \star \Psi \left(\frac{n}{P}; 0 \right) + \sum_{n'=1}^{\infty} \left[A_{n+n'} A_{n'} \star \Psi \left(\frac{n+n'}{P}; \frac{n'}{P} \right) + A_{n-n'} A_{n'} \star \Psi \left(\frac{n-n'}{P}; \frac{-n'}{P} \right) \right] \right\} \quad (14)$$

and

$$b_n = b_{-n}$$

where A_n are the Fourier coefficients for the line object as given in Eq. 12.

The function is called the transmission crosscoefficient [14] and characterizes the optical system including the state of partial coherence of the illumination. For a one-dimensional line object, following Ref. 15, the transmission crosscoefficient is given by

$$\Psi(\xi_1, \xi_2) = \int_{-\infty}^{\infty} \int_{-\infty}^{\infty} \mathcal{S}(\xi'', \eta'') \cdot F(\xi_1 + \xi'', \eta'') F^*(\xi_2 + \xi'', \eta'') d\eta'' d\xi'' \quad (15)$$

where $\mathcal{S}(\xi'', \eta'')$ is the two-dimensional intensity distribution in the condenser aperture, F is the two-dimensional equivalent of the pupil function, and $*$ denotes the complex conjugate (wide-field Kohler or critical illumination assumed). The function \mathcal{S} is sometimes called the effective source function [17] (assumed to be incoherent, i.e., the coherence interval is small compared with the effective source size).

Because of the dependence of R and \emptyset on angle of incidence the image structure will also vary with angle of incidence. This

formulation assumes that R and \emptyset are constant over the illuminating solid angle. If they are not, it is still possible to calculate the image from these equations. However, R and \emptyset become functions of μ and η and the integrals can no longer be separated as shown in Eqs. 14 and 15.

In this scalar theory approach, the line object is described by the planar function $t(x)$. Hence, there is no ambiguity about focus; the object thickness is much thinner than the depth of field of the optics. If the plane of the object is not coincident with the focal plane of the lens, the defocus aberration term is included in the pupil function,

$$F_{\text{defocus}}(\mu) = \exp(ika_2\mu^2) \text{Rec } \mu \mid \frac{M}{P} \quad (16)$$

where a_2 is the constant that indicates the amount of defocus in number of waves (units of λ), k is the wave number, and Rec is the rectangular function of width M/P , which defines the aperture diameter.

With lines patterned in thin layers (less than approximately $\lambda/4$ thick) and vertical edges, the images can be accurately described by these scalar equations and the coherent optical edge detection threshold T_c can be used for linewidth measurement [4].

$$T_c = 0.25 (1 + R + 2 \sqrt{R} \cos \emptyset), \quad (17)$$

However, in order to use T_c , R and \emptyset must be known. R (the ratio of reflectances on either side of the edge) is best determined from the image waveform. If \emptyset (the phase change at the edge from Eq. 6) is unknown, the dual threshold method [6] illustrated in Fig. 16(a) may be used to determine linewidth.

Because of the complex waveforms which result from the coherent imaging of line features of varying contrast with phase discont-

inuties present, best focus is difficult to determine. One objective criterion currently in use is minimization of Δ as defined in Fig. 16(b). This distance can also be tolerated to ensure that measurements made with inaccurate focus are rejected. That is, at best focus Δ is a minimum but by plotting Δ versus the change in linewidth with defocus, an acceptable range for Δ may be specified for a desired measurement accuracy.

In Fig. 17, calculated image waveforms are given for lines patterned in silicon dioxide on silicon and for chromium on glass. The computer software used to calculate the theoretical images is given in Appendix II. The reproducibility of these waveforms for linewidth measurement is determined principally by the accuracy of alignment of the line to be measured to the reference crosshair, accuracy of leveling of the wafer, and accuracy of focus. All of these operations should be automated so that they become operator independent and the required accuracy can be specified and maintained.

VECTOR THEORY FOR THICK-LAYER IMAGING

Scalar theory is unable to accurately predict the image profiles for line objects which violate the initial assumptions of infinitesimally thin (planar) objects and vertical edges characterized by abrupt discontinuities in R and ϕ . For patterned layers thicker than approximately one-quarter of the illumination wavelength, the multiple reflections which occur within semi-transparent layers result in constructive and destructive interference, which affects R and ϕ and the scattering patterns as well. In addition, both metals and dielectrics exhibit waveguide effects near edges which also influence the nature of the image waveforms. (See Fig. 18.) The major differences for thick layers as compared to thin layers are (1) the broadening of the minimum at the line edge, (2) enhanced maxima on either side of the edge particularly with sloping edge geometry, and (3) edge ringing which extends farther from the line edge in some cases.

Imaging of lines patterned in thick layers may be modeled using vector theory. For lines patterned in a thick layer with vertical edges, the complex dielectric constant of the material rather than the complex reflectance function is expanded in a Fourier series

$$\hat{\epsilon}(x) = \hat{n}_c^2 = \sum_m \epsilon_m \cos\left(\frac{2\pi mx}{P}\right) \quad (18)$$

The appropriate wave equation

$$\nabla^2 E_y + k_o^2 \hat{\epsilon} E_y = 0 \quad (\text{TE-mode})^* \quad (19)$$

and

$$\nabla^2 H_y - \frac{1}{\epsilon} \frac{\partial \epsilon}{\partial x} \frac{\partial H_y}{\partial x} + k_o^2 \hat{\epsilon} H_y = 0 \quad (\text{TM-mode}) \quad (20)$$

where $k_o = 2\pi/\lambda$ is solved for the E- and H-fields within the layer. In this case, when the Fourier series expansion for $\hat{\epsilon}(x)$ is substituted into Eq. (19), the resulting equation is Hill's equation [18], which has solutions of the form

$$E_y(x, z) = \sum_m A_m \exp(\alpha_m z) + A'_m \exp(-\alpha_m z) \cdot \sum_j B_{j,m} \exp(2\pi i j x / P)$$

where the α_m 's are the eigenvalues and the $B_{j,m}$'s are the eigen vector solutions to Hill's equation. The A_m and A'_m are weighting constants which must be determined from the boundary conditions. Each of these terms represents an inhomogeneous eigenfunction or waveguide mode which is supported by the line structure.

* Defined as that polarization component with its electric field parallel to the line being measured.

With a single plane wave incident, the boundary condition equations allow for solution for the Fourier series coefficients in the plane wave expansion for the reflected (scattered) field

$$E^R(x, z) = \sum_j E_j^R \exp \left\{ -ik_o \left[\left(\frac{\lambda j}{F} \right) x + K_j^R z \right] \right\} \quad (22)$$

For normal or nearly normal incidence, the magnitudes of the E- and H- fields are equal and no polarization effects are present. Therefore, the E_j^R coefficients in Eq. (22) can be substituted for the A_n 's in the scalar imaging equation (Eq.(14)). In this case, Eq. (22) may be regarded as representing the equivalent planar object which would produce the same image as the thick object of Eq. (18). The equivalent planar object is taken as located in the plane of the top surface of the thick layer. This concept is important to understanding the problem of focusing for thick layers.

For nonvertical edges, the single thick layer may be subdivided into a set of sublayers each of which may vary in linewidth, complex index of refraction and offset (to allow for asymmetric line objects). Such a representation is shown in Fig. 19. When boundary conditions are applied at each sublayer interface, the solution of the resulting equations yields the scattered field in the same form as Eq. (22). Thus any nonplanar structure can be represented by an equivalent planar structure and its image determined. For details of the method, see Refs. 5 and 19.

This method of computing both the reflected field and the corresponding microscope image requires no approximations of the type usually found in calculations of the scattered field, such as limits on the conductivity or slope of the surface. Limitations may be imposed, however, by the computation capability available. First, increasing the number of layers used to approximate the structure increases the computing time linearly. In most cases

of interest seven to nine layers were sufficient to produce significant results.

The second limitation is in the truncation of the series, i.e., the matrix sizes used in the computations. In this case, as for a single layer [4], all of the reflected plane waves which have diffraction angles less than $\pm \pi/2$ in the air are included. With $P = 12 \mu\text{m}$ and $\lambda = 0.53 \mu\text{m}$, 22 diffracted orders are included. This requires a 45×45 complex eigenvalue matrix and a 90×90 complex matrix for solution of the boundary condition equations. This choice necessarily truncates the series which represents the field in the layers with higher refractive index. This truncation does not appear to significantly affect the results except for very small linewidths and near resonances, that is, either where the thickness of the layer or the linewidth is approximately equal to the wavelength of the illumination.

Also, for grating objects with $P \leq 12 \mu\text{m}$, the assumed periodicity is true. However, for isolated line objects near resonances, $P = 12 \mu\text{m}$ is not large enough to eliminate the effect of the assumed adjacent lines on the calculated image. In order to calculate images of isolated lines, a larger period and, therefore, larger matrix sizes would have to be used.

As discussed earlier, this approach to the imaging of lines patterned in thick layers involves replacement of the thick line object by its equivalent planar object located in the plane coinciding with the top surface of the patterned layer. It can also be shown that displacement of the top surface of the thick layer (or equivalent planar object) along the optical axis of the imaging system introduces a focus error as in conventional scalar imaging equations with the accompanying loss of resolution and distortion of the image profiles.

At this time, no universal, simple, and accurate edge detection methods have been found for thick layer imaging. The complex

image structure in the vicinity of the line edge depends upon thickness and edge geometry as well as wavelength and other parameters of the imaging system. It is difficult to see how, in such a complex relationship of these parameters, a single number will be adequate to characterize line geometry.

Calculated images have been compared with experimentally measured images from the narrow-angle laser linewidth system. Some results are shown in Figs. 20 and 21. One of the major difficulties in getting agreement between theory and experiment is finding line objects with well characterized edge geometries.

ACCURACY AND PRECISION

Both the accuracy and precision of any metrology system needs to be established. Precision can be determined by repeated measurements on a control specimen. In the present case, the quality of the line specimens may limit precision. That is, specimens with rough edges cannot be placed in exactly the same position each time, and, therefore, the precision of the measurements is a function of edge roughness as well as system parameters. Unfortunately, the quality of most available processed wafers is not suitable for standard reference materials. Indications are that for the best thin layer materials available, the precision of the measurements when the coherent edge detection threshold is used is comparable to that of the photomask system used for calibration of SRM 475, which is approximately $\pm 0.05 \mu\text{m}$ (three standard deviations). The narrow-angle laser system at NBS has not yet reached the operational level of the photomask system. Until such time, there will be operator dependence due to focus, alignment and leveling errors. The difference here is that at the operational level all image scans which do not meet specified tolerance criteria are rejected automatically with an accompanying improvement in the long term precision of the system. The laser system has not been in routine use at this level long enough to get an accurate number for measurement precision.

Accuracy is customarily assessed based on fundamental physics considerations and/or comparison with other measurement techniques. In this case, at the level of accuracy being considered, comparison with other techniques cannot provide comparison numbers. There are no other fundamentally accurate optical techniques for dimensional measurements on thick objects with accuracies at the $0.05\text{ }\mu\text{m}$ ($\lambda/10$) level available at this time. A common recourse is to compare optical with scanning electron microscope (SEM) measurements. However, it has been shown that at this level SEM measurements are suspect [20] due to both electron beam interactions with the specimen and instrument errors. Therefore, comparison with SEM can only be expected to indicate gross errors at best. Even edge slope (or geometry) for thin layers ($< 200\text{ nm}$) can only be determined crudely in the SEM. (Magnifications of more than 100,000X are required.)

Therefore, accuracy needs to be assessed in terms of fundamental physics of the measurement process. For the photomask calibration system, edge slopes greater than approximately 70° produce images which are indistinguishable from vertical (90°) edges. This is supported by the fact that structure or variations which occur within a distance less than approximately $1/6$ the Airy disc diameter of the imaging objective do not affect the image. Hence, for lines with edge slopes greater than approximately 70° , there is an uncertainty in the measurement (for lines patterned in a 150 nm thick layer and 0.9 N.A.) of approximately $\pm 0.05\text{ }\mu\text{m}$ (worst case) if the measurement is taken to be the mean width. See Fig. 22. For the photomask case, SEM measurements on Cr-CrO masks corroborated this value.

For thin layers on wafers, the same argument may be applied with similar results. However, the agreement between theoretical and experimental image profiles must also be considered. In the wafer case, there is much more variation in materials and image profiles as well as greater system sensitivity to optical alignment, leveling, and focus errors. Therefore, while the narrow-angle laser

system has the capacity for accuracies on thin layers comparable to that of the photomask system, the accuracy should be assessed on a case-by-case basis with the above considerations taken into account.

For thick layers, assessment of accuracy is more complex. First, theory is based on a model which has yet to be fully evaluated. There are inappropriate assumptions in the modeling near resonances. Although the calculations are known to be in agreement for thin layers, the accuracy of the calculations for other cases has not been established. When discrepancies occur between calculated and experimentally measured image profiles, it is not known whether these differences are due to inaccuracies in the calculations, deviations of the system response from the ideal, poorly characterized line geometry, poorly known optical constants, or all of these. More work needs to be done on comparisons with line objects of known geometry, perhaps preferentially etched silicon samples, and on testing the accuracy of the calculated image profiles.

DESIGN OF LINEWIDTH CALIBRATION STANDARDS

Photomask materials have relatively little variation in optical constants. Hence, choice of a standard reference material was simplified. The most commonly used mask materials were chosen, CrO on Cr on glass, and an appropriate warning given about calibration of systems used to measure other materials was also given [21]. For wafers, there is an enormous variation in index of refraction and thickness of the layers found on wafers and, therefore, in R and \emptyset values as well. In fact, different combinations of materials may produce the same R , \emptyset values as well. Rather than sample all variables (R , \emptyset , and linewidth w) over the ranges of interest ($0 < R \leq 1$, $0 \leq \emptyset \leq \pi$, $0.5 \mu\text{m} < w < 5 \mu\text{m}$) which is impractical, it is possible to determine the nature of the expected errors, that is, their dependence on the variables R , \emptyset , and w and apply experimental design methodology to the design of a

standard. For linewidth measurements on wafers, the expected errors are known to be of low order [6]. Work by Dr. James Lechner, Carol Croarkin, and Ruth N. Varner at NBS resulted in the proposed optimal six-point design illustrated in Fig. 23. The expected error surface shown in Fig. 7(a) of Ref. 6 was found to fit a polynomial of the form

$$E(R, \phi) = (1-R) (A + BR + CR^2 + E \cos \phi + F \cos^2 \phi) \quad (23)$$

A search for a D-optimal design [22] was made, based on the polynomial model of the expected error surface. In combination with other factors such as ease of fabrication, the six-point design of Fig. 23 was selected as optimal. It is also a good design for polynomial surfaces of lower order such as those of Fig. 7(b) and (c) of Ref. 6. The design points $(R_i, \cos \phi_i)$ can be fabricated from two materials with a silicon substrate using the combinations shown in Table 2. In each case, only the top layer is patterned. This design is also relatively insensitive to small changes in R and ϕ such as would occur in normal fabrication of the standard. Thin-layer standards could thus be provided and calibrated with the present narrow-angle laser microscope. However, these standards would not be directly applicable for applications involving thick layers on silicon.

SUMMARY

This report has described the development of the narrow-angle laser linewidth measurement system at NBS and its application to calibration of linewidth measurement standard reference materials for the IC industry. This system represents a major move toward optical systems with well characterized waveforms suitable for accurate linewidth measurements at dimensions on the order of the illumination wavelength. In the course of its development, major theoretical advances have also been made in the theory of optical scattering from and imaging of objects with dimensions on the order of a micrometer.

ACKNOWLEDGMENTS

A number of people have contributed at various times to the developments described here. The original computer software for partially coherent imaging of line objects patterned in thin layers was written by Dr. Eric Kintner and later expanded and documented by Clinton R. Gable. Thanks are given to Ruth N. Varner for help in preparing the software for publication. Credit for the application of experimental design methodology to the design of a reference standard goes principally to Dr. James Lechner, Carol C. Croarkin, and Ruth N. Varner.

REFERENCES

1. Nyyssonen, D., "Optical linewidth measurements on wafers," Proc. SPIE Vol. 135, Developments in Semiconductor Microlithography III, 115-119 (1978).
2. Nyyssonen, D., "Calibration of optical systems for linewidth measurements on wafers," Proc. SPIE Vol. 221, Semiconductor Microlithography V, 119-126 (1980).
3. Nyyssonen, D., "Design of an optical linewidth standard reference material for wafers," Proc. SPIE Vol. 342, Integrated Circuit Metrology, 27-34 (1982).
4. Nyyssonen, D., "Theory of optical edge detection and imaging of thick layers," J. Opt. Soc. Am. 72, 1425-1436 (1982).
5. Nyyssonen, D., and Kirk, C., "Modeling the optical microscope images of thick layers for the purpose of linewidth measurement," Proc. SPIE Vol. 538, Optical Microlithography IV, 179-187 (1985).

6. Nyyssonen, D., "A practical method for edge detection and focusing for linewidth measurements on wafers," Opt. Eng. 26, 81-85 (1987).
7. Nyyssonen, D., "Focused-beam vs. conventional bright-field scanning microscopy for integrated circuit metrology," Proc. SPIE Vol. 565, Micron and Submicron Integrated Circuit Metrology, 180-186 (1985).
8. Stone, J. M., Radiation and Optics, (McGraw-Hill, New York, 1963) Chapter 16.
9. Driscoll, W. G., ed., Handbook of Optics, (McGraw-Hill, New York, 1978) pp. 8-42 to 8-43.
10. Chandler-Horowitz, D., "Ellipsometric accuracy and the principal angle of incidence," Proc. SPIE Vol. 342, Integrated Circuit Metrology, 121-130 (1982).
11. Scire, F. E. and E. C. Teague, "Piezodriven 50- μ m range state with subnanometer resolution", Rev. Sci. Instrum. 49, 1735-1740 (1978).
12. Kinzly, R. E. "Partially coherent imaging in a microdensitometer," J. Opt. Soc. Am. 62, 386-394 (1972).
13. Sheppard, C. J. R. and T. Wilson, "Image formation in scanning microscopes with partially coherent source and detector," Optica Acta 25, 315-325 (1978).
14. Wolf, E., "The radiant intensity from planar sources of any state of coherence," J. Opt. Soc. Am. 68, 1597-1605 (1978).
15. Born, M. And E. Wolf, Principles of Optics, 5th ed. (Pergamon, New York, 1975) pp. 530-532.

16. Kintner, E. C., "Method for the calculation of partially coherent imagery," Appl. Opt. 17, 2747-2753 (1978).
17. Hopkins, H. H., "Applications of coherence theory in microscopy and interferometry," J. Opt. Soc. Am. 47, 508-526 (1957).
18. Magnus, W. and S. Winkler, Hill's Equation (John Wiley and Sons, New York, 1966 and Dover, New York, 1979).
19. Nyyssonen, D., "Computer software for the computation of the scattered field and the optical microscope images of line objects patterned in thick layers," NBSIR 87-3618 (December 1987).
20. Postek, M. T. and D. C. Joy, "Microelectronics dimensional metrology in the scanning electron microscope," Solid State Tech. Part I 29, 145-150 (Nov. 1986) and Part II 29, 77-85 (Dec. 1986).
21. Nyyssonen, "Linewidth calibration for bright-chromium photo-masks," NBSIR 86-3357 (May 1986).
22. Raghavarao, D., Construction and Combinatorial Problems in Design of Experiments (John Wiley and Sons, New York, 1971).

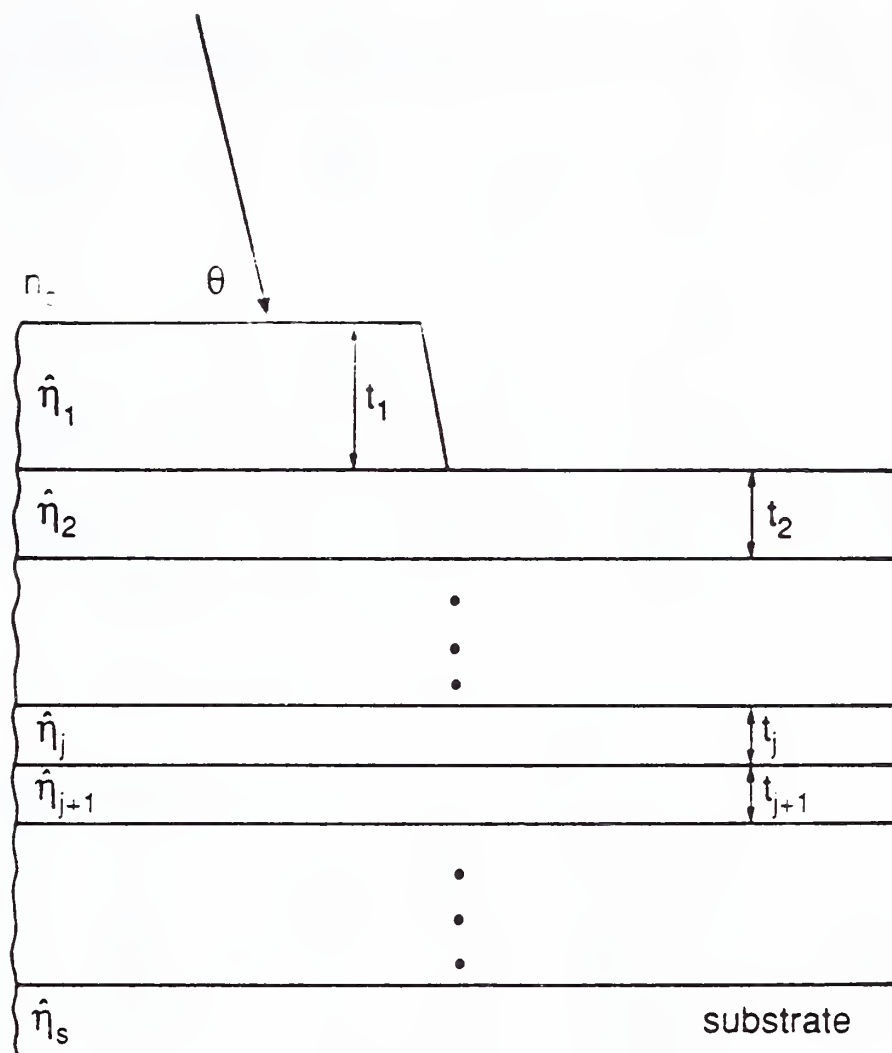


Fig. 1 Schematic of multi-layer structure on a wafer with definition of parameters used for calculation of R and ϕ .

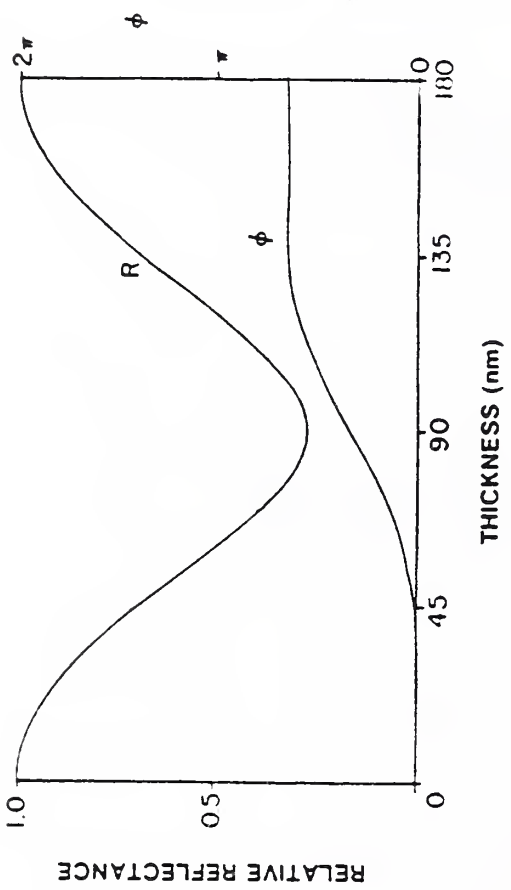


Fig. 2(a) Relative reflectance R and phase difference ϕ for silicon calculated from the Fresnel equations for varying thickness of silicon dioxide and monochromatic illumination (530 nm) at normal incidence.

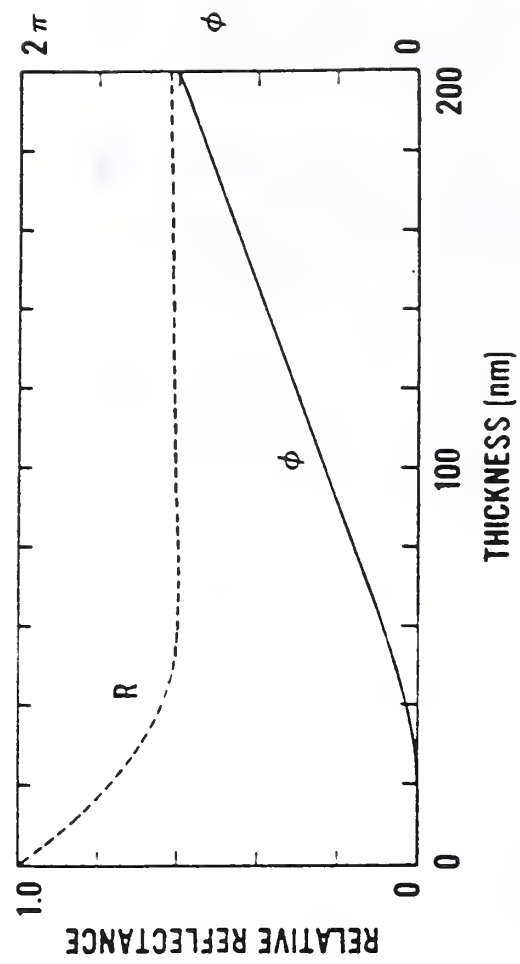


Fig. 2(b) Same as Figure 2(a), except for chromium on silicon.

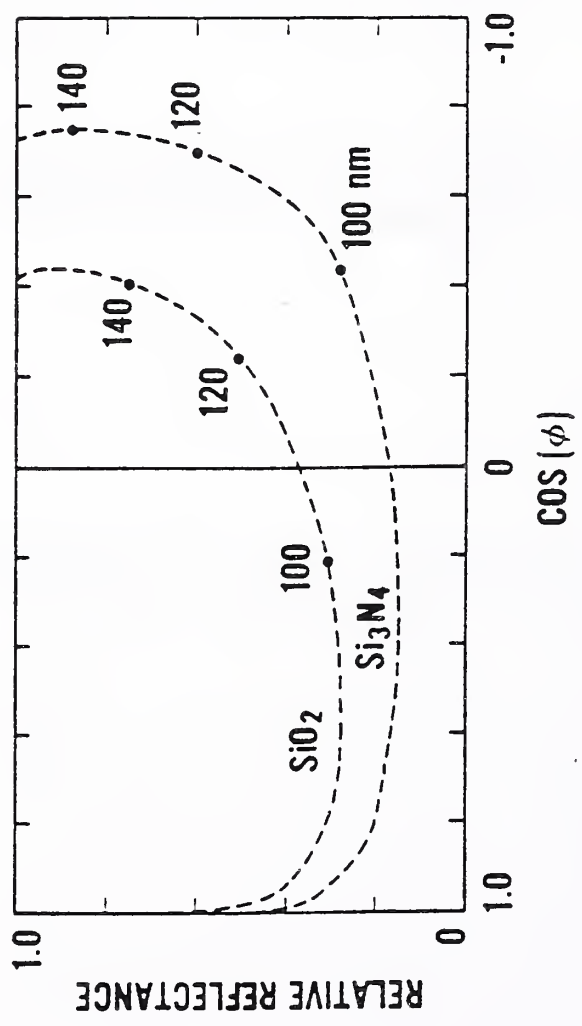


Fig. 2(c) Relative reflectance vs. the cosine of the phase difference for silicon dioxide and silicon nitride on silicon. Some of the corresponding thicknesses are indicated along each of the curves.

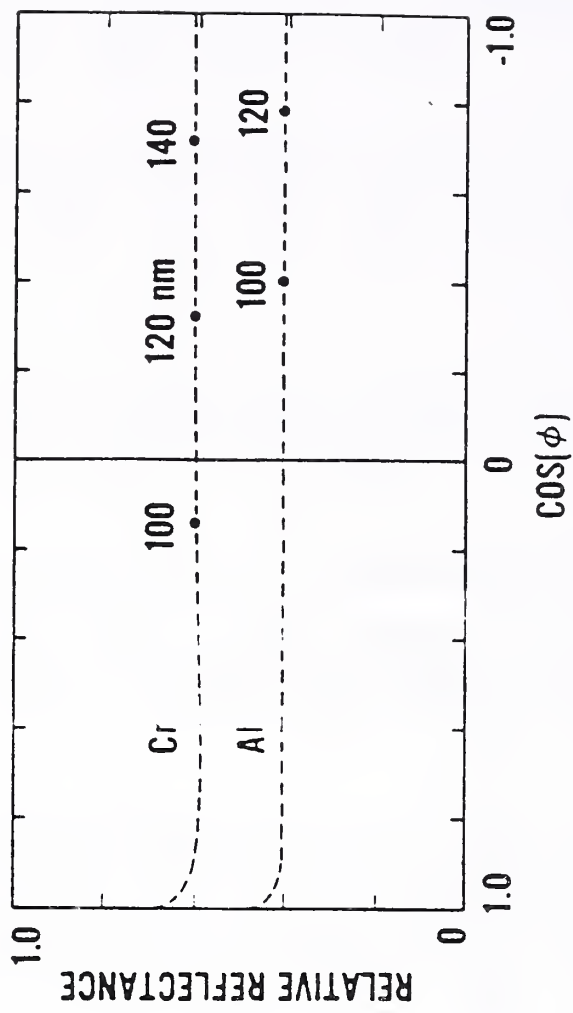


Fig. 2(d) Same as Figure 2(b), except for chromium and aluminum on silicon.

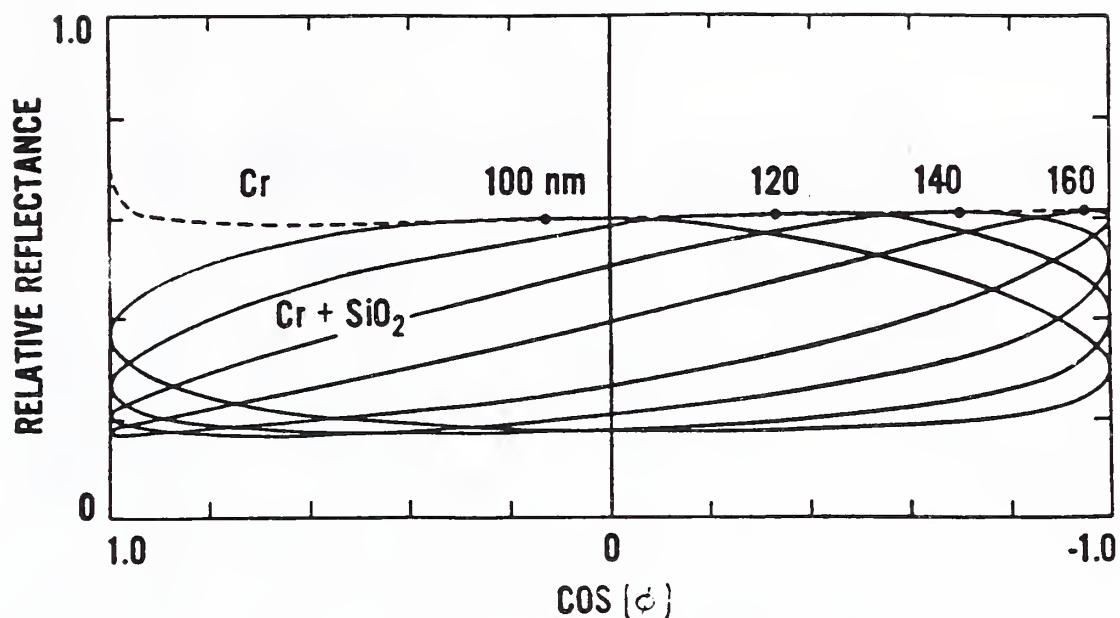


Fig. 3 Same as Fig. 2(b) for chromium with the addition of a silicon-dioxide layer of varying thickness between the chromium and silicon. The tangent point of each ellipse indicates the thickness of the chromium patterned layer. Varying the silicon dioxide between zero and 180 nm produces the ellipse.

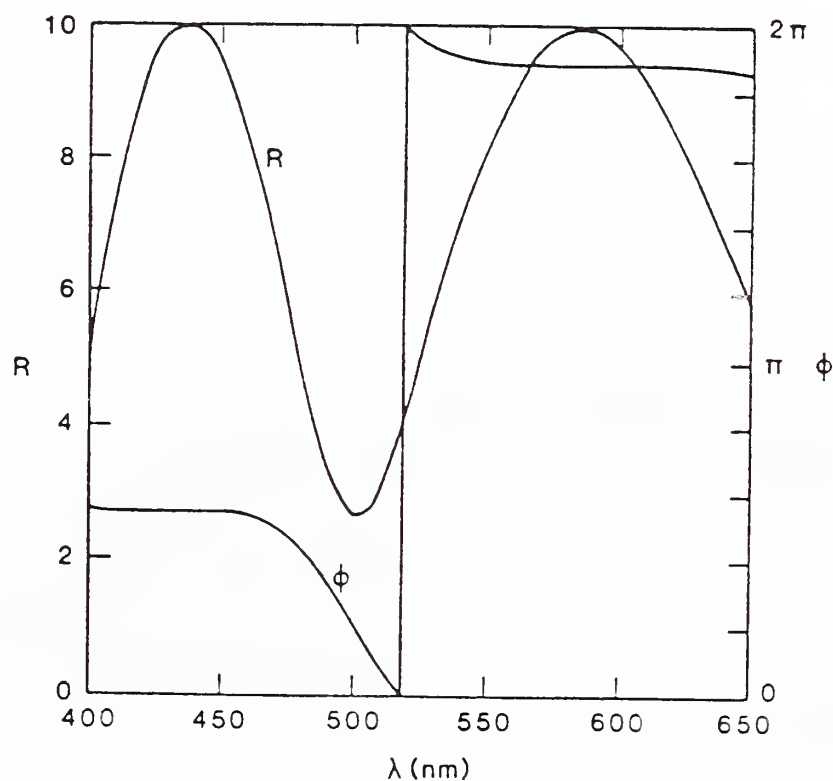


Fig. 4 Variation of R and ϕ with λ for a 600 nm thick layer of SiO_2 on Si.

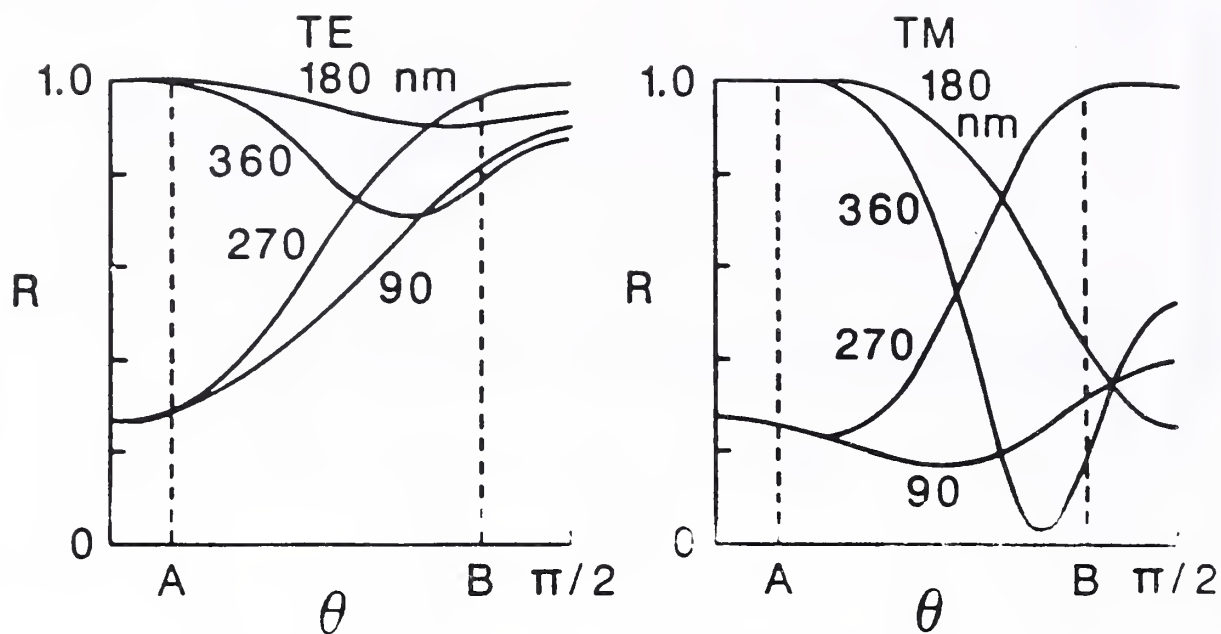


Fig. 5 Variation of R and ϕ with angle of incidence θ for thicknesses of SiO_2 on Si shown.

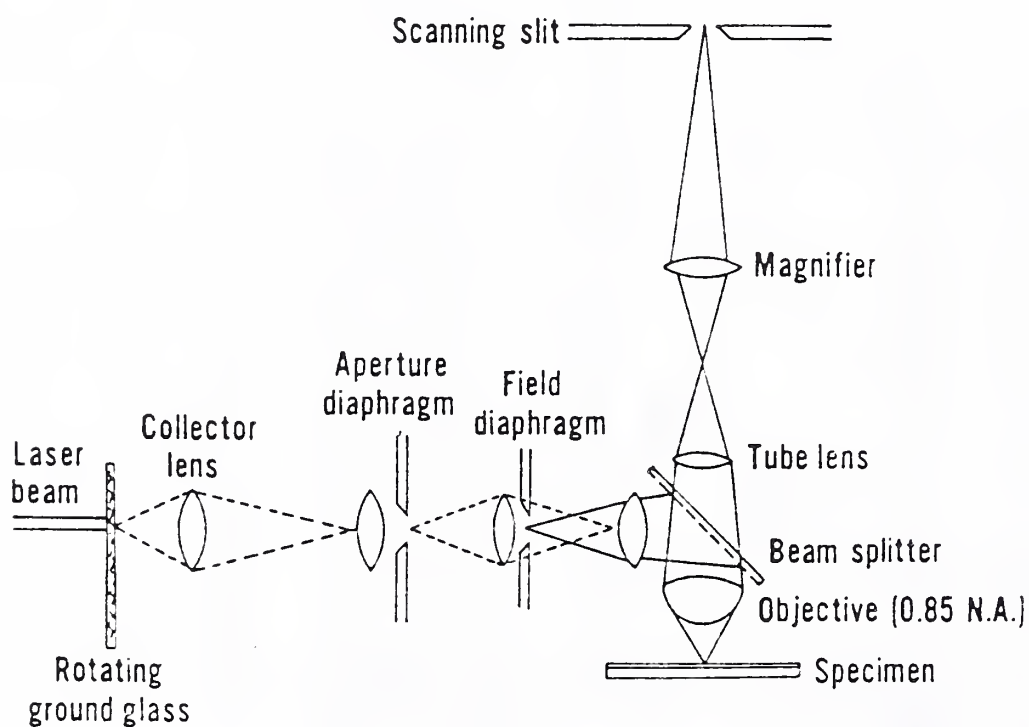


Fig. 6 Ray path for reflected-light laser-scanning microscope system.

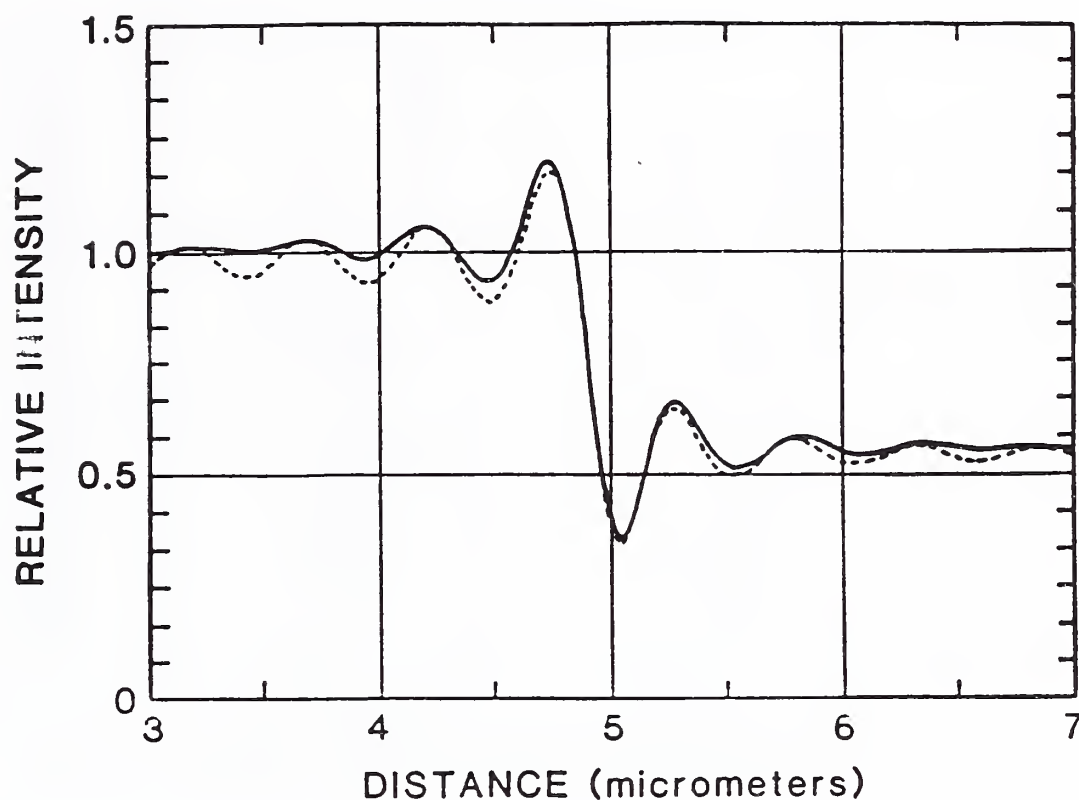


Fig. 7 Comparison of edge profiles calculated for fully coherent imaging (dashed curve) and for a coherence parameter of 0.2 (solid curve). Edge is located at 5 μm .

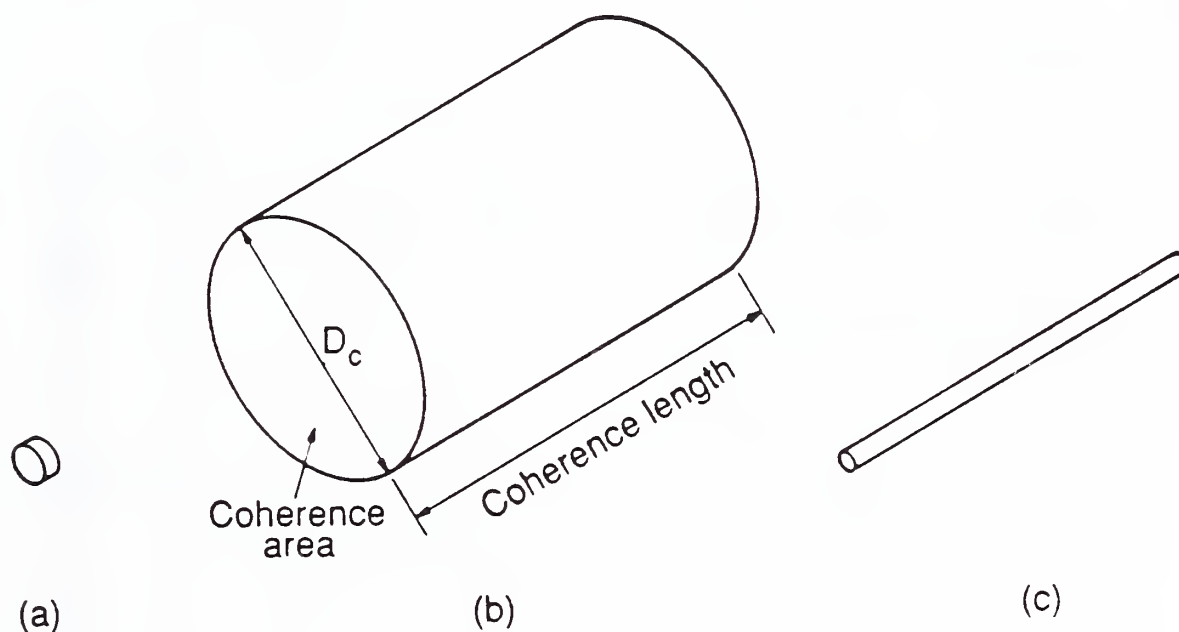


Fig. 8 Relative sizes of coherence volumes for microscopes using the sources indicated: (a) white light thermal source, (b) laser source, (c) narrow-angle laser system with rotating ground glass and laser source.

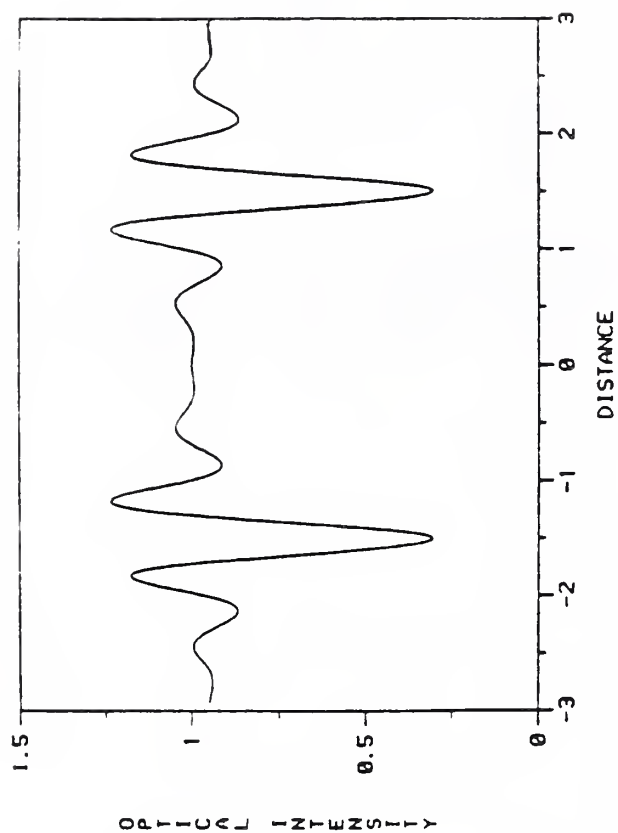


Fig. 9 Image waveform for 180 nm SiO₂ on Si.

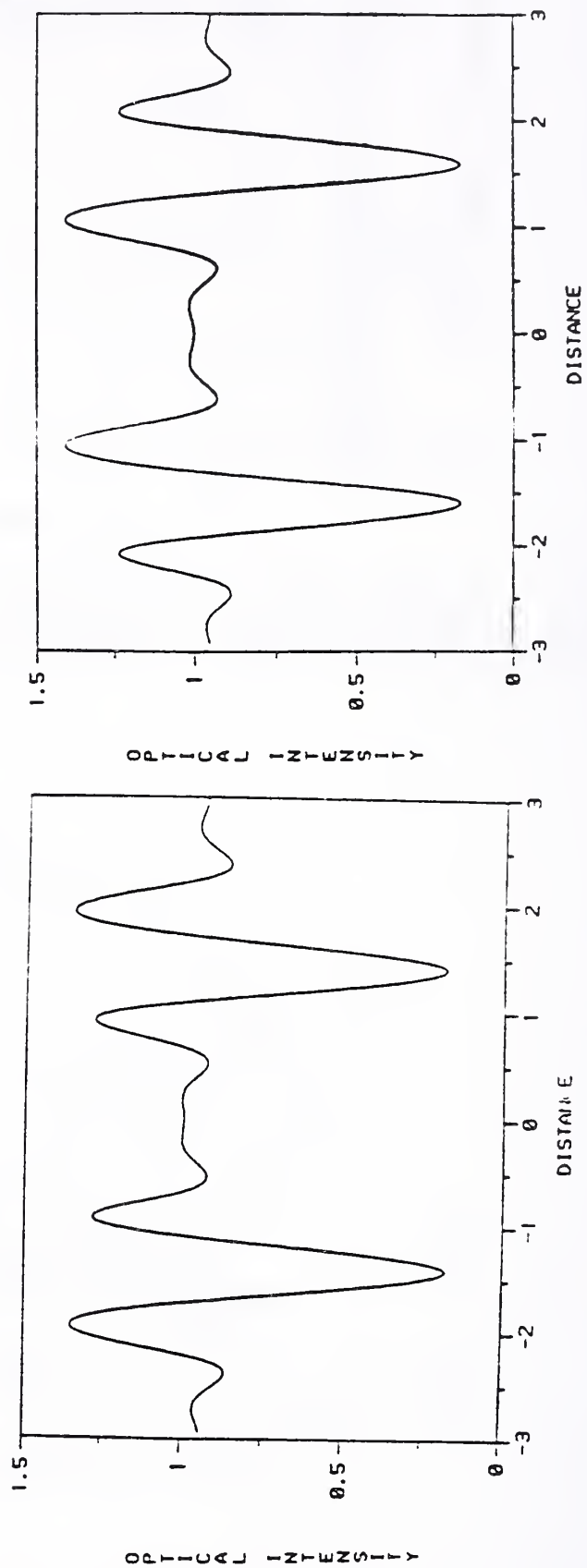
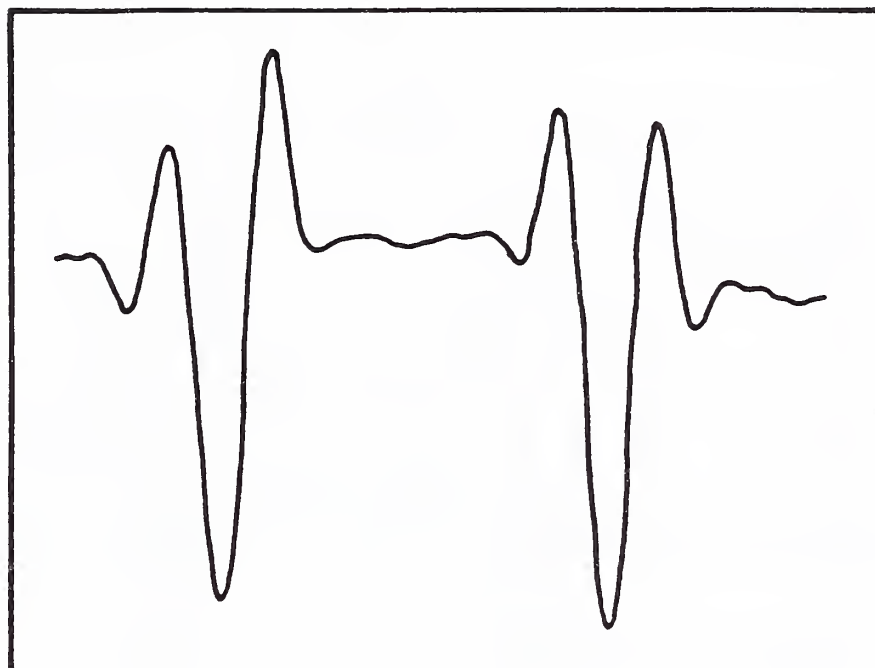


Fig. 10 Same as Figure 9 with defocus as indicated.

OPTICAL INTENSITY



DISTANCE IN MICROMETERS

Fig. 11 Image waveform with tilt present in wafer.
Note nonsymmetry.

OPTICAL INTENSITY

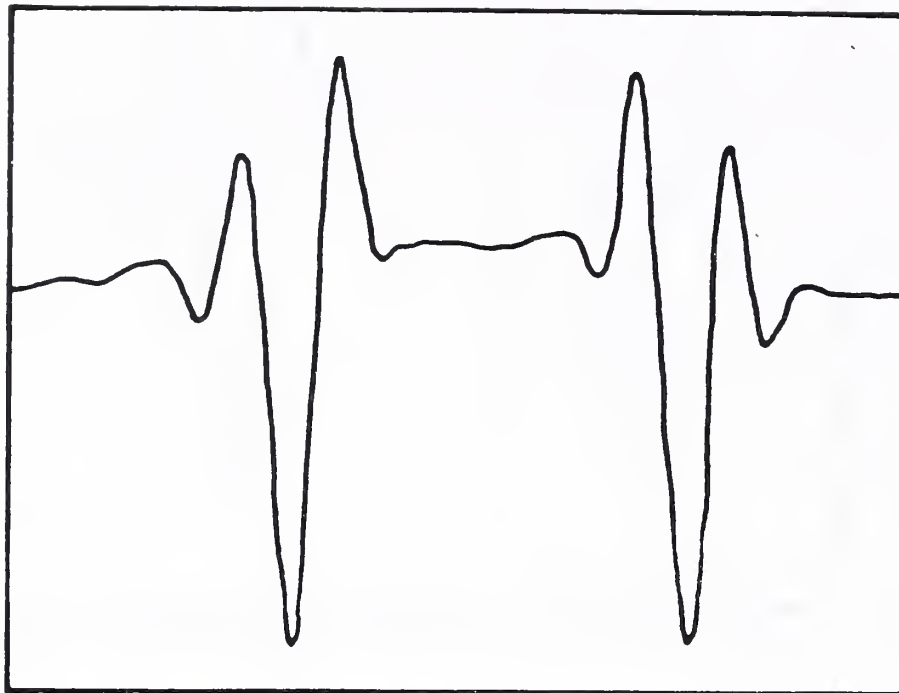


DISTANCE IN MICROMETERS

Fig. 12 Image waveform with misalignment present.

(a)

OPTICAL INTENSITY



DISTANCE IN MICROMETERS

OPTICAL INTENSITY



DISTANCE IN MICROMETERS

Fig. 13 Image waveform with slight misalignment and tilt (b) with correct alignment (a) shown for comparison.

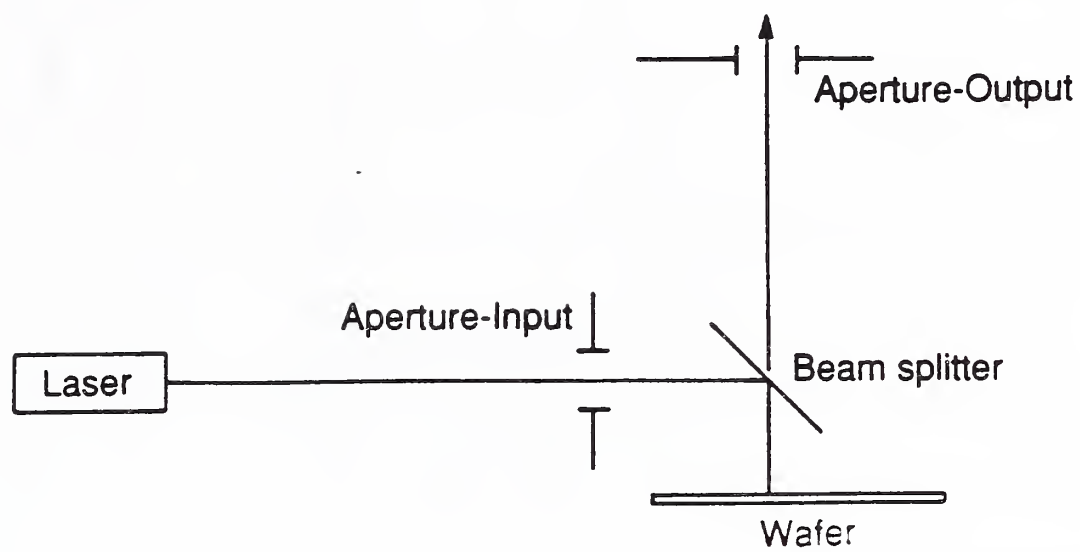


Fig. 14(a) Defining the optical axis of the system.

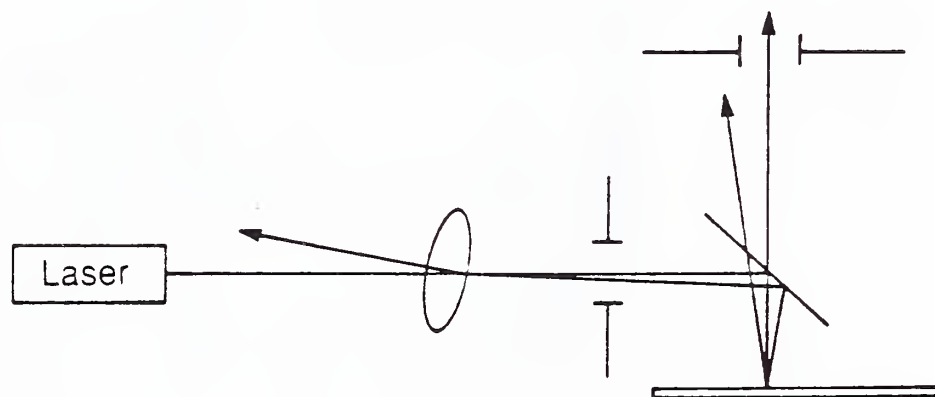


Fig. 14(b) Alignment errors with addition of lens.

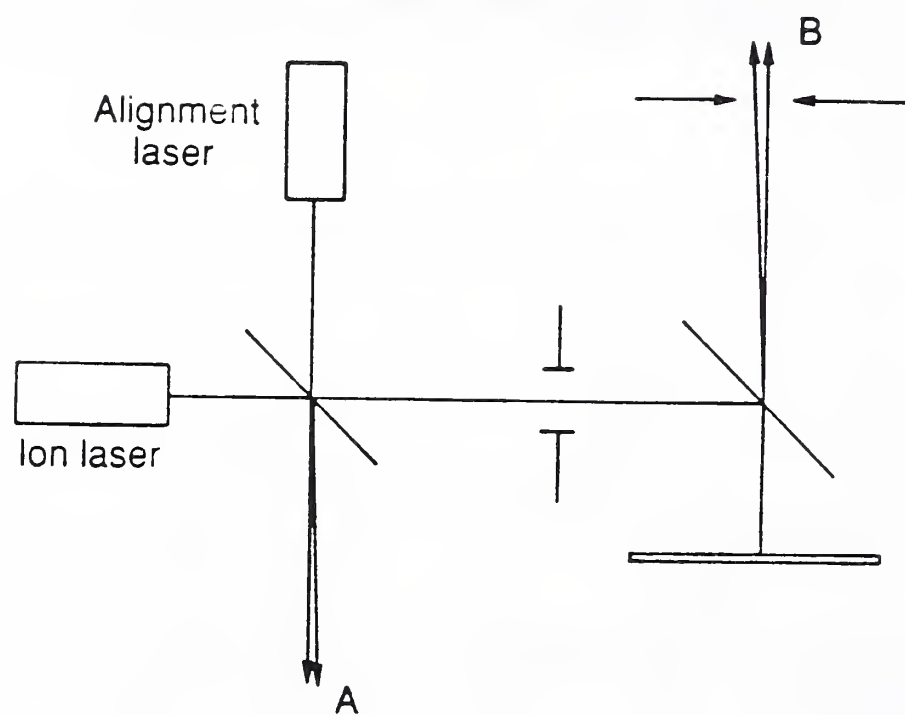


Fig. 15 Alignment laser beam and high power laser beam must be brought into coincidence at both A and B.

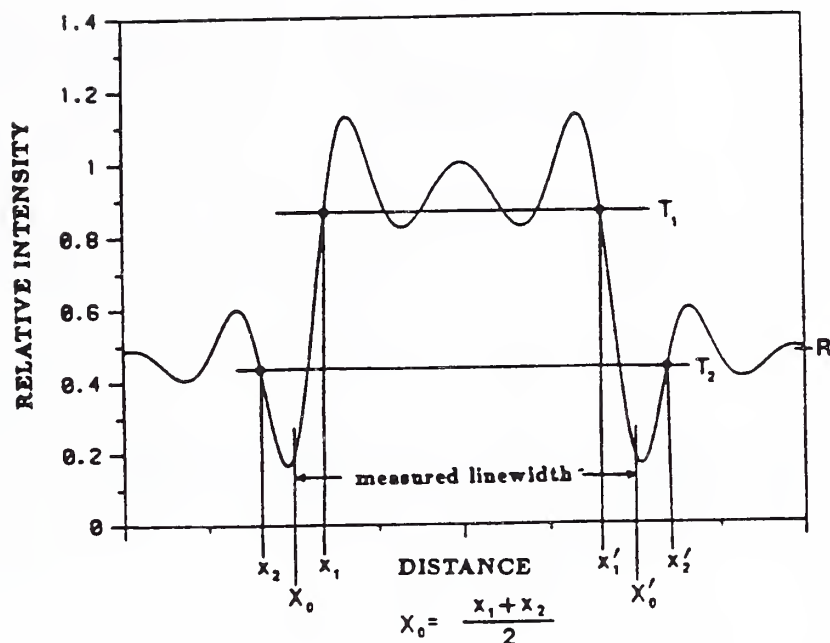


Fig. 16(a) Proposed dual-threshold edge detection criteria where $T_2 = RT$. In this paper, T_1 is taken to be 0.95 times the reflectance of either the line material or surround, whichever is higher.

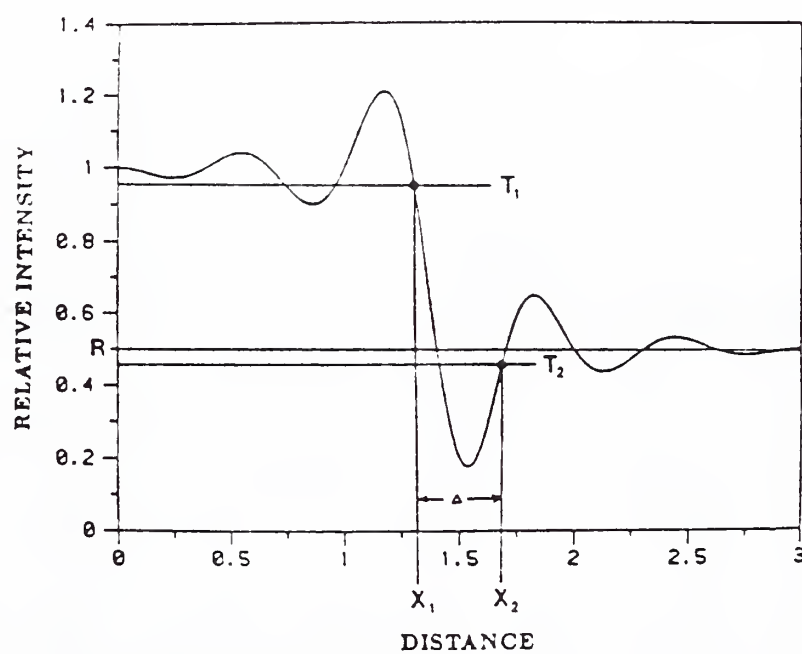


Fig. 16(b) Dual-threshold focus criterion for wafers. The edge width δ is a minimum at focus. For wafers, the threshold T_1 and T_2 are taken the same as in Fig. 16(a).

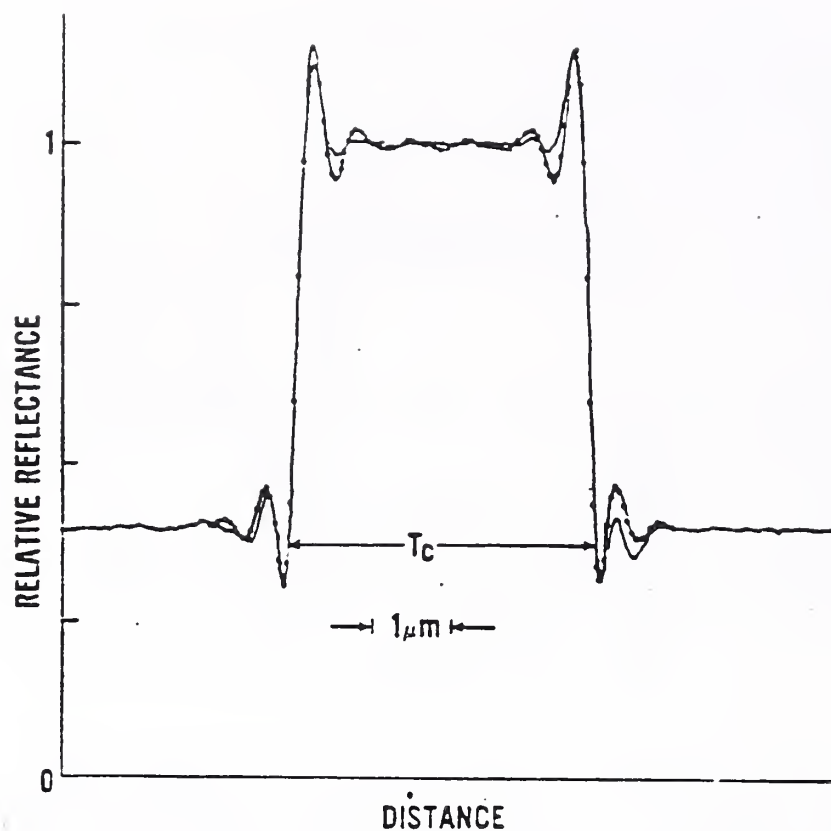


Fig. 17(a) Comparison of experimental (—) and theoretical (●) image profiles for a window etched in a 150-nm-thick layer of silicon dioxide on silicon (0.85 objective N.A., 0.2 condenser N.A., and 530-nm wavelength).

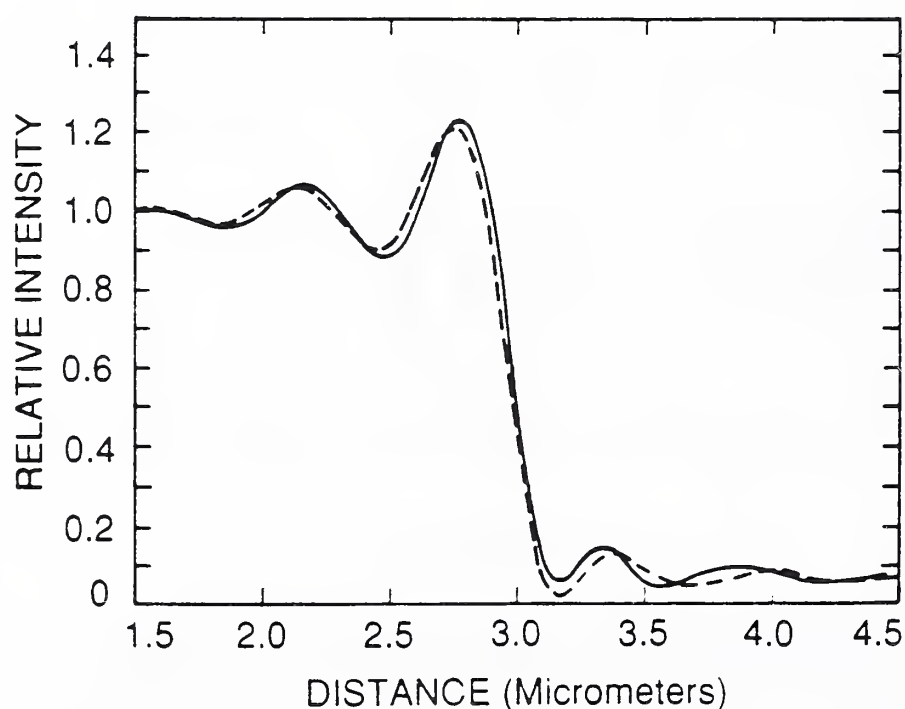


Fig. 17(b) Calculated image profiles from thick (vector, solid line) and thin (scalar, dotted line) models for a chromium on glass line.

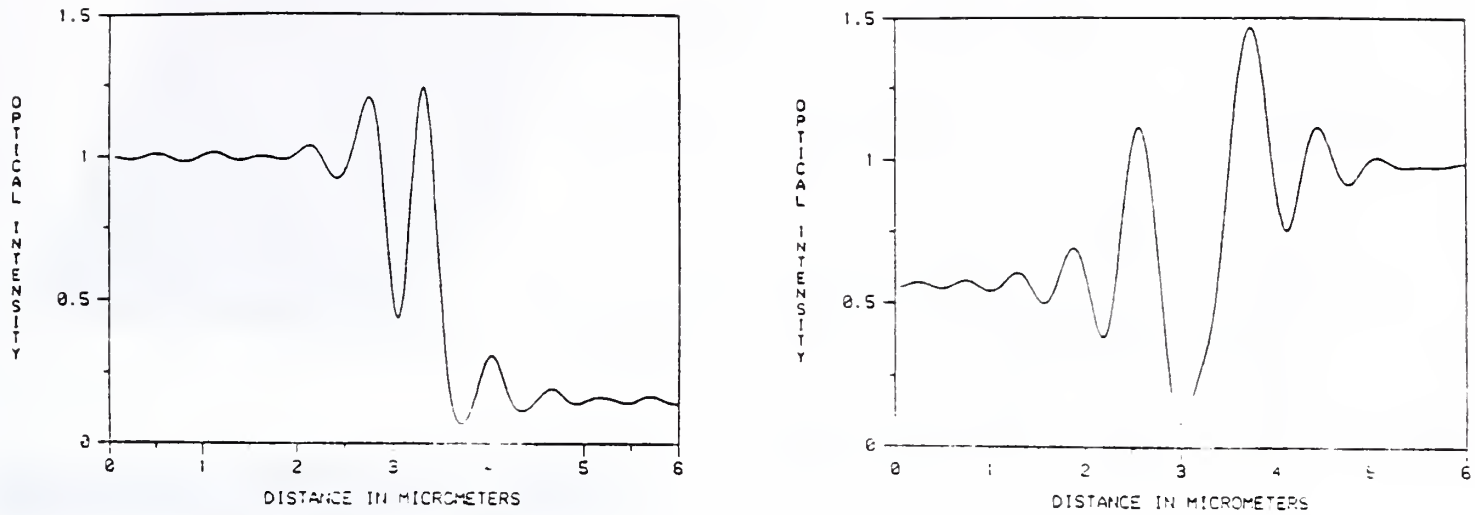


Fig. 18 Calculated image waveforms at edges of a single, vertical edge patterned layer for (a) Cr on SiO_2 on Si and (b) SiO_2 on Si.

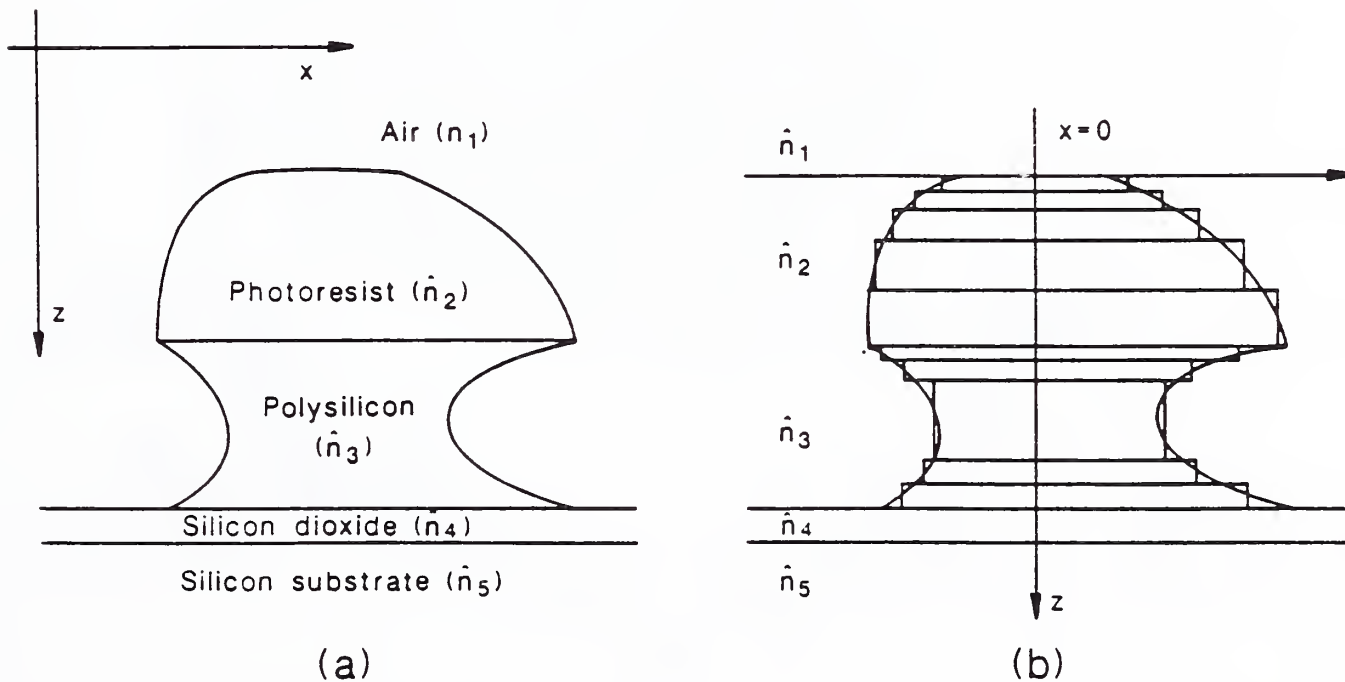


Fig. 19 Cross section of a typical thick line object (a) and the corresponding multilayer representation (b).

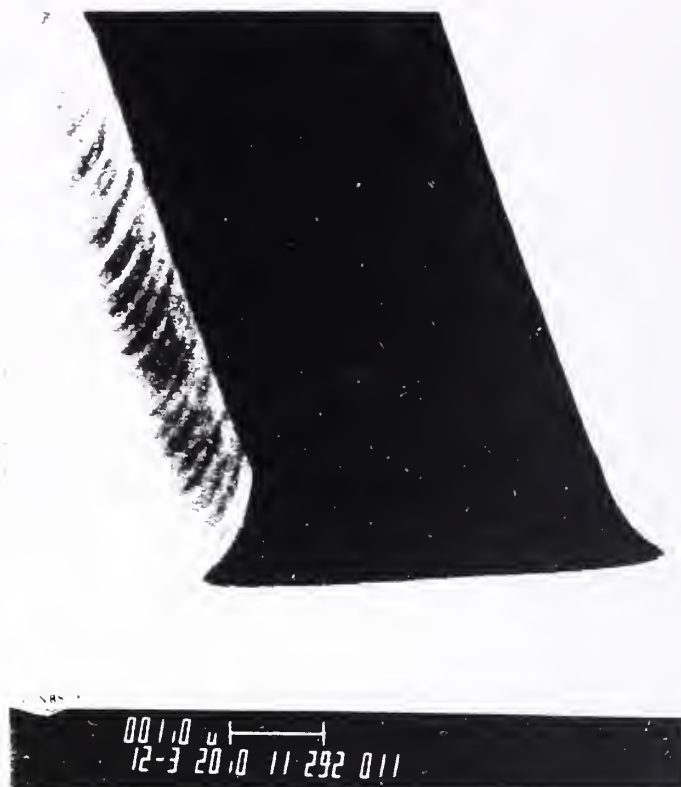
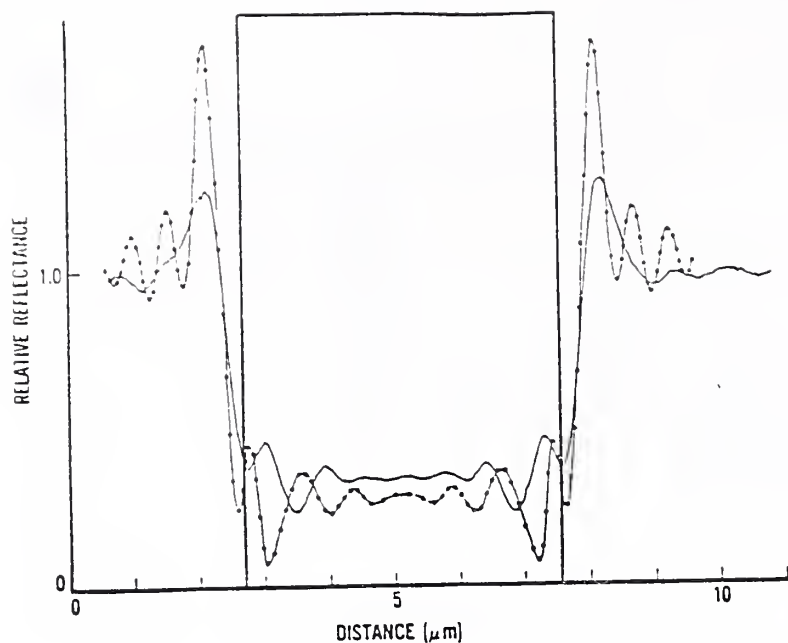


Fig. 20 (a) Comparison of experimental (solid curve) and theoretical () (based on waveguide model) image profiles for a window etched in a 616-nm-thick layer of silicon dioxide in silicon. The calculated curve is based on $\eta_0 = 1.46$, $\hat{\eta}_8 = 4.1 + i(0.06)$, 0.85 objective N.A., 0.14 condenser N.A., a wavelength of 514 nm, and a linewidth of 4.85 μm (b) SEM image of oxide line for wafer samples used in (a).

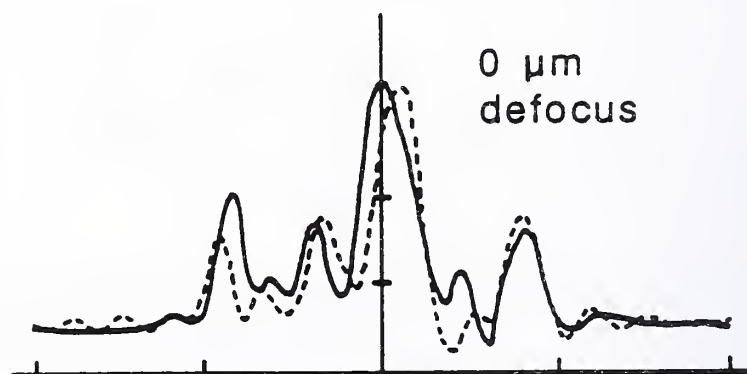
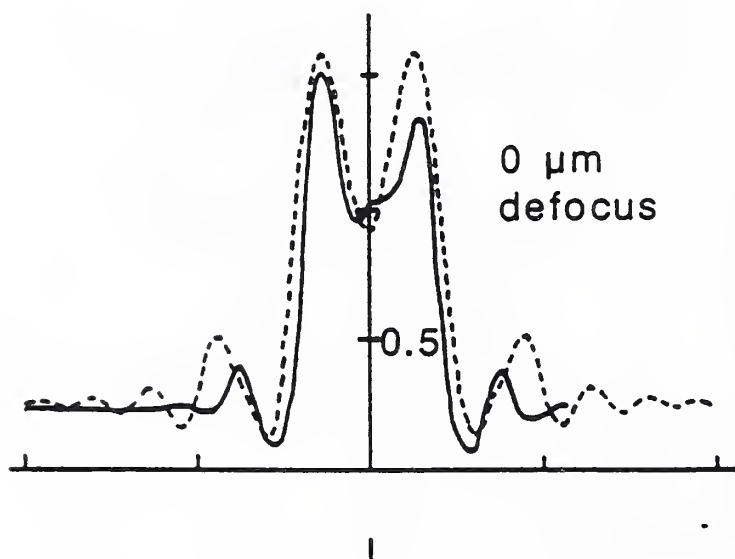


Fig. 21 Comparison of theoretical and experimental image profiles for 1 μm thick resist on Si for (a) vertical and (b) non-vertical.

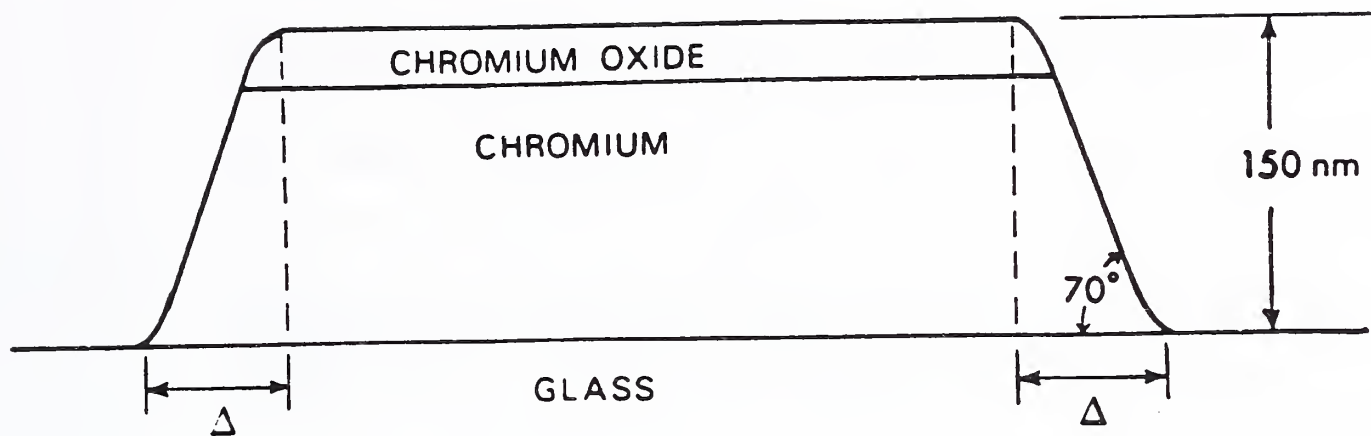


Fig. 22 Schematic of the profile for an opaque line on SRM 474 showing uncertainty U .

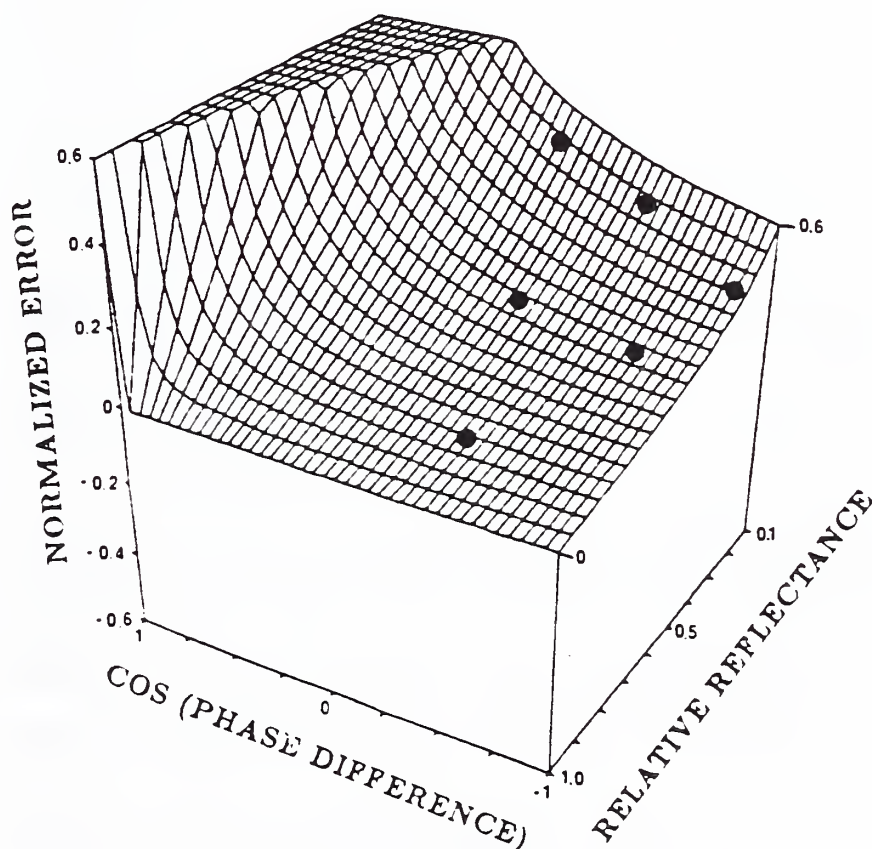


Fig. 23 Values of R and $\cos \phi$ (o) for six-point design super imposed on error surface. Corresponding to using the minima at the line edge as the edge detection threshold.

Appendix I - Software for Calculation of R and \emptyset
from the Fresnel Equations


```
1      PROGRAM TH2LR
2 C
3 C      THIS PROGRAM COMPUTES THE RELATIVE REFLECTANCE AND PHASE
4 C      DIFFERENCE FOR A PATTERNED LAYER WITH A SUBLAYER AND
5 C      SUBSTRATE BOTH OF WHICH MAY HAVE COMPLEX INDICES.
6 C
7 C      THIS PROGRAM WAS WRITTEN BY D. NYSSONEN, CD METROLOGY, INC.
8 C
9 C      *****
10 C
11 C      INTERMEDIATE LAYER THICKNESS IS HELD CONSTANT, WHILE THE
12 C      PATTERNED LAYER THICKNESS VARIES FROM 0 TO A MAXIMUM VALUE
13 C      (TO BE INPUT).  THE PATTERNED LAYER THICKNESSES ARE
14 C      INCREMENTED IN STEPS OF 0.002 MICROMETERS (20 ANGSTROMS).
15 C
16 C      *****
17 C
18 C      OUTPUT IS ON LOGICAL UNIT IOUT
19 C
20      DIMENSION T(2)
21      COMPLEX CM(2,2,2),DEL(2),CN(2),CBASE,CML(2,2),WAVEL,
22 *      X,Y,R
23      DATA IOUT/10/
24      OPEN(UNIT=IOUT,FILE='TAPE10')
25 C
26 C      WAVELENGTH OF LIGHT USED=0.53 MICROMETERS.
27 C
28      WAVEL=0.53
29 C
30 C      THICKNESS ENTERED FOR PATTERNED LAYER, T(1), IS MAXIMUM
31 C      FOR WHICH CALCULATIONS ARE MADE, INCREMENT IS 0.002 UM
32 C
33      PRINT*, 'INPUT THICKNESS AND COMPLEX INDICES OF LAYERS WITH',
34 *      ' PATTERNED LAYER FIRST'
35 C
36 C      ENTER MAX. THICKNESS OF PATTERNED LAYER IN MICROMETERS
37 C      FOLLOWED BY THE COMPLEX INDEX OF THE PATTERNED LAYER
38 C
39      READ*, T(1), CN(1)
40      PRINT*, 'INPUT THICKNESS AND COMPLEX INDEX OF',
41 *      ' INTERMEDIATE LAYER'
42 C
43 C      ENTER THICKNESS OF INTERMEDIATE LAYER IN MICROMETERS
44 C      FOLLOWED BY THE COMPLEX INDEX OF THE INTERMEDIATE LAYER,
45 C
46      READ*, T(2), CN(2)
47      PRINT*, 'INPUT COMPLEX INDEX OF SUBSTRATE'
48 C
49 C      ENTER COMPLEX INDEX OF SUBSTRATE (CBASE)
50 C
51      READ*, CBASE
52      WRITE(IOUT,*) 'FOR PATTERNED LAYER, MAX THICKNESS IS ', T(1),
53 *      ' AND INDEX IS ', CN(1)
54      WRITE(IOUT,*) 'FOR INTERMEDIATE LAYER, THICKNESS IS ', T(2),
55 *      ' AND INDEX IS ', CN(2)
```

```

56      WRITE(IOUT,*) 'INDEX OF SUBSTRATE IS ', CBASE
57      WRITE(IOUT,*)
58      WRITE(IOUT,*) 'THIS PROGRAM VARIES THICKNESS OF PATTERNED LAYER'
59      WRITE(IOUT,*)
60      WRITE(IOUT,*) '  THICK    R-PAT    R-INT    P-PAT    P-INT    DELAY',
61      *  'RNO    RM    PNORM    COS-P'
62      WRITE(IOUT,*)
63      TMAX=T(1)
64      T(1)=0.0
65      20 IF(T(1).GE.(TMAX-0.001)) GO TO 60
66      DO 40 J=1,2
67      DEL(J)=6.28318*CN(J)*T(J)/WAVEL
68      CM(J,1,1)=CCOS(DEL(J))
69      CM(J,1,2)=CSIN(DEL(J))/CN(J)*CMPLX(0.0,-1.0)
70      CM(J,2,1)=CSIN(DEL(J))*CN(J)*CMPLX(0.0,-1.0)
71      CM(J,2,2)=CM(J,1,1)
72      40 CONTINUE
73      CML(1,1)=CM(1,1,1)*CM(2,1,1)+CM(1,1,2)*CM(2,2,1)
74      CML(1,2)=CM(1,1,1)*CM(2,1,2)+CM(1,1,2)*CM(2,2,2)
75      CML(2,1)=CM(1,2,1)*CM(2,1,1)+CM(1,2,2)*CM(2,2,1)
76      CML(2,2)=CM(1,2,1)*CM(2,1,2)+CM(1,2,2)*CM(2,2,2)
77      X=CML(1,1)+CML(1,2)*CBASE
78      Y=CML(2,1)+CML(2,2)*CBASE
79      R=(X-Y)/(X+Y)
80      S=CABS(R)
81      RL=S**2
82      EL=ATAN2(AIMAG(R),REAL(R))
83      EL=EL/3.14159
84      X=CM(2,1,1)+CM(2,1,2)*CBASE
85      Y=CM(2,2,1)+CM(2,2,2)*CBASE
86      R=(X-Y)/(X+Y)
87      S=CABS(R)
88      RS=S**2
89      ES=ATAN2(AIMAG(R),REAL(R))
90      ES=ES/3.14159
91      C=4.0*T(1)/WAVEL
92      IF(RS.LT.RL) THEN
93      RO=RS/RL
94      ELSE
95      RO=RL/RS
96      END IF
97      EO=ES-EL+C
98      CSE=COS(3.14159*EO)
99      WRITE(IOUT,80)T(1),RL,RS,EL,ES,C,RO,EO,CSE
100 C
101 C      INCREMENT THE PATTERNED LAYER THICKNESS BY 0.002 UM
102 C
103      T(1)=T(1)+0.002
104      GO TO 20
105      60 CONTINUE
106      CLOSE(UNIT=IOUT)
107      STOP
108      80 FORMAT(9F8.3)
109      END
110 (EOF)

```

TEST CASE FOR TH2LR

1 FOR PATTERNED LAYER, MAX THICKNESS IS .2 AND INDEX IS (1.46,0.)
 2 FOR INTERMEDIATE LAYER, THICKNESS IS 0. AND INDEX IS (1.46,0.)
 3 INDEX OF SUBSTRATE IS (4.1,.1)

4
 5 THIS PROGRAM VARIES THICKNESS OF PATTERNED LAYER

	THICK	R-PAT	R-INT	P-PAT	P-INT	DELAY	RNORM	PNORM	COS-P
9	.000	.370	.370	-.996	-.996	.000	1.000	.000	1.000
10	.002	.369	.370	-.982	-.996	.015	.999	.001	1.000
11	.004	.369	.370	-.968	-.996	.030	.997	.002	1.000
12	.006	.367	.370	-.954	-.996	.045	.993	.003	1.000
13	.008	.366	.370	-.940	-.996	.060	.989	.004	1.000
14	.010	.363	.370	-.926	-.996	.075	.983	.005	1.000
15	.012	.361	.370	-.911	-.996	.091	.976	.006	1.000
16	.014	.358	.370	-.897	-.996	.106	.968	.007	1.000
17	.016	.354	.370	-.882	-.996	.121	.958	.007	1.000
18	.018	.350	.370	-.868	-.996	.136	.947	.008	1.000
19	.020	.346	.370	-.853	-.996	.151	.936	.008	1.000
20	.022	.341	.370	-.838	-.996	.166	.923	.008	1.000
21	.024	.336	.370	-.823	-.996	.181	.908	.008	1.000
22	.026	.330	.370	-.807	-.996	.196	.893	.008	1.000
23	.028	.324	.370	-.792	-.996	.211	.877	.007	1.000
24	.030	.318	.370	-.776	-.996	.226	.859	.006	1.000
25	.032	.311	.370	-.760	-.996	.242	.840	.005	1.000
26	.034	.303	.370	-.743	-.996	.257	.821	.004	1.000
27	.036	.296	.370	-.726	-.996	.272	.800	.002	1.000
28	.038	.288	.370	-.709	-.996	.287	.779	.000	1.000
29	.040	.280	.370	-.692	-.996	.302	.756	-.003	1.000
30	.042	.271	.370	-.674	-.996	.317	.733	-.005	1.000
31	.044	.262	.370	-.655	-.996	.332	.709	-.009	1.000
32	.046	.253	.370	-.636	-.996	.347	.685	-.013	.999
33	.048	.244	.370	-.617	-.996	.362	.660	-.017	.999
34	.050	.234	.370	-.597	-.996	.377	.634	-.022	.998
35	.052	.225	.370	-.576	-.996	.392	.608	-.028	.996
36	.054	.215	.370	-.554	-.996	.408	.582	-.034	.994
37	.056	.206	.370	-.532	-.996	.423	.556	-.041	.992
38	.058	.196	.370	-.510	-.996	.438	.530	-.049	.988
39	.060	.187	.370	-.486	-.996	.453	.505	-.057	.984
40	.062	.177	.370	-.461	-.996	.468	.480	-.067	.978
41	.064	.168	.370	-.436	-.996	.483	.455	-.077	.971
42	.066	.159	.370	-.409	-.996	.498	.431	-.089	.961
43	.068	.151	.370	-.381	-.996	.513	.408	-.101	.950
44	.070	.143	.370	-.352	-.996	.528	.387	-.115	.935
45	.072	.135	.370	-.322	-.996	.543	.366	-.130	.918
46	.074	.128	.370	-.291	-.996	.558	.347	-.146	.896
47	.076	.122	.370	-.259	-.996	.574	.330	-.164	.871
48	.078	.117	.370	-.225	-.996	.589	.315	-.182	.841
49	.080	.112	.370	-.190	-.996	.604	.302	-.202	.806
50	.082	.108	.370	-.154	-.996	.619	.291	-.223	.765
51	.084	.104	.370	-.118	-.996	.634	.282	-.244	.719
52	.086	.102	.370	-.080	-.996	.649	.276	-.267	.669
53	.088	.101	.370	-.042	-.996	.664	.272	-.290	.613
54	.090	.100	.370	-.003	-.996	.679	.270	-.313	.554

55	.092	.100	.370	.035	-.996	.694	.271	-.337	.491
56	.094	.102	.370	.073	-.996	.709	.275	-.360	.426
57	.096	.104	.370	.111	-.996	.725	.281	-.382	.361
58	.098	.107	.370	.148	-.996	.740	.289	-.404	.296
59	.100	.111	.370	.184	-.996	.755	.300	-.425	.233
60	.102	.116	.370	.219	-.996	.770	.313	-.445	.171
61	.104	.121	.370	.253	-.996	.785	.328	-.464	.113
62	.106	.127	.370	.286	-.996	.800	.344	-.482	.058
63	.108	.134	.370	.317	-.996	.815	.363	-.498	.007
64	.110	.142	.370	.347	-.996	.830	.383	-.513	-.041
65	.112	.149	.370	.376	-.996	.845	.404	-.527	-.084
66	.114	.158	.370	.404	-.996	.860	.427	-.540	-.124
67	.116	.167	.370	.431	-.996	.875	.451	-.551	-.161
68	.118	.176	.370	.457	-.996	.891	.475	-.562	-.194
69	.120	.185	.370	.481	-.996	.906	.500	-.572	-.224
70	.122	.194	.370	.505	-.996	.921	.526	-.581	-.250
71	.124	.204	.370	.528	-.996	.936	.552	-.588	-.274
72	.126	.214	.370	.551	-.996	.951	.578	-.596	-.296
73	.128	.223	.370	.572	-.996	.966	.604	-.602	-.315
74	.130	.233	.370	.593	-.996	.981	.630	-.608	-.332
75	.132	.242	.370	.613	-.996	.996	.655	-.613	-.347
76	.134	.252	.370	.633	-.996	1.011	.680	-.617	-.360
77	.136	.261	.370	.652	-.996	1.026	.705	-.621	-.372
78	.138	.270	.370	.670	-.996	1.042	.729	-.625	-.382
79	.140	.278	.370	.688	-.996	1.057	.752	-.628	-.391
80	.142	.286	.370	.706	-.996	1.072	.775	-.630	-.398
81	.144	.294	.370	.723	-.996	1.087	.796	-.632	-.404
82	.146	.302	.370	.740	-.996	1.102	.817	-.634	-.409
83	.148	.309	.370	.757	-.996	1.117	.837	-.636	-.414
84	.150	.316	.370	.773	-.996	1.132	.856	-.637	-.417
85	.152	.323	.370	.789	-.996	1.147	.874	-.638	-.419
86	.154	.329	.370	.805	-.996	1.162	.890	-.638	-.421
87	.156	.335	.370	.820	-.996	1.177	.906	-.639	-.422
88	.158	.340	.370	.835	-.996	1.192	.920	-.639	-.422
89	.160	.345	.370	.850	-.996	1.208	.933	-.639	-.422
90	.162	.350	.370	.865	-.996	1.223	.945	-.638	-.421
91	.164	.354	.370	.880	-.996	1.238	.956	-.638	-.420
92	.166	.357	.370	.894	-.996	1.253	.966	-.637	-.418
93	.168	.360	.370	.909	-.996	1.268	.974	-.637	-.416
94	.170	.363	.370	.923	-.996	1.283	.982	-.636	-.414
95	.172	.365	.370	.937	-.996	1.298	.988	-.635	-.412
96	.174	.367	.370	.951	-.996	1.313	.993	-.634	-.409
97	.176	.368	.370	.965	-.996	1.328	.996	-.633	-.406
98	.178	.369	.370	.979	-.996	1.343	.999	-.632	-.403
99	.180	.370	.370	.993	-.996	1.358	1.000	-.631	-.400
100	.182	.370	.370	-.993	-.996	1.374	1.000	1.370	-.397
101	.184	.369	.370	-.978	-.996	1.389	.999	1.371	-.394
102	.186	.368	.370	-.964	-.996	1.404	.996	1.372	-.391
103	.188	.367	.370	-.950	-.996	1.419	.992	1.373	-.388
104	.190	.365	.370	-.936	-.996	1.434	.987	1.374	-.385
105	.192	.363	.370	-.922	-.996	1.449	.981	1.375	-.382
106	.194	.360	.370	-.908	-.996	1.464	.974	1.376	-.380
107	.196	.357	.370	-.893	-.996	1.479	.965	1.377	-.378
108	.198	.353	.370	-.879	-.996	1.494	.956	1.377	-.377


```
1      PROGRAM TH2SV
2  C
3  C      THIS PROGRAM COMPUTES THE RELATIVE REFLECTANCE AND PHASE DIFFER-
4  C      ENCE FOR A PATTERNED LAYER WITH A SUBLAYER AND SUBSTRATE BOTH OF
5  C      WHICH MAY HAVE COMPLEX INDICES.
6  C
7  C      THIS PROGRAM WAS WRITTEN BY D. NYSSONEN, CD METROLOGY, INC.
8  C
9  C      *****
10 C
11 C      PATTERNED LAYER THICKNESS IS HELD CONSTANT, WHILE THE
12 C      INTERMEDIATE LAYER THICKNESS VARIES FROM 0 TO A MAXIMUM
13 C      VALUE (TO BE INPUT). THE INTERMEDIATE LAYER THICKNESSES
14 C      ARE INCREMENTED IN STEPS OF 0.002 MICROMETERS 20 ANGSTROMS).
15 C
16 C      *****
17 C
18 C      OUTPUT IS ON LOGICAL UNIT IOUT
19 C
20      DIMENSION T(2)
21      COMPLEX CM(2,2,2),DEL(2),CN(2),CBASE,CML(2,2),WAVEL,
22 *      X,Y,R
23      DATA IOUT/10/
24      OPEN(IOUT,FILE='TAPE10')
25 C
26 C      WAVELENGTH OF LIGHT USED=0.53 MICROMETERS.
27 C
28      WAVEL=0.53
29 C
30 C      THICKNESS ENTERED FOR INTERMEDIATE LAYER IS MAXIMUM THICKNESS FOR
31 C      WHICH CALCULATIONS ARE MADE, INCREMENT IS 0.002 UM
32 C
33      PRINT*, 'ENTER THE NUMBER OF DIFFERENT PATTERN LAYER'
34 C
35      PRINT*, 'THICKNESSES TO BE EXPLORED'
36 C
37      READ*,K
38      DO 60 L=1,K
39      PRINT*, 'INPUT THICKNESS AND COMPLEX INDICES OF LAYERS WITH',
40 *      ' PATTERNED LAYER FIRST'
41 C
42      READ *, T(1), CN(1)
43      PRINT*, ' INPUT MAX. THICKNESS AND COMPLEX INDICES OF',
44 *      ' INTERMEDIATE LAYER'
45 C
46      READ*, T(2), CN(2)
47      PRINT*, 'INPUT COMPLEX INDEX OF SUBSTRATE'
48 C
49      READ*, CBASE
50      WRITE(IOUT,*) 'FOR PATTERNED LAYER, THICKNESS IS ', T(1),
51 *      ' AND INDEX IS ', CN(1)
52      WRITE(IOUT,*) 'FOR INTERMEDIATE LAYER, THICKNESS IS ', T(2),
53 *      ' AND INDEX OF ', CN(2)
54      WRITE(IOUT,*) 'INDEX OF SUBSTRATE IS ', CBASE
```

```

55      WRITE(IOUT,*)
56      WRITE(IOUT,*) 'THIS PROGRAM VARIES THICKNESS OF INTERMEDIATE',
57      * ' LAYER'
58      WRITE(IOUT,*) ' THICK  R-PAT  R-INT  P-PAT  P-INT  DELAY',
59      * ' RNO  RM  PNORM  COS-P'
60      TMAX=T(2)
61      T(2)=0.0
62      DO 40 J=1,2
63          DEL(J)=6.28318*CN(J)*T(J)/WAVEL
64          CM(J,1,1)=COS(DEL(J))
65          CM(J,1,2)=SIN(DEL(J))/CN(J)*CMPLX(0.0,-1.0)
66          CM(J,2,1)=SIN(DEL(J))*CN(J)*CMPLX(0.0,-1.0)
67          CM(J,2,2)=CM(J,1,1)
68      40 CONTINUE
69          CML(1,1)=CM(1,1,1)*CM(2,1,1)+CM(1,1,2)*CM(2,2,1)
70          CML(1,2)=CM(1,1,1)*CM(2,1,2)+CM(1,1,2)*CM(2,2,2)
71          CML(2,1)=CM(1,2,1)*CM(2,1,1)+CM(1,2,2)*CM(2,2,1)
72          CML(2,2)=CM(1,2,1)*CM(2,1,2)+CM(1,2,2)*CM(2,2,2)
73          X=CML(1,1)+CML(1,2)*CBASE
74          Y=CML(2,1)+CML(2,2)*CBASE
75          R=(X-Y)/(X+Y)
76          S=CABS(R)
77          RL=S**2
78          EL=ATAN2(AIMAG(R),REAL(R))
79          EL=EL/3.14159
80          X=CM(2,1,1)+CM(2,1,2)*CBASE
81          Y=CM(2,2,1)+CM(2,2,2)*CBASE
82          R=(X-Y)/(X+Y)
83          S=CABS(R)
84          RS=S**2
85          ES=ATAN2(AIMAG(R),REAL(R))
86          ES=ES/3.14159
87          C=4.0*T(1)/WAVEL
88          IF(RS.LT.RL)THEN
89              RO=RS/RL
90          ELSE
91              RO=RL/RS
92          END IF
93          EO=ES-EL+C
94          CSE=COS(3.14159*EO)
95          WRITE(IOUT,80)T(2),RL,RS,EL,ES,C,RO,EO,CSE
96      C
97          IF(T(2).GE.TMAX)THEN
98              GO TO 60
99          ENDIF
100         T(2)=T(2)+0.002
101         GO TO 20
102     60 CONTINUE
103     CLOSE(UNIT=IOUT)
104     STOP
105     80 FORMAT(9F8.3)
106     END
107 (EOR)

```

TEST CASE FOR TH2SV

1 FOR PATTERNED LAYER, THICKNESS IS .08 AND INDEX IS (2.9,4.2)
 2 FOR INTERMEDIATE LAYER, THICKNESS IS .2 AND INDEX OF (1.46,0.)
 3 INDEX OF SUBSTRATE IS (4.1,.1)

4	THIS PROGRAM VARIES THICKNESS OF INTERMEDIATE LAYER								
5	THICK	R-PAT	R-INT	P-PAT	P-INT	DELAY	RNORM	PNORM	COS-P
6	.000	.647	.370	-.897	-.996	.604	.572	.505	-.015
7	.002	.647	.369	-.897	-.982	.604	.571	.519	-.059
8	.004	.647	.369	-.897	-.968	.604	.570	.533	-.103
9	.006	.647	.367	-.897	-.954	.604	.568	.547	-.147
10	.008	.647	.366	-.897	-.940	.604	.565	.561	-.191
11	.010	.647	.363	-.897	-.926	.604	.562	.575	-.234
12	.012	.647	.361	-.897	-.911	.604	.558	.590	-.278
13	.014	.647	.358	-.897	-.897	.604	.553	.604	-.321
14	.016	.647	.354	-.897	-.882	.604	.548	.618	-.364
15	.018	.647	.350	-.897	-.868	.604	.542	.633	-.406
16	.020	.647	.346	-.897	-.853	.604	.535	.648	-.448
17	.022	.647	.341	-.897	-.838	.604	.527	.663	-.490
18	.024	.647	.336	-.897	-.823	.604	.519	.678	-.531
19	.026	.647	.330	-.897	-.807	.604	.510	.693	-.571
20	.028	.647	.324	-.897	-.792	.604	.501	.709	-.611
21	.030	.647	.318	-.897	-.776	.604	.491	.725	-.649
22	.032	.647	.311	-.897	-.760	.604	.480	.741	-.687
23	.034	.647	.303	-.897	-.743	.604	.469	.758	-.724
24	.036	.647	.296	-.897	-.726	.604	.457	.774	-.759
25	.038	.647	.288	-.897	-.709	.604	.445	.792	-.793
26	.040	.647	.280	-.897	-.692	.604	.432	.809	-.826
27	.042	.647	.271	-.897	-.674	.604	.419	.827	-.856
28	.044	.647	.262	-.897	-.655	.604	.405	.846	-.885
29	.046	.647	.253	-.897	-.636	.604	.391	.865	-.911
30	.048	.647	.244	-.897	-.617	.604	.377	.884	-.934
31	.050	.647	.234	-.897	-.597	.604	.362	.904	-.955
32	.052	.647	.225	-.897	-.576	.604	.348	.925	-.972
33	.054	.647	.215	-.897	-.554	.604	.333	.946	-.986
34	.056	.647	.206	-.897	-.532	.604	.318	.968	-.995
35	.058	.647	.196	-.897	-.510	.604	.303	.991	-1.000
36	.060	.647	.187	-.897	-.486	.604	.288	1.015	-.999
37	.062	.647	.177	-.897	-.461	.604	.274	1.040	-.992
38	.064	.647	.168	-.897	-.436	.604	.260	1.065	-.979
39	.066	.647	.159	-.897	-.409	.604	.246	1.092	-.959
40	.068	.647	.151	-.897	-.381	.604	.233	1.119	-.930
41	.070	.647	.143	-.897	-.352	.604	.221	1.148	-.894
42	.072	.647	.135	-.897	-.322	.604	.209	1.178	-.847
43	.074	.647	.128	-.897	-.291	.604	.199	1.209	-.791
44	.076	.647	.122	-.897	-.259	.604	.189	1.242	-.725
45	.078	.647	.117	-.897	-.225	.604	.180	1.276	-.648
46	.080	.647	.112	-.897	-.190	.604	.173	1.310	-.561
47	.082	.647	.108	-.897	-.154	.604	.166	1.346	-.464
48	.084	.647	.104	-.897	-.118	.604	.161	1.383	-.359
49	.086	.647	.102	-.897	-.080	.604	.158	1.421	-.247
50	.088	.647	.101	-.897	-.042	.604	.155	1.459	-.129
51	.090	.647	.100	-.897	-.003	.604	.155	1.497	-.009
52	.092	.647	.100	-.897	.035	.604	.155	1.536	.112
53	.094	.647	.102	-.897	.073	.604	.157	1.574	.230

55	.096	.647	.104	-.897	.111	.604	.161	1.612	.344
56	.098	.647	.107	-.897	.148	.604	.165	1.649	.450
57	.100	.647	.111	-.897	.184	.604	.171	1.685	.548
58	.102	.647	.116	-.897	.219	.604	.179	1.720	.637
59	.104	.647	.121	-.897	.253	.604	.187	1.754	.715
60	.106	.647	.127	-.897	.286	.604	.197	1.786	.783
61	.108	.647	.134	-.897	.317	.604	.207	1.818	.840
62	.110	.647	.142	-.897	.347	.604	.219	1.848	.888
63	.112	.647	.149	-.897	.376	.604	.231	1.877	.926
64	.114	.647	.158	-.897	.404	.604	.244	1.905	.956
65	.116	.647	.167	-.897	.431	.604	.258	1.932	.977
66	.118	.647	.176	-.897	.457	.604	.272	1.957	.991
67	.120	.647	.185	-.897	.481	.604	.286	1.982	.998
68	.122	.647	.194	-.897	.505	.604	.301	2.006	1.000
69	.124	.647	.204	-.897	.528	.604	.315	2.029	.996
70	.126	.647	.214	-.897	.551	.604	.330	2.051	.987
71	.128	.647	.223	-.897	.572	.604	.345	2.073	.974
72	.130	.647	.233	-.897	.593	.604	.360	2.094	.957
73	.132	.647	.242	-.897	.613	.604	.375	2.114	.937
74	.134	.647	.252	-.897	.633	.604	.389	2.133	.913
75	.136	.647	.261	-.897	.652	.604	.403	2.152	.888
76	.138	.647	.270	-.897	.670	.604	.417	2.171	.859
77	.140	.647	.278	-.897	.688	.604	.430	2.189	.829
78	.142	.647	.286	-.897	.706	.604	.443	2.207	.796
79	.144	.647	.294	-.897	.723	.604	.455	2.224	.762
80	.146	.647	.302	-.897	.740	.604	.467	2.241	.727
81	.148	.647	.309	-.897	.757	.604	.479	2.257	.690
82	.150	.647	.316	-.897	.773	.604	.489	2.274	.653
83	.152	.647	.323	-.897	.789	.604	.499	2.290	.614
84	.154	.647	.329	-.897	.805	.604	.509	2.305	.574
85	.156	.647	.335	-.897	.820	.604	.518	2.321	.534
86	.158	.647	.340	-.897	.835	.604	.526	2.336	.493
87	.160	.647	.345	-.897	.850	.604	.534	2.351	.451
88	.162	.647	.350	-.897	.865	.604	.541	2.366	.409
89	.164	.647	.354	-.897	.880	.604	.547	2.380	.367
90	.166	.647	.357	-.897	.894	.604	.552	2.395	.324
91	.168	.647	.360	-.897	.909	.604	.557	2.409	.281
92	.170	.647	.363	-.897	.923	.604	.561	2.424	.237
93	.172	.647	.365	-.897	.937	.604	.565	2.438	.194
94	.174	.647	.367	-.897	.951	.604	.568	2.452	.150
95	.176	.647	.368	-.897	.965	.604	.570	2.466	.106
96	.178	.647	.369	-.897	.979	.604	.571	2.480	.062
97	.180	.647	.370	-.897	.993	.604	.572	2.494	.018
98	.182	.647	.370	-.897	-.993	.604	.572	.508	-.026
99	.184	.647	.369	-.897	-.978	.604	.571	.522	-.070
100	.186	.647	.368	-.897	-.964	.604	.569	.536	-.114
101	.188	.647	.367	-.897	-.950	.604	.567	.550	-.158
102	.190	.647	.365	-.897	-.936	.604	.564	.565	-.201
103	.192	.647	.363	-.897	-.922	.604	.561	.579	-.245
104	.194	.647	.360	-.897	-.908	.604	.557	.593	-.288
105	.196	.647	.357	-.897	-.893	.604	.552	.607	-.331
106	.198	.647	.353	-.897	-.879	.604	.546	.622	-.374
107	.200	.647	.349	-.897	-.864	.604	.540	.637	-.416
108	.202	.647	.345	-.897	-.849	.604	.533	.652	-.458

Appendix II - Software for Calculation of Partially Coherent
Imaging of Planar Line Objects

```

1      PROGRAM PCIMAG2
2 C    PROFPLAY.MAIN
3 C
4 C*****
5 C
6 C    THIS IS THE MAIN PROGRAM FOR COMPUTING PARTIALLY COHERENT
7 C    IMAGERY OF 1-D PERIODIC OBJECTS.
8 C
9 C    THE COMPUTATIONS EMPLOY THE METHODS OF FOURIER OPTICS.
10 C
11 C    THIS PROGRAM CONTROLS THE FLOW OF THE CALCULATIONS BY TESTING
12 C    CERTAIN INPUT PARAMETERS. IT ALLOWS FOR THE CHOICE OF 1-D OR 2-D
13 C    OPTICS, AND THE INPUT PARAMETERS CAN BE CHANGED WITHOUT HALTING
14 C    THE EXECUTION OF THE PROGRAM.
15 C
16 C*****
17 C
18 C    PARAMETER DEFINITIONS -
19 C
20 C          WIDTH      -      LINEWIDTH OF OBJECT IN MICROMETERS
21 C          WT         -      HALF-WIDTH OF FOREGROUND OBJECT
22 C          PER        -      PERIOD
23 C          XIR        -      FUNDAMENTAL FREQUENCY
24 C
25 C*****
26 C
27      CHARACTER*2 ANSWER
28      CHARACTER*5 TYPE
29      CHARACTER*12 SIZE
30      COMMON WIDTH,WAVE,OBJ,SSO,SAO,AB2,AB4,AP,TBO,PB,TTO,PT,SLIT,
31      *      DATAS(13)
32      COMMON/PAR/PI,TWOPI
33      COMMON/MN/XIR,WT,PER,NX
34      COMMON/IM/DUM1(2000),NX1,DUM2,DUM3,DUM4
35      COMMON/IO/INA,IOUTA,IOUTB
36      DATA INA,IOUTA,IOUTB/10,16,40/
37      PI=4.0*ATAN(1.0)
38      TWOPI=2.0*PI
39      OPEN (UNIT=INA,FILE='INDATA')
40      OPEN (UNIT=IOUTA,FILE='PRTDATA')
41      OPEN (UNIT=IOUTB,FILE='PLOTDAT')
42 C
43 C*****
44 C
45 C    SUMMARY OF THE INPUT/OUTPUT STRUCTURE.
46 C-----
47 C
48 C          FILE      VARIABLE      LOGICAL UNIT      DEFINITION
49 C
50 C          INDATA      INA          10              INPUT DATA FILE
51 C          PRTDATA      IOUTA        16              OUTPUT DATA FILE - PRINTER
52 C          PLOTDAT      IOUTB        40              OUTPUT DATA FILE - PLOTTER
53 C
54 C*****
55 C
56      PRINT*
57      READ(INA,*)ANSWER
58 C
59 C*****
60 C

```

```
61 C READ THE INPUT PARAMETERS THAT CHARACTERIZE THE OPTICAL SYSTEM.
62 C CONVERT INPUT DATA FOR INTENSITY TRANSMITTANCE (OR REFLECTANCE)
63 C AND PHASE OF THE OBJECT TO COMPLEX AMPLITUDE TRANSMITTANCE
64 C (OR REFLECTANCE).
65 C
66 C*****
67 C
68 C 100 CALL RDATA
69 C
70 C*****
71 C
72 C TEST 'WIDTH' INPUT PARAMETER.
73 C THE WIDTH CAN VARY FROM 0.01 TO 10.00 MICROMETERS.
74 C
75 C NOTE: WIDTH IS MULTIPLIED BY 2 WHEN CALCULATING 'NX' IN ORDER
76 C TO VIEW THE BEHAVIOR OF THE INTENSITY PROFILE OF LINES
77 C OR SPACES FURTHER FROM THE EDGE.
78 C
79 C AN ERROR MESSAGE OCCURS IF THE WIDTH LIES OUTSIDE THIS RANGE-
80 C THE PROGRAM THEN DEMANDS A NEW SET OF INPUT DATA
81 C
82 C*****
83 C
84 C 200 IF(WIDTH.GT.2.5.OR.WIDTH.LE.10.0) THEN
85 C     WT=0.1
86 C     PER=5.0*WIDTH
87 C     SIZE='GREATER THAN'
88 C     NX=100.0*WIDTH+0.0001
89 C ELSEIF(WIDTH.LE.2.5.AND.WIDTH.GT.0.0) THEN
90 C     WT=WIDTH/10.0
91 C     PER=5.0
92 C     SIZE='LESS THAN'
93 C     NX=100.0*WIDTH*2.0+0.0001
94 C ELSE
95 C     PRINT*, 'ERROR IN WIDTH. PROGRAM STOPS.'
96 C     STOP
97 C ENDIF
98 C XIR=WAVE/(PER*OBJ)
99 C
100 C*****
101 C
102 C COMPUTE THE COMPLEX FOURIER COEFFICIENTS, A(N), OF A PERIODIC
103 C OBJECT WITH A SYMMETRIC RECTANGULAR WAVEFORM.
104 C
105 C*****
106 C
107 C CALL OBJECT
108 C
109 C*****
110 C
111 C COMPUTE THE REAL FOURIER COEFFICIENTS, C(N), WHICH CHARACTERIZE
112 C THE INTENSITY DISTRIBUTION IN THE IMAGE PLANE.
113 C
114 C ('CROS1D' IS CALLED FOR 1-D OPTICS, WHILE 'CROS2D' IS CALLED FOR
115 C 2-D OPTICS.)
116 C
117 C*****
118 C
119 C IF(ANSWER.EQ.'1D') THEN
120 C     CALL CROS1D
```

```
121      ELSE
122      CALL CROS2D
123      ENDIF
124 C
125 C*****
126 C
127 C  INCLUDE THE EFFECT OF A SCANNING SLIT IN THE IMAGE PLANE BY
128 C  ADJUSTING THE VALUES OF THE REAL FOURIER COEFFICIENTS, C(N).
129 C  (THIS IS NOT NECESSARY IF THE SLIT IS LESS THAN 0.01 MICROMETERS
130 C  IN WIDTH.)
131 C
132 C*****
133 C
134      IF(SLIT.GE.0.01) CALL CSLIT
135 C
136 C*****
137 C
138 C  CALCULATE THE INTENSITY DISTRIBUTION OF A PLANAR OBJECT USING
139 C  PARTIALLY COHERENT IMAGING FORMULAS.
140 C
141 C*****
142 C
143      CALL IMAGE
144 C
145 C*****
146 C
147 C  TEST FOREGROUND TRANSMITTANCE IN ORDER TO SET CERTAIN PARAMETERS
148 C  PRIOR TO NORMALIZATION.
149 C
150 C*****
151 C
152      IF(TTO.EQ.1.0)THEN
153          NUM=1
154          TYPE='SPACE'
155      ELSE
156          NUM=NX1
157          TYPE='LINE'
158      ENDIF
159 C
160 C*****
161 C
162      CALL YNORM(NUM)
163 C
164 C*****
165 C
166 C  PRINT A TABLE OF NORMALIZED INTENSITY VERSUS DISTANCE ONTO
167 C  AN OUTPUT DEVICE.  ALSO PRINT TWO COLUMNS OF INTENSITY AND
168 C  DISTANCE OUT TO FILE PLOTDAT FOR PLOTTING PURPOSES.
169 C
170 C*****
171 C
172      CALL PRINT(TYPE,SIZE,ANSWER)
173 C
174 C*****
175 C
176      CLOSE(UNIT=INA)
177      CLOSE(UNIT=IOUTA)
178      CLOSE(UNIT=IOUTB)
179      STOP
180      END
```



```
181 C
182 C*****
183 C
184 C THIS SUBROUTINE COMPUTES THE COMPLEX FOURIER COEFFICIENTS, A(N), OF
185 C A PERIODIC OBJECT WITH A SYMMETRIC RECTANGULAR WAVEFORM.
186 C
187 C THE COMPUTED COEFFICIENTS ARE STORED IN LABELED COMMON/ACOE/.
188 C
189 C*****
190 C
191 C SUBROUTINE OBJECT
192 C
193 C*****
194 C
195 C COMPLEX TB, TT, A(100), A0, CC
196 C COMMON/ACOE/ A, A0
197 C COMMON/MN/DUM1,WT,DUM2,DUM3
198 C COMMON/RD1/TB,TT
199 C COMMON/PI/PI,TWOPI
200 C
201 C*****
202 C
203 C SEE EQUATION #21A, 'METHOD FOR THE CALCULATION OF PARTIALLY COHERENT
204 C IMAGERY', ERIC KINTNER, J. APPLIED OPTICS, VOL.17, NO.17, PAGE 2747
205 C
206 C A0=TB+2.0*(TT-TB)*WT
207 C
208 C COMPUTE CONSTANT COMMON TO ALL COEFFICIENTS.
209 C
210 C CC=(TT-TB)/PI
211 C
212 C NOTE THE USE OF THE IDENTITY -
213 C SIN(N*X) = 2.0*COS(X)*SIN((N-1)*X) - SIN((N-2)*X).
214 C
215 C COSN=COS(TWOPI*WT)
216 C S=0.0
217 C S1=-SIN(TWOPI*WT)
218 C DO 300 N=1, 100
219 C S2=S1
220 C S1=S
221 C S=2.0*COSN*S1-S2
222 C A(N)=CC*S/N
223 C 300 CONTINUE
224 C RETURN
225 C END
226 C
227 C*****
228 C
229 C THIS SUBROUTINE COMPUTES THE REAL FOURIER COEFFICIENTS, C(N), WHEN
230 C THE 1-D OPTION OF THE PROGRAM IS SELECTED.
231 C
232 C*****
233 C
234 C SUBROUTINE CROS1D
235 C
236 C*****
237 C
238 C COMMON WIDTH,WAVE,OBJ,SSO,SAO,AB2,AB4,AP
239 C COMMON/MN/XIR,DUM1,DUM2,DUM3
240 C COMMON/RD2/SS,SA
```

```

241      COMMON/CROS/C(325),LJ,LJ1,C0
242      COMPLEX CCF1D, A
243 C
244 C*****
245 C
246 C  SEE EQUATION #18, 'METHOD FOR THE CALCULATION OF PARTIALLY COHERENT
247 C  IMAGERY', ERIC KINTNER, J. APPLIED OPTICS, VOL.17, NO.17, PAGE 2747
248 C  FOR THE MATHEMATICAL FORMULATION OF THE FOURIER COEFFICIENTS, C(N).
249 C
250 C*****
251 C
252 C  COMPUTE THE NUMBER OF FOURIER COEFFICIENTS NEEDED IN THE SUMMATION
253 C  WITHOUT EFFECTING THE ACCURACY.
254 C
255      LJ=2.0/XIR+1.0
256      LJ1=LJ+1
257      LN0=(1.0+SS)/XIR+1.0
258 C
259 C  TEMPORARILY SET AB2 AND AB4 TO ZERO BEFORE ENTERING CCF1D FUNCTION
260 C  THROUGH CNORM1.
261 C
262      TEMP1=AB2
263      TEMP2=AB4
264      AB2=0.0
265      AB4=0.0
266 C
267 C  COMPUTE NORMALIZING FACTOR FOR COEFFICIENTS (CNO).  THIS IS DONE
268 C  THROUGH THE FUNCTION CNORM1.
269 C
270      CNO=CNORM1(SA)
271 C
272 C  SET AB2 AND AB4 BACK TO THEIR ORIGINAL VALUES.
273 C
274      AB2=TEMP1
275      AB4=TEMP2
276 C
277 C  CALCULATE THE FOURIER COEFFICIENTS CORRESPONDING TO THE PRIMARY
278 C  AXIS FIRST (C0).
279 C
280      C0=CABS(A(0))*2.0*CCF1D(0.0,0,0)
281      DO 300 N=1, LN0
282          C0=C0+REAL(CABS(A(N))*2*CCF1D(XIR,N,N)
283      1      +CABS(A(-N))*2*CCF1D(XIR,-N,-N))
284      300 CONTINUE
285      C0=C0/CNO
286 C
287 C  COMPUTE FOURIER COEFFICIENTS, C(N), VIA EQUATION #18 (KINTNER'S REF.)
288 C
289      DO 500 J=1, LJ
290          LN=LN0+J
291          CT=REAL(A(J)*CONJG(A(0))*CCF1D(XIR,J,0))
292          DO 400 N=1, LN
293              CT=CT+REAL(A(J+N)*CONJG(A(N))*CCF1D(XIR,J+N,N)
294      1      +A(J-N)*CONJG(A(-N))*CCF1D(XIR,J-N,-N))
295      400 CONTINUE
296          C(J)=CT/CNO
297      500 CONTINUE
298      RETURN
299      END
300 C

```

```

301 C*****
302 C
303 C THIS FUNCTION RETRIEVES THE FOURIER COEFFICIENTS FROM COMMON/A/.
304 C IT IS CALLED FROM THE FUNCTION CCF1D AND CCF2D.
305 C
306 C*****
307 C
308 C     COMPLEX FUNCTION A(N)
309 C
310 C*****
311 C
312 C     COMPLEX AA(100), A0
313 C     COMMON/ACOE/ AA, A0
314 C
315 C*****
316 C
317 C     NA=IABS(N)
318 C     IF(NA .GT. 100) THEN
319 C         A=(0.0,0.0)
320 C         RETURN
321 C     ELSEIF(NA .EQ. 0) THEN
322 C         A=A0
323 C         RETURN
324 C     ELSE
325 C         A=AA(NA)
326 C         RETURN
327 C     ENDIF
328 C     END
329 C
330 C*****
331 C
332 C FUNCTION TO NORMALIZE IMAGERY.
333 C FOR BRIGHT-FIELD IMAGERY, FIELD IS UNITY.
334 C FOR DARK-FIELD IMAGERY, FIELD WITHOUT SOURCE STOP IS UNITY.
335 C
336 C THIS FUNCTION IS CALLED FROM THE SUBROUTINE CROS1D (ONLY NEEDED
337 C WHEN THE 1-D OPTION OF THE PROGRAM IS USED).
338 C
339 C*****
340 C
341 C     FUNCTION CNORM1(SA)
342 C
343 C*****
344 C
345 C     IF(SA .GE. 1.0) THEN
346 C         CNORM1=1.0
347 C         RETURN
348 C     ELSE
349 C         CNORM1=REAL(CCF1D(0.0,0,0))
350 C         RETURN
351 C     ENDIF
352 C     END
353 C
354 C*****
355 C
356 C FUNCTION TO NORMALIZE IMAGERY.
357 C FOR BRIGHT-FIELD IMAGERY, FIELD IS UNITY.
358 C FOR DARK-FIELD IMAGERY, FIELD WITHOUT SOURCE STOP IS UNITY.
359 C
360 C THIS FUNCTION IS CALLED FROM THE SUBROUTINE CROS2D (ONLY NEEDED

```

```

361 C WHEN THE 2-D OPTION OF THE PROGRAM IS USED).
362 C
363 C*****
364 C
365 FUNCTION CNORM2(SA)
366 C
367 C*****
368 C
369 IF(SA .GE. 1.0) THEN
370 CNORM2=1.0
371 RETURN
372 ELSE
373 CNORM2=REAL(CCF2D(0.0,0,0))
374 RETURN
375 ENDIF
376 END
377 C
378 C*****
379 C
380 C FUNCTION TO COMPUTE THE TRANSMISSION CROSS-COEFFICIENT FOR A
381 C ONE DIMENSIONAL PARTIALLY COHERENT IMAGING SYSTEM WITH
382 C DEFOCUSING, SPHERICAL ABERRATION, AND GAUSSIAN APODIZATION OF
383 C BOTH SOURCE AND PUPIL.
384 C
385 C (USED ONLY WITH THE 1-D OPTION OF THE PROGRAM)
386 C
387 C*****
388 C
389 COMPLEX FUNCTION CCF1D(XIR,N1,N2)
390 C
391 C*****
392 C
393 C PARAMETER DEFINITIONS -
394 C XIR - FUNDAMENTAL FREQUENCY.
395 C N1 - HARMONIC FOR FIRST FREQUENCY.
396 C N2 - HARMONIC FOR SECOND FREQUENCY.
397 C SS - SOURCE SIZE.
398 C SA - SOURCE APODIZATION.
399 C AB2 - DEFOCUSING
400 C AB4 - SPHERICAL ABERRATION.
401 C AP - PUPIL APODIZATION.
402 C
403 C ROUTINE ASSUMES THAT (N1 .GE. N2)
404 C
405 C*****
406 C
407 COMPLEX ZERO, SUM, Y
408 COMMON WIDTH,WAVE,OBJ,SSO,SAO,AB2,AB4,AP
409 COMMON/RD2/SS,SA
410 COMMON/PAR/PI,TWOPI
411 DATA ZERO,EPS/(0.0 ,0.0),0.01/
412 DATA N0/10/
413 C
414 C*****
415 C
416 X1=N1*XIR
417 X2=N2*XIR
418 CCF1D=ZERO
419 C
420 C IN THE COHERENT LIMIT, USE ALTERNATE ROUTINE.

```



```

421 C
422     IF(SS .LT. EPS) GOTO 100
423 C
424 C RETURN WITH ZERO IF SOURCE AND TWO PUPILS DO NOT INTERSECT.
425 C
426     IF((X1-X2) .GT. 2.0) RETURN
427     IF((X1-1.0) .GT. SS) RETURN
428     IF(-(1.0+X2) .GT. SS) RETURN
429 C
430 C DETERMINE LIMITS OF INTEGRATION. ASSUME LIMITS DETERMINED BY
431 C PUPILS UNLESS SOURCE IS SMALLER.
432 C
433     RL2=1.0-X1
434     RL1=-(1.0+X2)
435     IF(SS .LT. RL2) RL2=SS
436     IF(-SS .GT. RL1) RL1=-SS
437 C
438 C SET UP INTEGRATION BY SIMPSON'S RULE.
439 C SCALE THE INTEGRATION INTERVAL TO BE APPROXIMATELY EQUAL FOR
440 C ALL CASES.
441 C (N0 IS THE APPROXIMATE NUMBER OF INTERVALS PER UNIT LENGTH.)
442 C
443     NC=1.0+(RL2-RL1)*N0
444     DC=(RL2-RL1)/NC
445     DC2=DC/2.0
446     Q=RL1
447     Q1=Q+X1
448     Q2=Q+X2
449     QQ1=Q1*Q1
450     QQ2=Q2*Q2
451     AR=SA*Q*Q+AP*(QQ1+QQ2)
452     AI=TWOPI*(AB2*(QQ1-QQ2)+AB4*(QQ1*QQ1-QQ2*QQ2))
453     SUM=CEXP(CMPLX(AR,AI))
454     DO 50 N=1, NC
455         QN=RL1+N*DC
456         Q=QN-DC2
457         Q1=Q+X1
458         Q2=Q+X2
459         QQ1=Q1*Q1
460         QQ2=Q2*Q2
461         AR=SA*Q*Q+AP*(QQ1+QQ2)
462         AI=TWOPI*(AB2*(QQ1-QQ2)+AB4*(QQ1*QQ1-QQ2*QQ2))
463         Y=CEXP(CMPLX(AR,AI))
464         SUM=SUM+4.0*Y
465         Q=QN
466         Q1=Q+X1
467         Q2=Q+X2
468         QQ1=Q1*Q1
469         QQ2=Q2*Q2
470         AR=SA*Q*Q+AP*(QQ1+QQ2)
471         AI=TWOPI*(AB2*(QQ1-QQ2)+AB4*(QQ1*QQ1-QQ2*QQ2))
472         Y=CEXP(CMPLX(AR,AI))
473         SUM=SUM+2.0*Y
474     50 CONTINUE
475 C
476 C EXTRA FACTOR OF TWO IN DENOMINATOR CORRECTLY NORMALIZES RESULT.
477 C
478     CCF1D=(SUM-Y)*DC2/6.0
479     RETURN
480 C

```

```

481 C  ALTERNATE ROUTINE FOR COHERENT LIMIT.
482 C
483     100 IF(ABS(X1) .GT. 1.0) RETURN
484         IF(ABS(X2) .GT. 1.0) RETURN
485         QQ1=X1*X1
486         QQ2=X2*X2
487         AR=AP*(QQ1+QQ2)
488         AI=TWOPI*(AB2*(QQ1-QQ2)+AB4*(QQ1*QQ1-QQ2*QQ2))
489         CCF1D=CEXP(CMPLX(AR,AI))
490         RETURN
491     END
492 C *****
493 C
494 C  FUNCTION TO COMPUTE TRANSMISSION CROSS-COEFFICIENT FOR CIRCULAR
495 C  OPTICAL SYSTEM (ANNULAR SOURCE) WITH NO ABERRATIONS OR
496 C  APODIZATION.
497 C
498 C  (USED ONLY WITH THE 2-D OPTION OF THE PROGRAM)
499 C
500 C *****
501 C
502 C  PARAMETER DEFINITIONS -
503 C      XIR - FUNDAMENTAL FREQUENCY.
504 C      N1  - HARMONIC FOR FIRST FREQUENCY.
505 C      N2  - HARMONIC FOR SECOND FREQUENCY.
506 C      SS  - OUTER RADIUS OF SOURCE ANNULUS.
507 C      SA  - INNER RADIUS OF SOURCE ANNULUS.
508 C
509 C      ROUTINE ASSUMES THAT (N1 .GE. N2).
510 C
511 C *****
512 C
513 C      COMPLEX FUNCTION CCF2D(XIR,N1,N2)
514 C
515 C *****
516 C
517 C      COMMON/RD2/SS,SA
518 C      COMMON/PAR/PI,TWOPI
519 C
520 C *****
521 C
522 C      X1=N1*XIR
523 C      X2=N2*XIR
524 C      CCF2D=(0.0,0.0)
525 C
526 C  USE ALTERNATE ROUTINE FOR COHERENT SOURCE.
527 C
528 C      IF(SS .LT. 0.01) THEN
529 C          GOTO 2000
530 C      ENDIF
531 C
532 C  RETURN WITH ZERO IF SOURCE AND PUPILS DO NOT INTERSECT.
533 C
534 C      IF((X1-X2) .GT. 2.0) RETURN
535 C      IF((X1-1.0) .GT. SS) RETURN
536 C      IF(-(1.0+X2) .GT. SS) RETURN
537 C
538 C  MAXIMUM AND MINIMUM EXTENT OF INTERSECTION OF TWO PUPILS.
539 C
540 C      XMAX=X2+1.0

```

```
541      XMIN=X1-1.0
542      IFLAG=0
543 C
544 C SET FLAG IF SOURCE IS ANNULAR - TWO SEPARATE PASSES REQUIRED.
545 C
546      IF(SA .GT. 0.01) IFLAG=1
547      XS=SS
548 100 XS2=XS*XS
549 C
550 C IF SOURCE SIZE IS LESS THAN PUPIL SIZE, USE ALTERNATE ROUTINE.
551 C
552      IF(XS .LT. 1.0) GOTO 400
553      IF(XS .LT. XMAX .OR. -XS .GT. XMIN) GOTO 200
554 C
555 C IF SOURCE ENVELOPES AREA COMMON TO BOTH PUPILS, CALCULATE THIS
556 C AREA.
557 C
558      Y=AREA(1.0,1.0,(X1-X2))
559      GOTO 1100
560 200 IF(XS2 .LE. (X1*X2+1.0)) GOTO 300
561 C
562 C IF REQUIRED AREA IS BOUNDED BY SOURCE AND BOTH PUPILS, CALCULATE
563 C THIS AREA.
564 C
565      Y=AREA(1.0,1.0,(X1-X2))+AREA(XS,1.0,AMIN1(ABS(X1),ABS(X2)))-PI
566      GOTO 1100
567 C
568 C IF REQUIRED AREA IS BOUNDED ONLY BY SOURCE AND ONE PUPIL,
569 C CALCULATE THIS AREA.
570 C
571 300 Y=AREA(XS,1.0,AMAX1(ABS(X1),ABS(X2)))
572      GOTO 1100
573 C
574 C ALTERNATE ROUTINE FOR SOURCE SMALLER THAN PUPIL.
575 C
576 C FIND WHETHER BOUNDARY OF SOURCE EXTENDS BEYOND THE AREA COMMON
577 C TO BOTH PUPILS, IN EITHER DIRECTION.
578 C
579 400 IFL1=0
580      IFL2=0
581      IF (XMIN .LE. -XS) IFL1=1
582      IF(XMAX .GE. XS) IFL2=1
583      IF(IFL1+IFL2-1) 900, 600, 500
584 C
585 C IF SOURCE IS ENVELOPED BY AREA COMMON TO BOTH PUPILS, CALCULATE
586 C AREA OF SOURCE.
587 C
588 500 Y=PI*XS2
589      GOTO 1100
590 C
591 C IF REQUIRED AREA IS BOUNDED BY SOURCE AND EITHER PUPIL (ALONE),
592 C CALCULATE AREA IN COMMON BETWEEN SOURCE AND THIS PUPIL.
593 C (ZERO IS IMPOSSIBLE IN IF-STATEMENT AT 600.)
594 C
595 600 IF(IFL1-IFL2) 700, 1100, 800
596 700 Y=AREA(1.0,XS,ABS(X1))
597      GOTO 1100
598 800 Y=AREA(1.0,XS,ABS(X2))
599      GOTO 1100
600 900 IF((X1*X2+1.0) .LE. XS2) GOTO 1000
```

```
601 C
602 C IF REQUIRED AREA IS BOUNDED BY SOURCE AND BOTH PUPILS, CALCULATE
603 C THIS AREA.
604 C
605 C     Y=AREA(1.0,XS,ABS(X1))+AREA(1.0,XS,ABS(X2))-PI*XS2
606 C     GOTO 1100
607 C
608 C IF SOURCE ENVELOPES AREA COMMON TO BOTH PUPILS, CALCULATE THIS
609 C AREA.
610 C
611 C 1000 Y=AREA(1.0,1.0,(X1-X2))
612 C     GOTO 1100
613 C
614 C CHECK FLAG FOR CIRCULAR SOURCE, OR FIRST OR SECOND PASS WITH
615 C ANNULAR SOURCE.
616 C
617 C 1100 IF(IFLAG-1) 1500, 1600, 1700
618 C
619 C FOR CIRCULAR SOURCE, NORMALIZE AND RETURN.
620 C
621 C 1500 CCF2D=Y/PI
622 C     RETURN
623 C
624 C FOR FIRST PASS WITH ANNULAR SOURCE, SAVE RESULTS FROM OUTER
625 C BOUNDARY OF ANNULUS, SET INNER BOUNDARY AS BOUNDARY OF INNER
626 C SOURCE.
627 C
628 C 1600 IFLAG=2
629 C     CCF2D=Y
630 C     Y=0.0
631 C     XS=SA
632 C     IF((X1-1.0) .GT. SA) GOTO 1100
633 C     IF(-(X2+1.0) .GT. SA) GOTO 1100
634 C     GOTO 100
635 C
636 C FOR SECOND PASS WITH ANNULAR SOURCE, SUBTRACT RESULTS OF INNER
637 C SOURCE FROM SAVED RESULTS OF OUTER SOURCE. NORMALIZE AND RETURN.
638 C
639 C 1700 CCF2D=(CCF2D-Y)/PI
640 C     RETURN
641 C
642 C ALTERNATE ROUTINE FOR COHERENT SOURCE.
643 C
644 C 2000 IF(ABS(X1) .GT. 1.0) RETURN
645 C     IF(ABS(X2) .GT. 1.0) RETURN
646 C     CCF2D=(1.0,0.0)
647 C     RETURN
648 C     END
649 C
650 C*****
651 C
652 C FUNCTION TO COMPUTE THE AREA COMMON TO TWO DISPLACED CIRCLES.
653 C
654 C FOR THE MATHEMATICAL FORMULATION PERTAINING TO THIS FUNCTION,
655 C SEE THE APPENDIX OF 'METHOD FOR THE CALCULATION OF PARTIALLY COHERENT
656 C IMAGERY', ERIC KINTNER, J. APPLIED OPTICS, VOL.17, NO.17, PAGE 2750.
657 C
658 C*****
659 C
660 C PARAMETER DEFINITIONS -
```



```

661 C      R1 - RADIUS OF FIRST CIRCLE.
662 C      R2 - RADIUS OF SECOND CIRCLE.
663 C      D  - SEPARATION BETWEEN FOCII OF TWO CIRCLES.
664 C
665 C  ROUTINE ASSUMES SOME CONTACT EXISTS, AND EXPECTS ALL THREE
666 C  PARAMETERS TO BE POSITIVE.
667 C
668 C*****
669 C
670 C      FUNCTION AREA(R1,R2,D)
671 C      COMMON/PAR/PI,TWOPI
672 C
673 C*****
674 C
675 C  TRAP FOR CONCENTRIC CIRCLES.
676 C
677 C      IF(D .LT. 0.001) GOTO 100
678 C
679 C  FIND ANGLE IN EACH CIRCLE SUBTENDED BY COMMON AREA. NOTE TRAPS
680 C  TO SUPPRESS ERRORS IN ARC-COSINE ROUTINES.
681 C
682 C      D2=D*D
683 C      RADII=R1*R1-R2*R2
684 C      DENOM=2.0*D
685 C      T=(D2+RADII)/(DENOM*R1)
686 C      IF(T .GT. 1.0) T=1.0
687 C      THETA1=ACOS(T)
688 C      T=(D2-RADII)/(DENOM*R2)
689 C      IF(T .GT. 1.0) T=1.0
690 C      THETA2=ACOS(T)
691 C
692 C  COMPUTE HALF-LENGTH OF CHORD COMMON TO THE TWO COMPUTED ANGLES.
693 C
694 C      C=R1*SIN(THETA1)
695 C
696 C  COMPUTE THE AREA OF THE REGION OF OVERLAP.
697 C
698 C      AREA=(R1**2*THETA1+R2**2*THETA2)-C*D
699 C      RETURN
700 C
701 C  IF CIRCLES ARE CONCENTRIC, CALCULATE AREA OF SMALLER CIRCLE.
702 C
703 C  100 AREA=PI*(AMIN1(R1,R2))**2
704 C      RETURN
705 C      END
706 C*****
707 C
708 C  THIS SUBROUTINE CORRECTS THE FOURIER COEFFICIENTS, C(N), FOR THE
709 C  EFFECT OF THE SCANNING SLIT IN THE IMAGE PLANE.
710 C
711 C*****
712 C
713 C      SUBROUTINE CSLIT
714 C
715 C*****
716 C
717 C      COMMON WIDTH,WAVE,OBJ,SSO,SAO,AB2,AB4,AP,TBO,PB,TTO,PT,SLIT
718 C      COMMON/MN/XIR,DUM1,DUM2,DUM3
719 C      COMMON/CROS/C(325),LJ
720 C      COMMON/PAR/PI,TWOPI

```

```
721 C
722 C*****
723 C
724 C  SEE EQUATION #19 IN 'METHOD FOR THE CALCULATION OF PARTIALLY COHERENT
725 C  IMAGERY', ERIC KINTNER, J. APPLIED OPTICS, VOL.17, NO.17, PAGE 2747
726 C  FOR THE MATHEMATICAL FORMULATIONS RELATING TO THIS SUBROUTINE.
727 C
728 C*****
729 C
730     ARG=PI*XIR*(SLIT*OBJ/WAVE)
731     COSN2=2.0*COS(ARG)
732     S=0.0
733     S1=-SIN(ARG)
734     DO 700 J=1, LJ
735         S2=S1
736         S1=S
737         S=COSN2*S1-S2
738         C(J)=C(J)*S/(J*ARG)
739 700 CONTINUE
740     RETURN
741     END
742 C
743 C*****
744 C
745 C  THIS SUBROUTINE COMPUTES THE REAL FOURIER COEFFICIENTS, C(N), WHEN
746 C  THE 2-D OPTION OF THE PROGRAM IS SELECTED.
747 C
748 C*****
749 C
750     SUBROUTINE CROS2D
751 C
752 C*****
753 C
754     COMMON/MN/XIR,DUM1,DUM2,DUM3
755     COMMON/RD2/SS,SA
756     COMMON/CROS/C(325),LJ,LJ1,C0
757     COMPLEX CCF2D, A
758 C
759 C*****
760 C
761 C  SEE EQUATION #18 IN 'METHOD FOR THE CALCULATION OF PARTIALLY COHERENT
762 C  IMAGERY', ERIC KINTNER, J. APPLIED OPTICS, VOL.17, NO.17, PAGE 2747
763 C  FOR THE MATHEMATICAL FORMULATION OF THE FOURIER COEFFICIENTS, C(N).
764 C
765 C*****
766 C
767 C  COMPUTE THE NUMBER OF FOURIER COEFFICIENTS NEEDED IN THE SUMMATION
768 C
769     LJ=2.0/XIR+1.0
770     LJ1=LJ+1
771     LN0=(1.0+SS)/XIR+1.0
772 C
773 C  COMPUTE THE NORMALIZING FACTOR FOR THE COEFFICIENTS (CN0).  THIS
774 C  IS DONE THROUGH THE FUNCTION CNORM2.
775 C
776     CN0=CNORM2(SA)
777 C
778 C  CALCULATE THE FOURIER COEFFICIENTS CORRESPONDING TO THE PRIMARY
779 C  AXIS FIRST (C0):
780 C
```

```

781      C0=CABS(A(0))*2*CCF2D(0.0,0,0)
782      DO 300 N=1, LN0
783          C0=C0+REAL(CABS(A(N))*2*CCF2D(XIR,N,N)
784      1      +CABS(A(-N))*2*CCF2D(XIR,-N,-N))
785      300 CONTINUE
786      C0=C0/CN0
787 C
788 C  COMPUTE FOURIER COEFFICIENTS, C(N), VIA EQUATION #18 (KINTNER'S REF.)
789 C
790      DO 500 J=1, LJ
791          LN=LN0+J
792          CT=REAL(A(J)*CONJG(A(0))*CCF2D(XIR,J,0))
793          DO 400 N=1, LN
794              CT=CT+REAL(A(J+N)*CONJG(A(N))*CCF2D(XIR,J+N,N)
795      1      +A(J-N)*CONJG(A(-N))*CCF2D(XIR,J-N,-N))
796      400 CONTINUE
797          C(J)=CT/CN0
798      500 CONTINUE
799      RETURN
800      END
801 C
802 C*****
803 C
804 C  THIS SUBROUTINE NORMALIZES ALL OF THE INTENSITY VALUES STORED IN
805 C  THE ARRAY YLIST(N).
806 C
807 C*****
808 C
809      SUBROUTINE YNORM(NUM)
810 C
811 C*****
812 C
813      COMMON/IM/YLIST(2000),NX1,YMAXBN,DUM1,YMAXAN
814 C
815 C*****
816 C
817 C  SINCE SCANNING IS ASSUMED TO START FROM THE CENTER OF THE LINE
818 C  OBJECT (CORRESPONDING TO X=0), THE INTENSITY VALUES ARE NORMALIZED
819 C  RELATIVE TO THE FOREGROUND INTENSITY WHEN THE INPUT VALUE FOR THE
820 C  INTENSITY TRANSMITTANCE (TTO) IS 1.0.
821 C  OTHERWISE, THE INTENSITY VALUES ARE NORMALIZED RELATIVE TO THE
822 C  BACKGROUND INTENSITY CORRESPONDING TO AN INPUT OF 1.0 FOR THE
823 C  BACKGROUND INTENSITY (TBO).
824 C
825 C*****
826 C
827 C  YMAXAN.....THE MAXIMUM INTENSITY VALUE AFTER NORMALIZATION
828 C
829      YMAXAN=YMAXBN/YLIST(NUM)
830      CONST=YLIST(NUM)
831      DO 100 I=1,NX1
832          YLIST(I)=YLIST(I)/CONST
833      100 CONTINUE
834      RETURN
835      END
836 C
837 C*****
838 C
839 C  THIS SUBROUTINE READS THE INPUT PARAMETERS THAT CHARACTERIZE THE
840 C  OPTICAL SYSTEM TO BE MODELED.  THE COMPLEX AMPLITUDE TRANSMITTANCE

```



```

841 C (OR REFLECTANCE) IS THEN CALCULATED FROM THE INPUTTED INTENSITY
842 C TRANSMITTANCE AND PHASE OF THE OBJECT.
843 C
844 C*****
845 C
846 C SUBROUTINE RDATA
847 C
848 C*****
849 C
850 C PARAMETER DEFINITIONS -
851 C
852 C WIDTH - LINEWIDTH OF OBJECT IN MICROMETERS
853 C WAVE - WAVELENGTH OF LIGHT IN MICROMETERS
854 C OBJ - OBJECTIVE NUMERICAL APERTURE
855 C SSO - CONDENSER NUMERICAL APERTURE
856 C SAO - NUMERICAL APERTURE OF CENTRAL OBSTRUCTION OF ANNULAR
857 C CONDENSER (SET TO ZERO FOR BRIGHT FIELD IMAGE)
858 C AB2 - AMOUNT OF DEFOCUS IN WAVES
859 C AB4 - AMOUNT OF SPHERICAL ABERRATION IN WAVES
860 C AP - GAUSSIAN APODIZATION PARAMETER
861 C (MUST BE ZERO UNLESS USING 1-D OPTICS)
862 C TBO - INTENSITY TRANSMITTANCE OF BACKGROUND
863 C PB - PHASE IN UNITS OF PI OF BACKGROUND
864 C TTO - INTENSITY TRANSMITTANCE OF LINE OBJECT
865 C PT - PHASE OF LINE OBJECT
866 C SLIT - EFFECTIVE SCANNING SLIT WIDTH IN MICROMETERS
867 C SS - COHERENCE PARAMETER
868 C SA - NORMALIZED RADIUS OF CENTRAL OBSTRUCTION
869 C TB - COMPLEX AMPLITUDE TRANSMITTANCE OF BACKGROUND
870 C TT - COMPLEX AMPLITUDE TRANSMITTANCE OF LINE OBJECT
871 C
872 C*****
873 C
874 C COMMON WIDTH,WAVE,OBJ,SSO,SAO,AB2,AB4,AP,TBO,PB,TTO,PT,SLIT,
875 C * DATAS(13)
876 C COMPLEX TB,TT
877 C COMMON/IO/INA,IOUTA,IOUTB
878 C COMMON/RD1/TB,TT
879 C COMMON/RD2/SS,SA
880 C COMMON/PAR/PI,TWOPI
881 C
882 C*****
883 C
884 C READ THE INPUT PARAMETERS AND STORE THEM IN THE ARRAY 'DATAS(N)'
885 C
886 C READ(INA,*)(DATAS(I),I=1,13)
887 C
888 C ASSIGN VARIABLE NAMES TO EACH ELEMENT OF ARRAY 'DATAS':
889 C
890 C WIDTH=DATAS(1)
891 C WAVE=DATAS(2)
892 C OBJ=DATAS(3)
893 C SSO=DATAS(4)
894 C SAO=DATAS(5)
895 C AB2=DATAS(6)
896 C AB4=DATAS(7)
897 C AP=DATAS(8)
898 C TBO=DATAS(9)
899 C PB=DATAS(10)
900 C TTO=DATAS(11)

```



```

901      PT=DATAS(12)
902      SLIT=DATAS(13)
903      SS=SSO/OBJ
904      SA=SAO/OBJ
905      AMPL=SQRT(TBO)
906      PHASE=PI*PB
907      TB=CMPLX(AMPL*COS(PHASE),AMPL*SIN(PHASE))
908      AMPL=SQRT(TTO)
909      PHASE=PI*PT
910      TT=CMPLX(AMPL*COS(PHASE),AMPL*SIN(PHASE))
911      RETURN
912      END
913 C
914 C *****
915 C
916 C THIS SUBROUTINE PRINTS A TABLE OF DISTANCE VERSUS INTENSITY VALUES
917 C FOR THE PARTIALLY COHERENT IMAGING OF PERIODIC OBJECTS OUT TO
918 C FILE 'PRTDATA'.
919 C
920 C TWO COLUMNS CONSISTING OF X-VALUES AND CORRESPONDING INTENSITY
921 C VALUES ARE OUTPUT TO FILE 'PLOTDAT'. THESE VALUES MAY BE USED AS
922 C A PLOT FILE TO PRODUCE A THEORETICAL OPTICAL PROFILE FOR THE LINE
923 C OBJECT.
924 C
925 C *****
926 C
927      SUBROUTINE PRINT(TYPE,SIZE,ANSWER)
928 C
929 C *****
930 C
931      COMMON WIDTH,WAVE,OBJ,SSO,SAO,AB2,AB4,AP,TBO,PB,TTO,PT,SLIT
932      COMMON/IO/INA,IOUTA,IOUTB
933      COMMON/IM/YLIST(2000),NX1,YMAXBN,XMAX,YMAXAN
934      CHARACTER*5 TYPE
935      CHARACTER*12 SIZE
936      CHARACTER*2 ANSWER
937 C
938 C *****
939 C
940 C PRINT PERTINENT INFORMATION FOLLOWED BY A TABLE OF INTENSITY VALUES
941 C FOR THE DISTANCE TRAVERSED:
942 C
943      WRITE(IOUTA,1) TYPE, SIZE
944      WRITE(IOUTA,2) NX1
945      WRITE(IOUTA,3) YMAXBN
946      WRITE(IOUTA,4) YMAXAN
947      WRITE(IOUTA,5) XMAX
948      IF(ANSWER.EQ.'2D') THEN
949          PRINT*, ' 2-D OPTION SELECTED'
950      ELSE
951          PRINT*, ' 1-D OPTION SELECTED'
952      ENDIF
953      WRITE(IOUTA,*)
954      WRITE(IOUTA,*)
955      WRITE(IOUTA,6)
956      WRITE(IOUTA,7)WIDTH,WAVE,OBJ,SSO,SAO,AB2,AB4,AP,TBO,PB,TTO,PT,SLIT
957      WRITE(IOUTA,8)
958      WRITE(IOUTA,9)
959      WRITE(IOUTA,10)
960      NA=1

```

```
961      NB=10
962      X=0.0
963 100  WRITE(IOUTA,11) X, (YLIST(NP), NP=NA,NB)
964      NA=NA+10
965      NB=NB+10
966      X=X+0.1
967      IF(NB.GT.NX1) NB=NX1
968      IF(NA.GT.NX1) GOTO 200
969      GOTO 100
970 C
971 C  THE FOLLOWING CODE PRINTS TWO COLUMNS OF DISTANCE AND INTENSITY
972 C  VALUES OUT TO FILE 'PLOTDAT'.  SINCE YLIST(N) ONLY CONTAINS INTENSITY
973 C  VALUES STARTING FROM THE CENTER OF THE LINE OBJECT, A ROUTINE HAS BEEN
974 C  DEVELOPED TO REPEAT THE CORRESPONDING INTENSITY VALUES FOR NEGATIVE
975 C  X-VALUES (LYING TO THE LEFT OF THE LINE OBJECT'S CENTER).
976 C  THIS ROUTINE ALSO COMPARES THE SLOPE OF A SET OF (X,Y) POINTS
977 C  AND PRINTS ONLY THOSE POINTS WHICH HAVE INTENSITY VALUE DIFFERENCES
978 C  GREATER THAN 0.001.  IN THIS WAY, THE PLOT FILE GENERATED MAY
979 C  BECOME MORE EFFICIENT BY ELIMINATING UNNECESSARY POINTS.
980 C
981 C  THIS PORTION OF CODE PRINTS OUT CORRESPONDING NEGATIVE X-VALUES
982 C  AND INTENSITY VALUES - STARTS FROM YLIST(NX1) AND GOES TO YLIST(1):
983 C
984 200  N=NX1
985      J=0
986 C
987 C  J IS COUNTER FOR NUMBER OF POINTS APART TO COMPARE WITH (UP TO 15)
988 C  SUBTRACT J BECAUSE WE ARE HEADING TOWARDS CENTER OF PROFILE...YLIST(1)
989 C
990 300  N=N-J
991      J=0
992      DO 400 I=1,15
993          J=J+1
994          DIFF=ABS(YLIST(N)-YLIST(N-I))
995 C
996 C  IF YLSIT(1) HAS BEEN REACHED, SWITCH TO SECOND PART OF ROUTINE (BELOW)
997 C
998      IF((N-I).LE.1) GOTO 600
999      IF(DIFF.GE.0.001) GOTO 500
1000 400  CONTINUE
1001 500  X=(N-J-1)*0.01
1002      WRITE(IOUTB,12) YLIST(N-J), -X
1003      GOTO 300
1004 C
1005 C  THIS PORTION OF CODE PRINTS OUT THE POSITIVE X-VALUES AND
1006 C  INTENSITY VALUES - STARTS FROM YLIST(1) AND GOES TO YLIST(NX1):
1007 C
1008 600  X=0.0
1009      WRITE(IOUTB,12) YLIST(1), X
1010 C
1011 C  START AT LOWEST INDEX NUMBER OF ARRAY AND WORK UP TO HIGHEST.
1012 C
1013      N=1
1014      J=0
1015 C
1016 C  ADD J BECAUSE WE START WITH YLIST(1) AND PROCEED TO YLIST(NX1).
1017 C
1018 700  N=N+J
1019      J=0
1020      DO 800 I=1,15
```

```

1021      J=J+1
1022      DIFF=ABS(YLIST(N)-YLIST(N+I))
1023      IF((N+I).GE.NX1) GOTO 1000
1024      IF(DIFF.GE.0.001) GOTO 900
1025      800 CONTINUE
1026      900 X=(N+J-1)*0.01
1027      WRITE(IOUTB,12) YLIST(N+J), X
1028      GOTO 700
1029      1000 X=(NX1-1)*0.01
1030      WRITE(IOUTB,12) YLIST(NX1), X
1031      WRITE(IOUTB,*)'END OF DATA'
1032      1100 ENDFILE 40
1033      RETURN
1034      1 FORMAT(1X//1X,'THE FOLLOWING DATA CORRESPONDS TO A ',A5/1X,
1035      *      A12,' 2.5 MICROMETERS IN WIDTH: '/')
1036      2 FORMAT(1X,'THE NUMBER OF DATA POINTS = ',I4/)
1037      3 FORMAT(1X,'THE MAXIMUM INTENSITY VALUE BEFORE NORMALIZATION =',
1038      *      F7.4)
1039      4 FORMAT(1X,'THE MAXIMUM INTENSITY VALUE AFTER NORMALIZATION =',
1040      *      F7.4)
1041      5 FORMAT(1X,'THE CORRESPONDING X-VALUE TO THESE MAXIMUM INTENSITIES
1042      *      =',F6.2//)
1043      6 FORMAT(1X,5HWIDTH,6H WAVE,4H OBJ,5H SSO,5H SAO,5H AB2,5H AB4,
1044      *      5H AP,6H TBO,6H PB,6H TTO,6H PT,6H SLIT)
1045      7 FORMAT(1X,8(F5.2),4(F6.2),F5.2//)
1046      8 FORMAT(1X,'LEFT-MOST RELATIVE INTENSITY VALUES CORRESPONDING TO
1047      *      STEPS OF')
1048      9 FORMAT(1X,'X-VALUES 0.01 MICROMETERS FROM LEFT TO RIGHT')
1049      10 FORMAT(1X,'_____')
1050      *      '_____'
1051      11 FORMAT(1X,F6.2,2X,10F6.3)
1052      12 FORMAT(1X,F7.4,3X,F7.2)
1053      END
1054 C
1055 C*****
1056 C
1057 C THIS SUBROUTINE COMPUTES THE IMAGE INTENSITY IN THE OBJECT PLANE
1058 C BY AN INVERSE FOURIER TRANSFORM METHOD.
1059 C
1060 C*****
1061 C
1062 C SUBROUTINE IMAGE
1063 C
1064 C*****
1065 C
1066 C COMMON WIDTH,WAVE,OBJ
1067 C COMMON/MN/DUM1,DUM2,PER,NX
1068 C COMMON/CROS/C(325),LJ,LJ1,C0
1069 C COMMON/IM/YLIST(2000),NX1,YMAXBN,XMAX,DUM3
1070 C COMMON/PAR/PI,TWOPI
1071 C
1072 C*****
1073 C
1074 C THE MATHEMATICAL FORMULATIONS RELATING TO THIS SUBROUTINE CAN
1075 C BE FOUND IN EQUATIONS #14 AND #17 IN 'METHOD FOR THE CALCULATION
1076 C OF PARTIALLY COHERENT IMAGERY', ERIC KINTNER, J. APPLIED OPTICS,
1077 C VOL.17, NO.17, PAGE 2747.
1078 C
1079 C*****
1080 C

```

```

1081 C  PARAMETER DEFINITIONS -
1082 C
1083 C  NX1      - TOTAL NUMBER OF CALCULATED IMAGE POINTS
1084 C  YMAXBN  - MAXIMUM INTENSITY VALUE BEFORE NORMALIZATION
1085 C  XMAX    - X-VALUE CORRESPONDING TO THE MAXIMUM INTENSITY VALUE
1086 C  X      - TRANSVERSE DISTANCE ACROSS THE OBJECT (STARTING AT X=0)
1087 C  Y      - INTENSITY VALUE CORRESPONDING TO EACH X-VALUE OF
1088 C           OBJECT
1089 C  YLIST(N) - ARRAY THAT CONTAINS EACH INTENSITY VALUE CORRESPONDING
1090 C           TO ACCENDING VALUES OF X.
1091 C
1092 C *****
1093 C
1094 C      X0=0.01
1095 C      NX1=NX+1
1096 C      YMBN=0.0
1097 C      DO 900 N=1, NX1
1098 C          X=(N-1)*X0
1099 C
1100 C  NOTE THE USE OF THE IDENTITY:
1101 C      COSNX = 2*COS(X)*COS(N-1)*X - COS(N-2)*X
1102 C
1103 C      COSN=COS(TWOPI*X/PER)
1104 C      COSN2=2.0*COSN
1105 C      CK1=0.0
1106 C      CK=0.0
1107 C      DO 800 J=1, LJ
1108 C          CK2=CK1
1109 C          CK1=CK
1110 C          CK=COSN2*CK1-CK2+2.0*C(LJ1-J)
1111 C 800 CONTINUE
1112 C          CK2=CK1
1113 C          CK1=CK
1114 C          CK=COSN2*CK1-CK2+C0
1115 C          Y=CK-COSN*CK1
1116 C          IF(Y .LE. YMBN) THEN
1117 C              GOTO 850
1118 C          ENDIF
1119 C          XM=X
1120 C          YMBN=Y
1121 C 850 YLIST(N)=Y
1122 C 900 CONTINUE
1123 C      XMAX=XM
1124 C      YMAXBN=YMBN
1125 C      RETURN
1126 C      END
1127 (EOR)

```


TEST CASE FOR PCIMAG2

INPUT DATA

Line
No.

1	'1D'												
2	3.00	.53	.85	.17	.00	.00	.00	.00	1.00	0.00	1.00	1.00	0.20
	▲ linewidth	▲ wavelength	▲ N.A. obj	▲ N.A. cond	} these parameters used for dark field		▲ defocus	▲ spherical aberration	▲ background R	▲ background Ø	▲ R for line	▲ Ø for line	▲ slit width at object plane

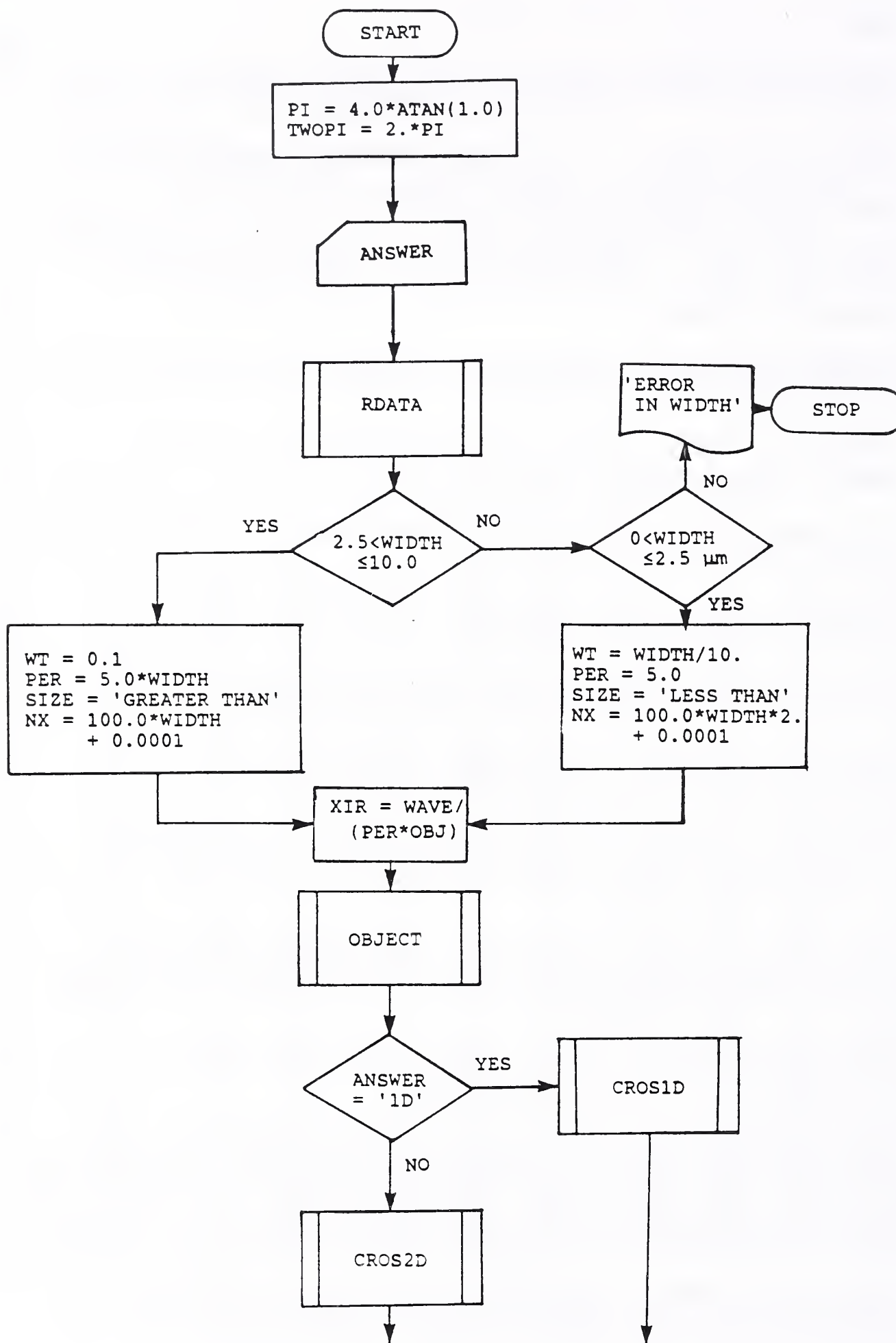
Notes:

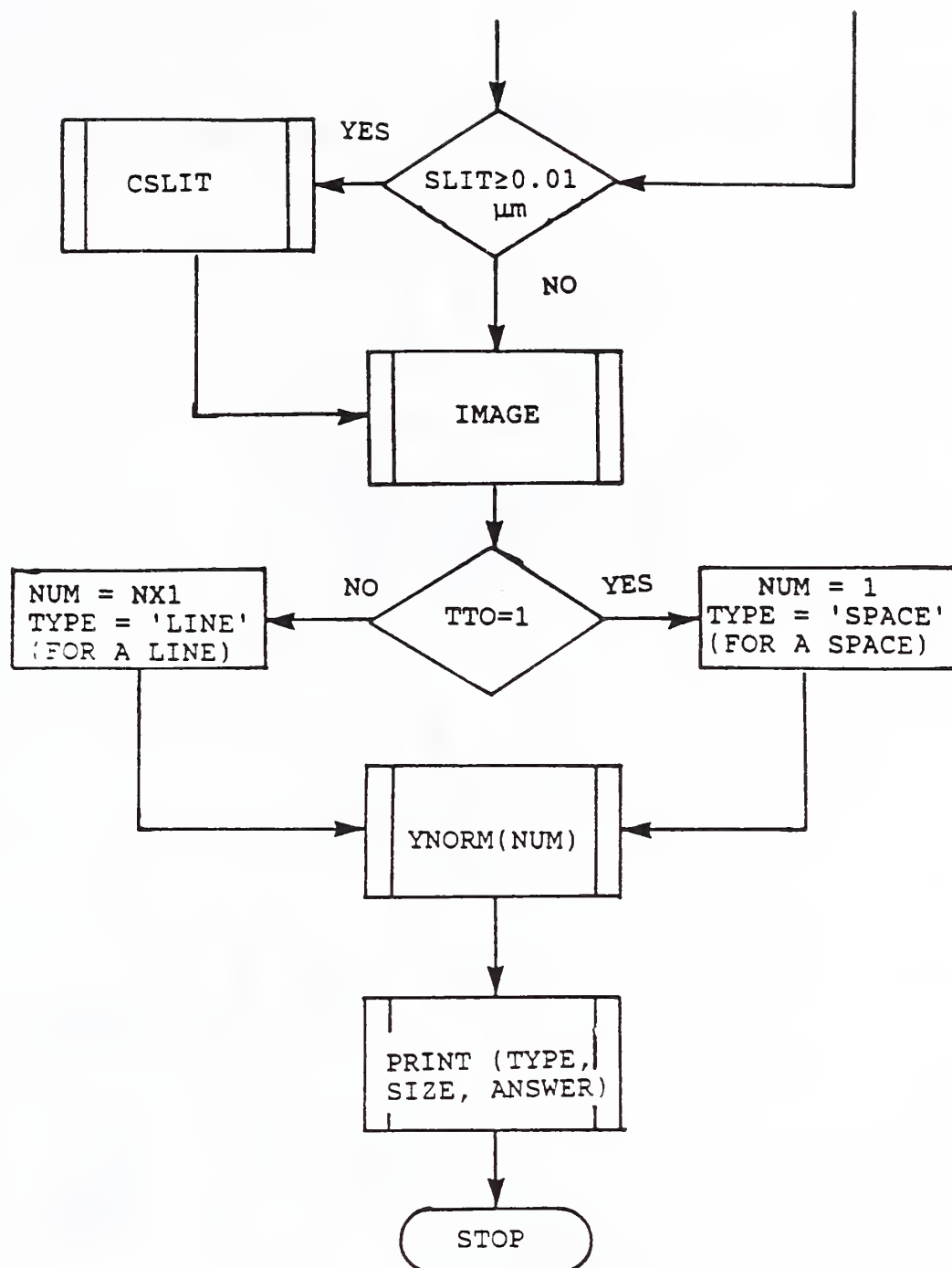
- 1) phase angles are given in units of π
- 2) both defocus and spherical aberrations are given in "number of waves"
- 3) all distances are given in μm

List of Program Elements

1. MAIN
2. Subroutine OBJECT - Calculates Fourier series coefficients for input line object.
3. Subroutine CROS1D - Calculates Fourier coefficients of the image for 1-D optics using transmission cross-coefficients.
4. Function A(N) - Retrieves Fourier coefficients for the line object from calculated array assuming symmetric object.
5. Function CNORM1 - Normalizes transmission cross-coefficients for 1-D optics.
6. Function CNORM2 - Normalizes transmission cross-coefficients for 2-D optics.
7. Function CCF1D - Calculates transmission cross-coefficients for 1-D optics.
8. Function CCF2D - Calculates transmission cross-coefficients for 2-D optics.
9. Function AREA - Calculates the overlapping area of circular lens apertures; used by CCF2D.
10. Subroutine CSLIT - Multiplies image Fourier coefficients by scanning slit function.
11. Subroutine CROS2D - Calculates Fourier coefficients of the image for 2-D optics using transmission cross-coefficients.
12. Subroutine YNORM - Normalizes the image to 1.0 at either the center or the edge of the image, whichever has the higher intensity.
13. Subroutine RDATA - Reads input data and sets up parameters used in calculations.
14. Subroutine PRINT - Creates two print files, one for printing of a table of image data (optical intensity vs. distance) and the second for a plot file. The plot file reduces the number of data points by eliminating values for which there is less than a 0.1% change in intensity.
15. Subroutine IMAGE - Calculates the image intensity vs. distance from the image Fourier coefficients.

1. FLOW DIAGRAM FOR 'MAIN' PROGRAM





NOTES:

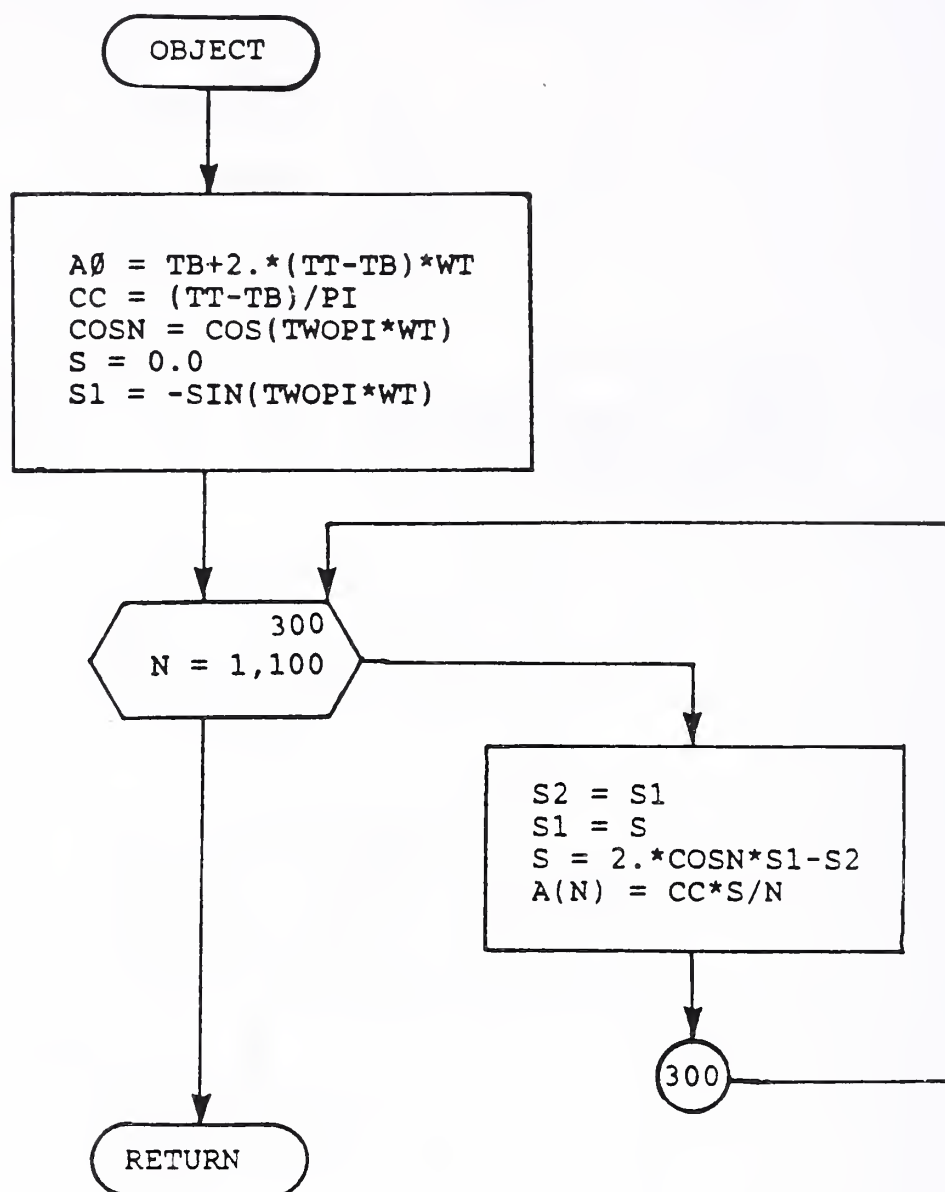
PER = PERIOD

WT = NORMALIZED WIDTH

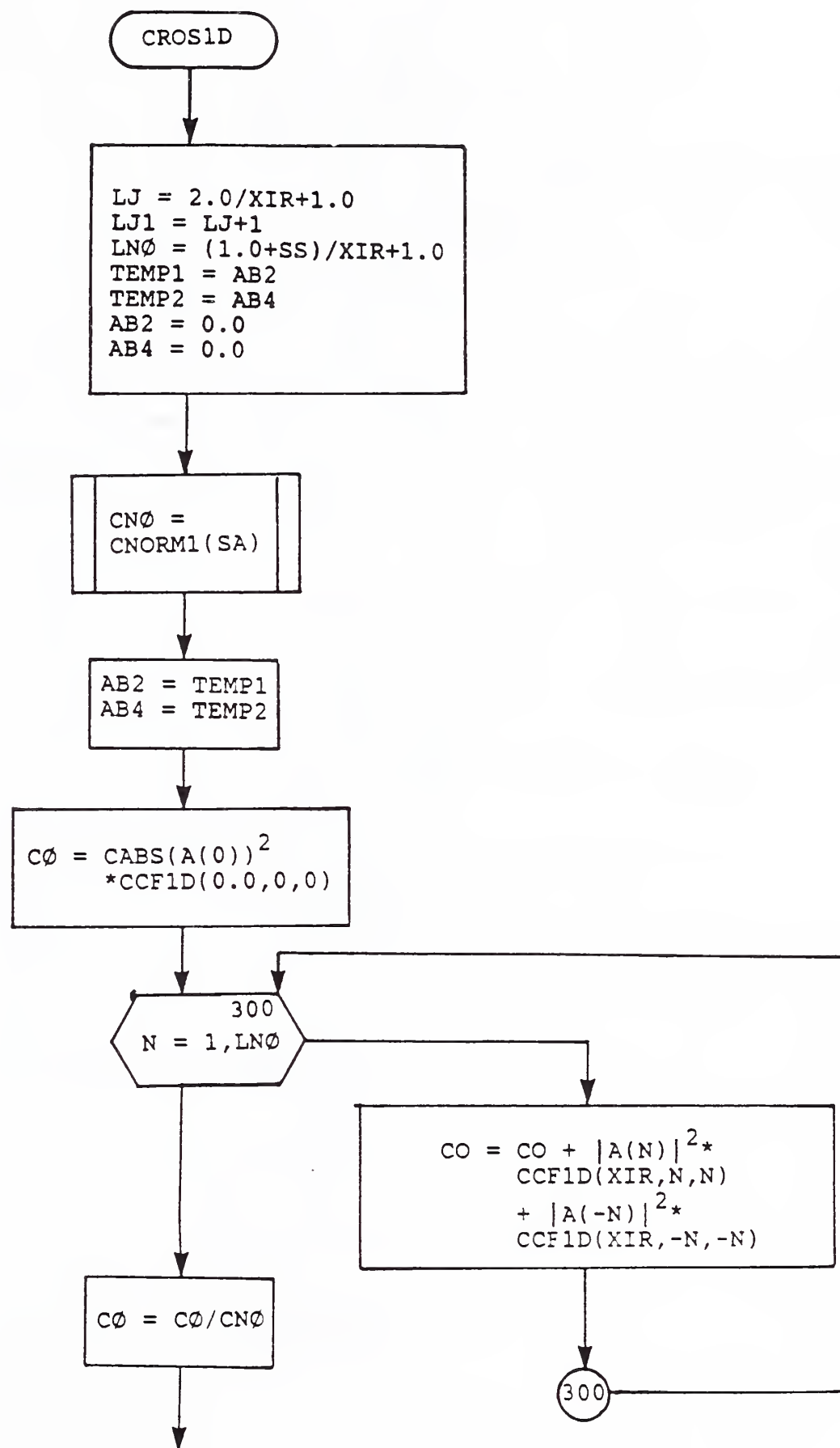
XIR = NORMALIZED FREQUENCY

NX = INCREMENT OF DISTANCE IN IMAGE

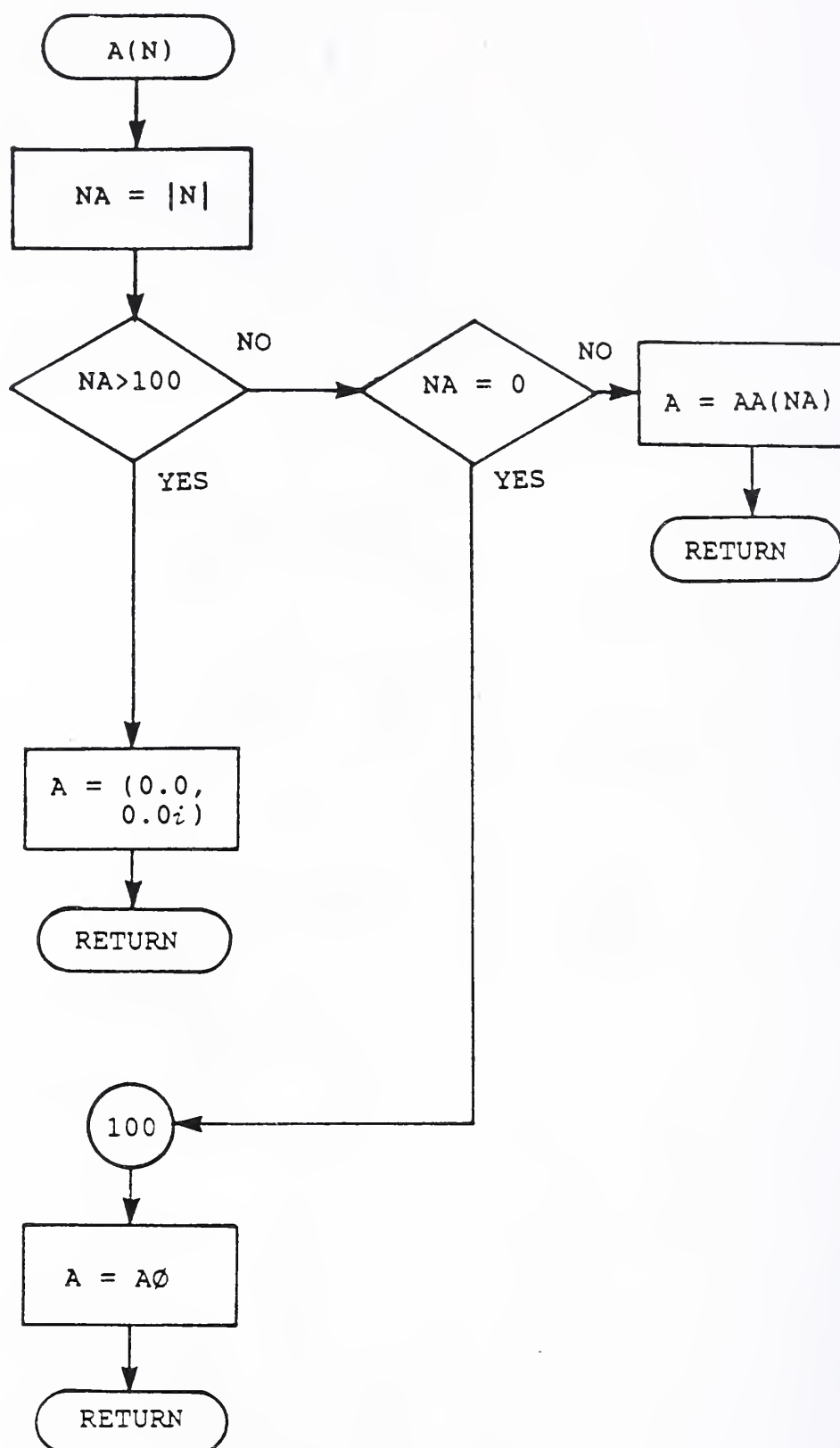
2. FLOW DIAGRAM OF SUBROUTINE 'OBJECT'

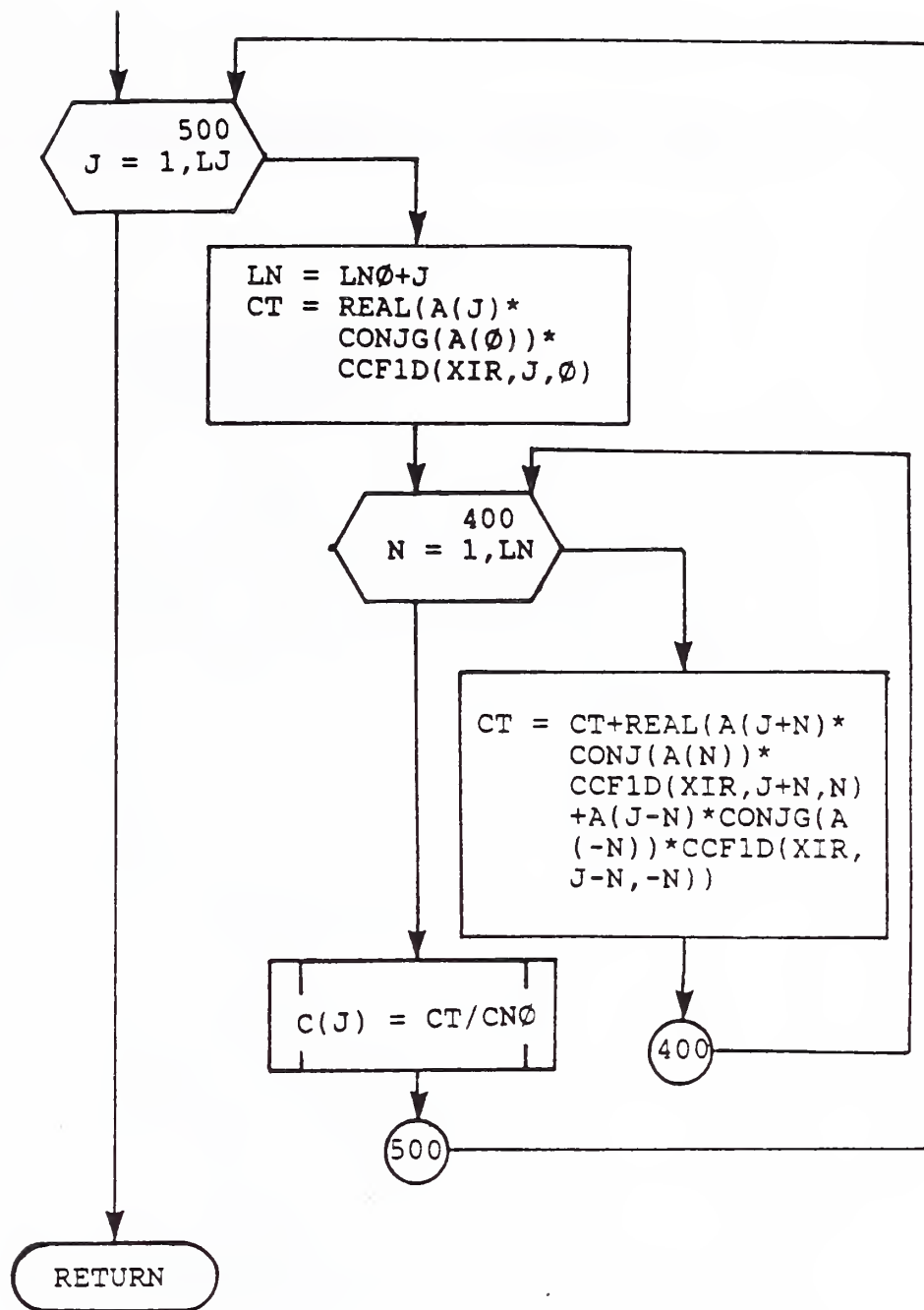


3. FLOW DIAGRAM OF SUBROUTINE 'CROS1D'

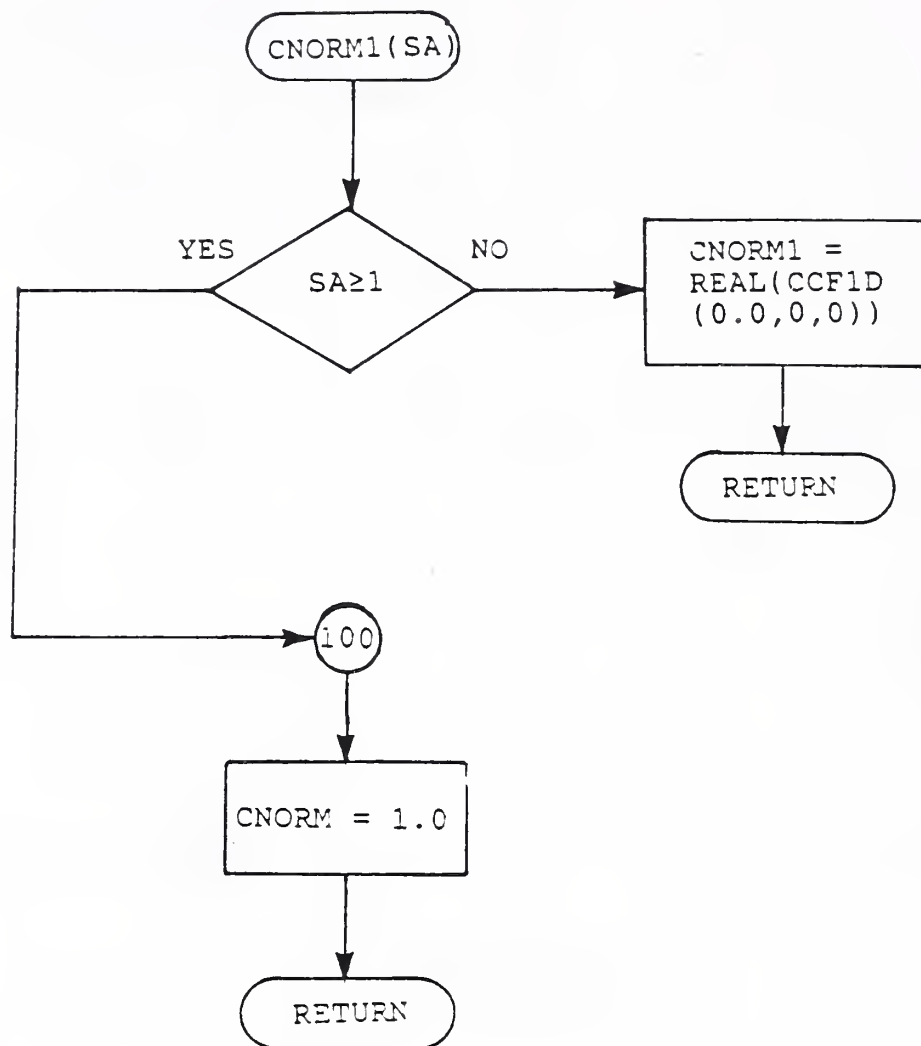


4. FLOW DIAGRAM OF THE FUNCTION 'A(N)'

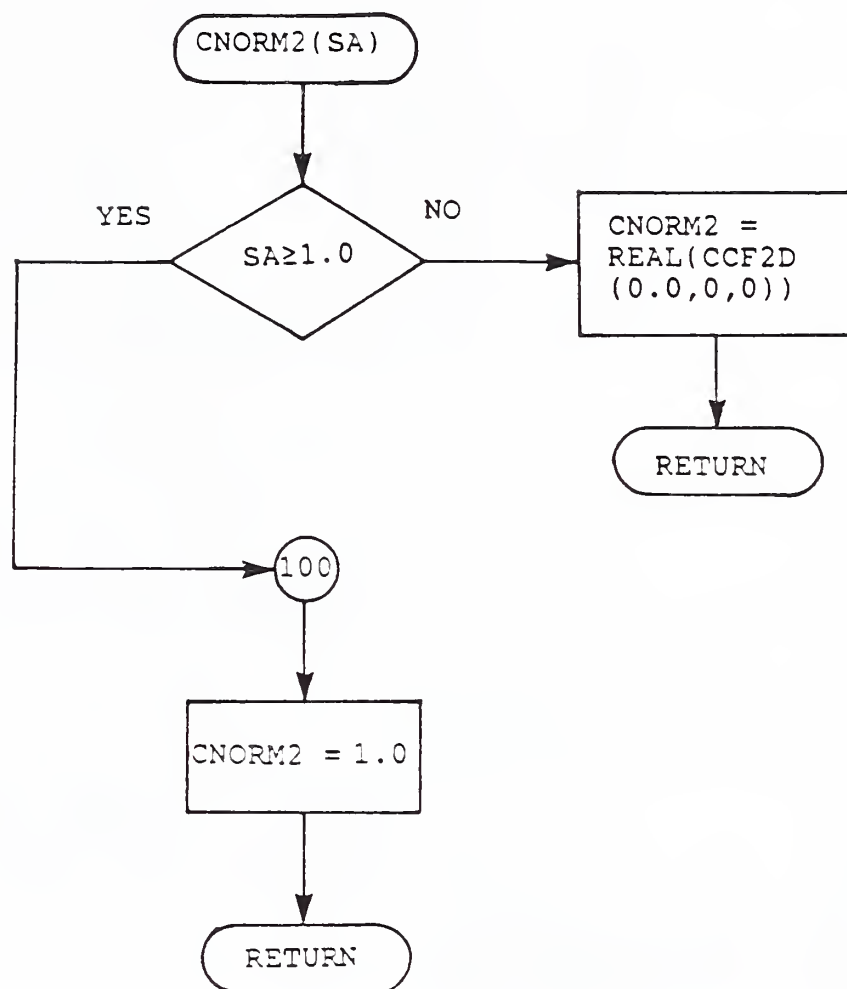




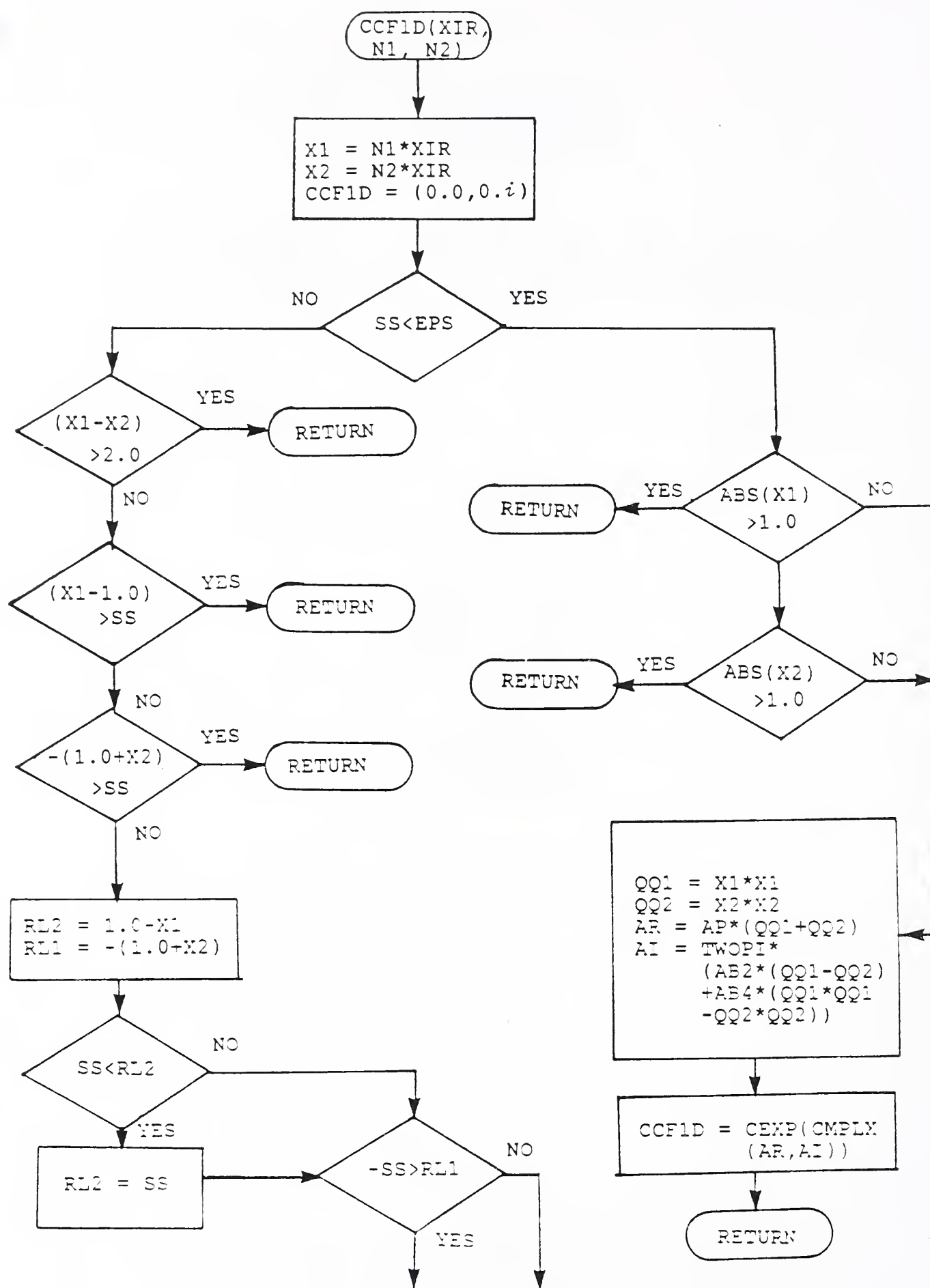
5. FLOW DIAGRAM OF THE FUNCTION 'CNORM1'

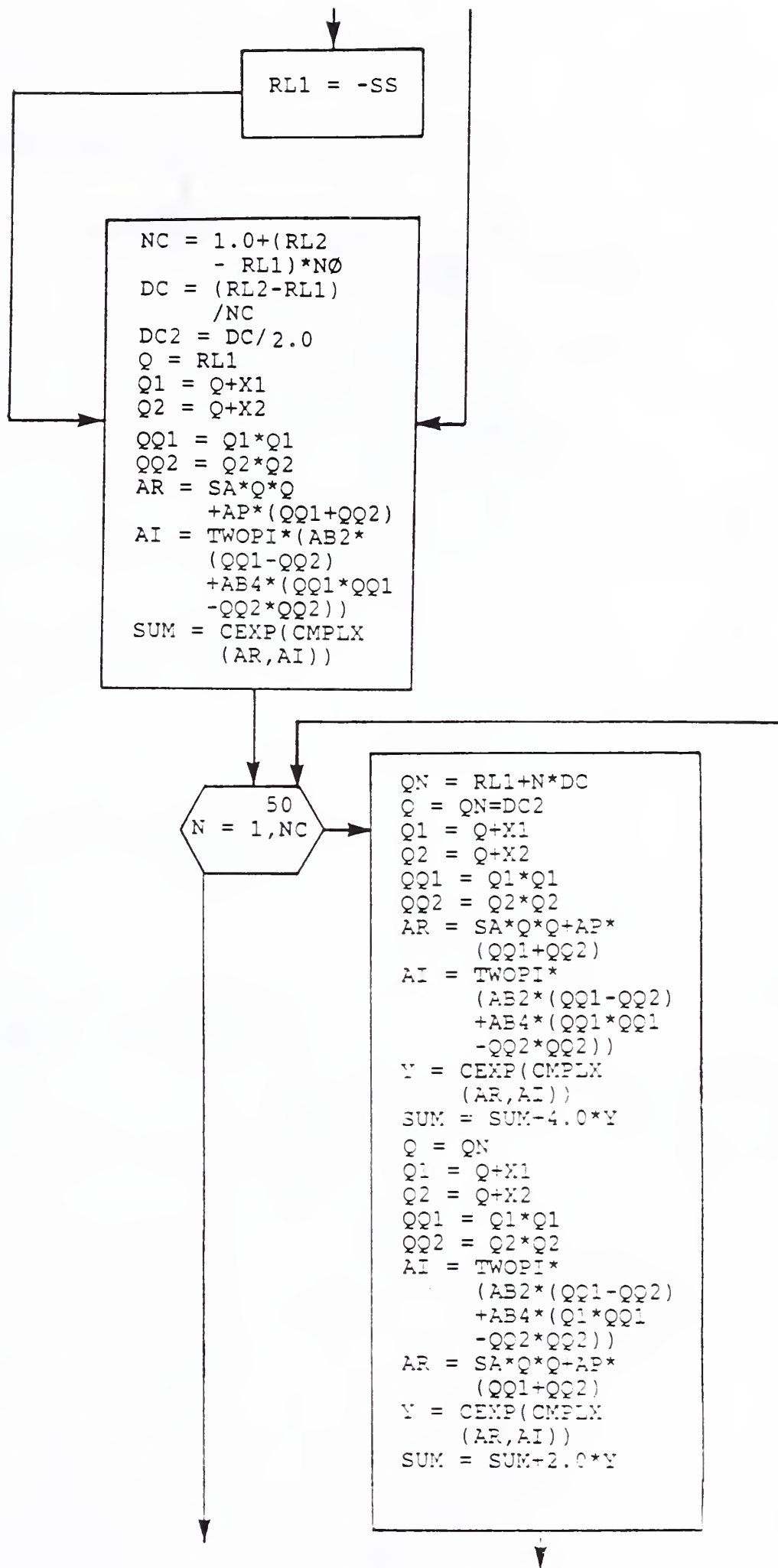


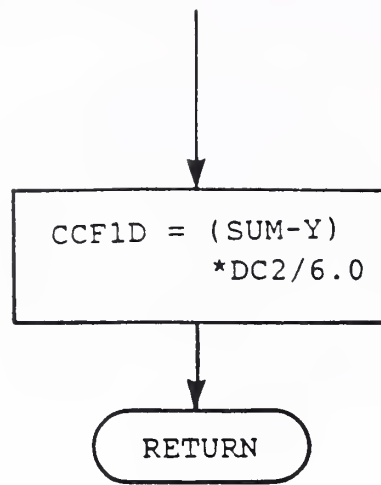
6. FLOW DIAGRAM OF FUNCTION 'CNORM2'



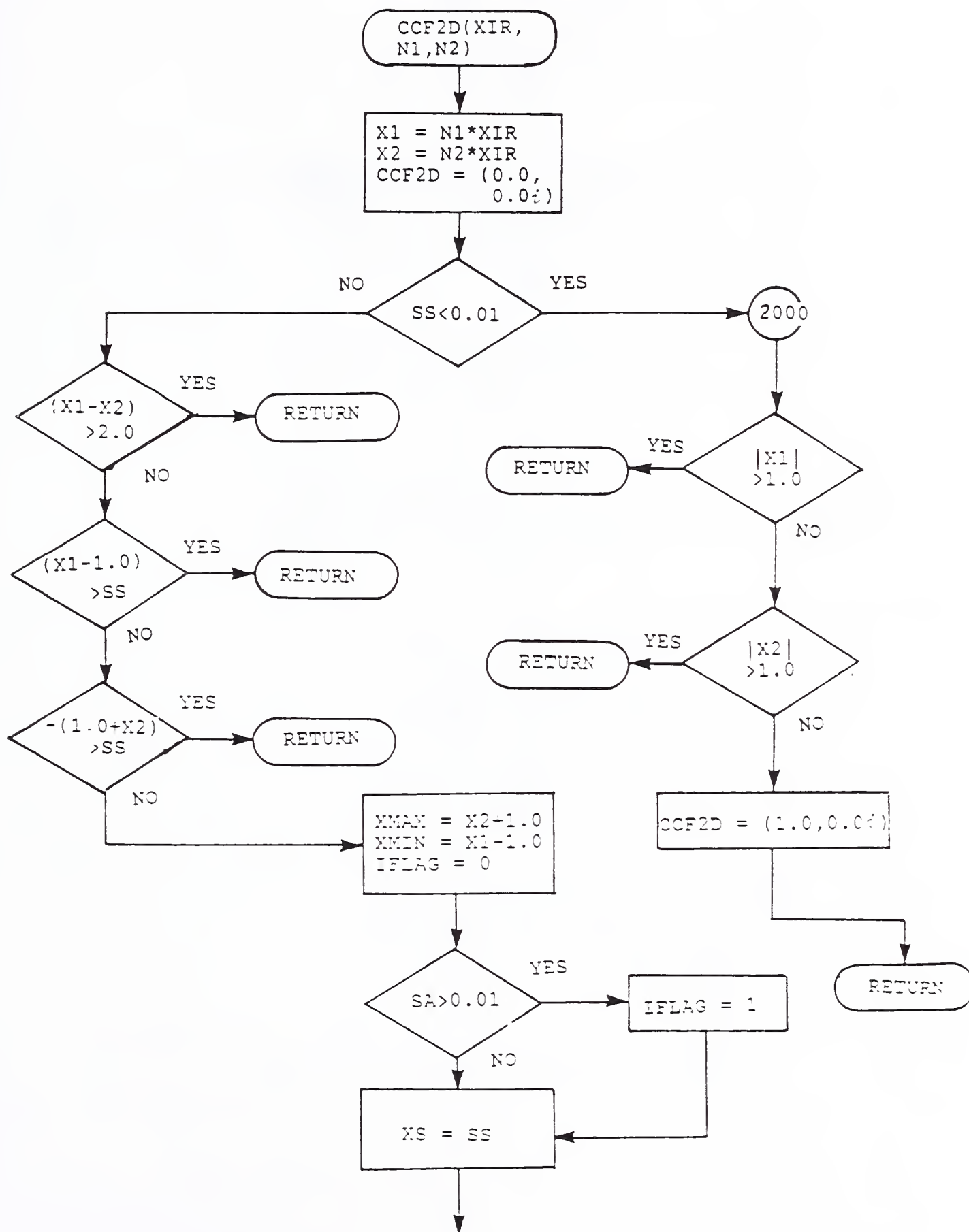
7. FLOW DIAGRAM OF FUNCTION CCF1D (XIR,N1,N2)

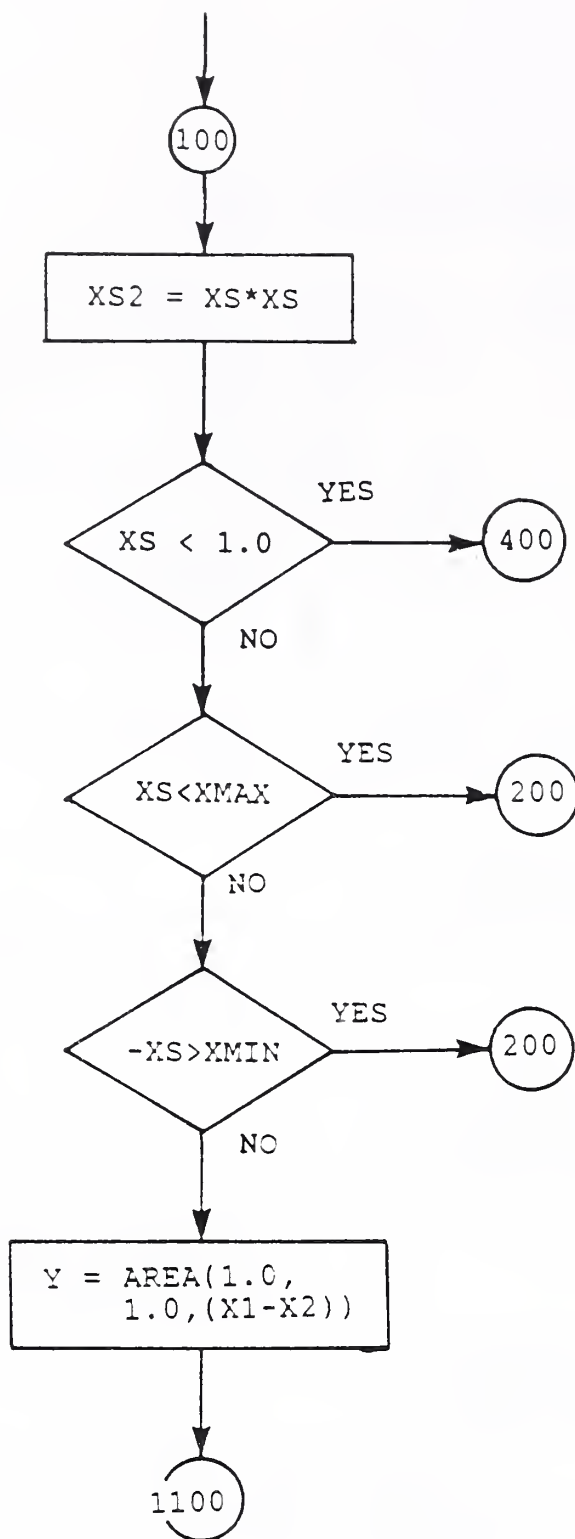


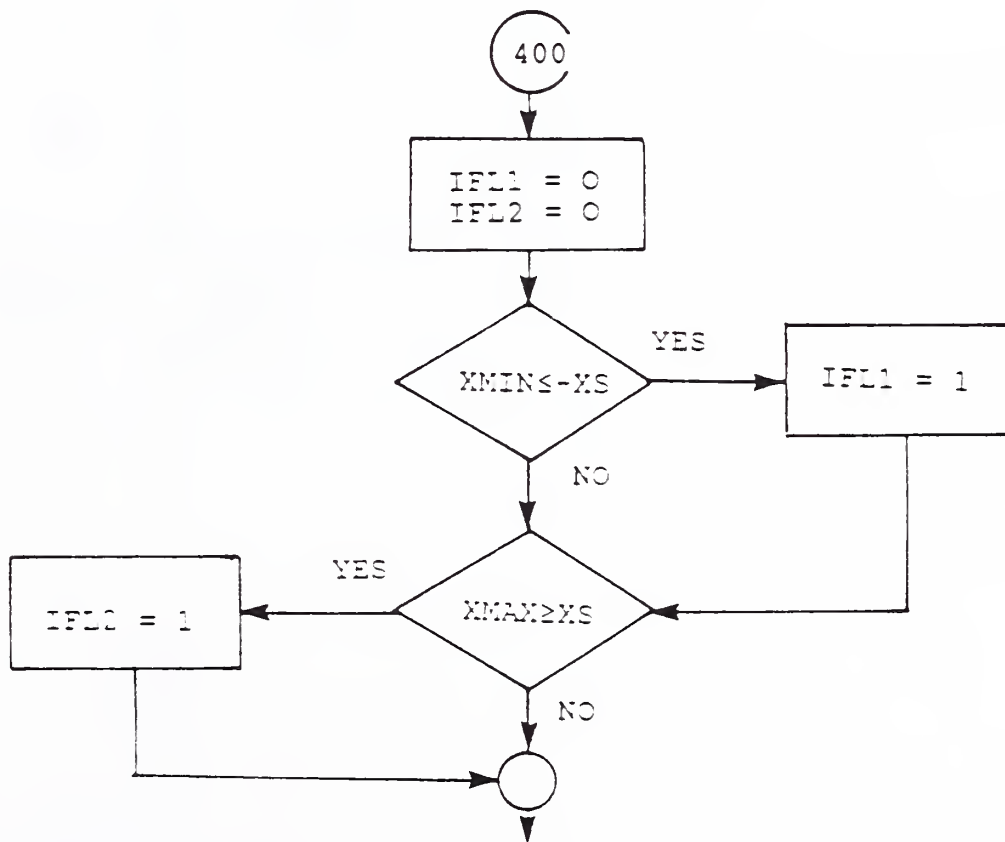
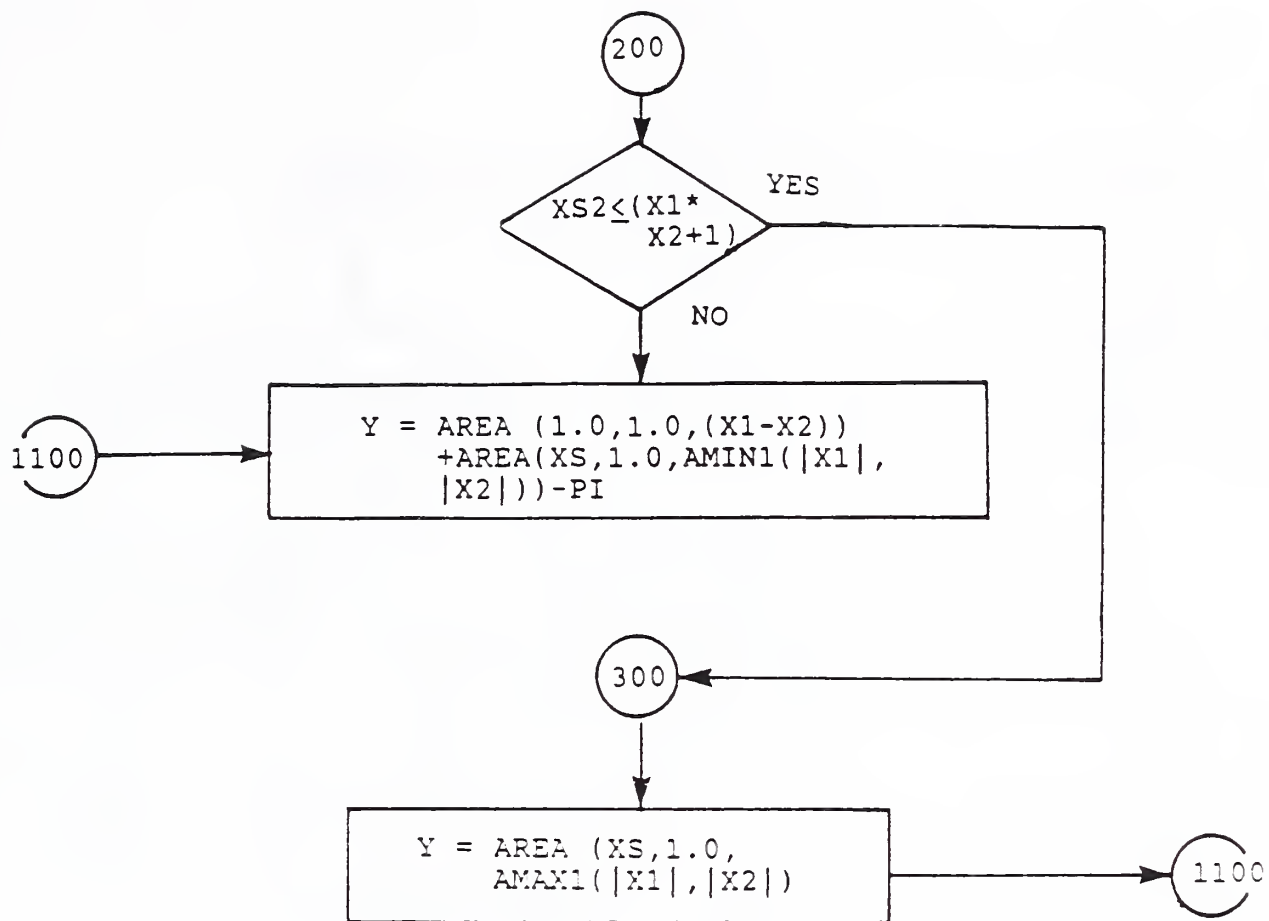


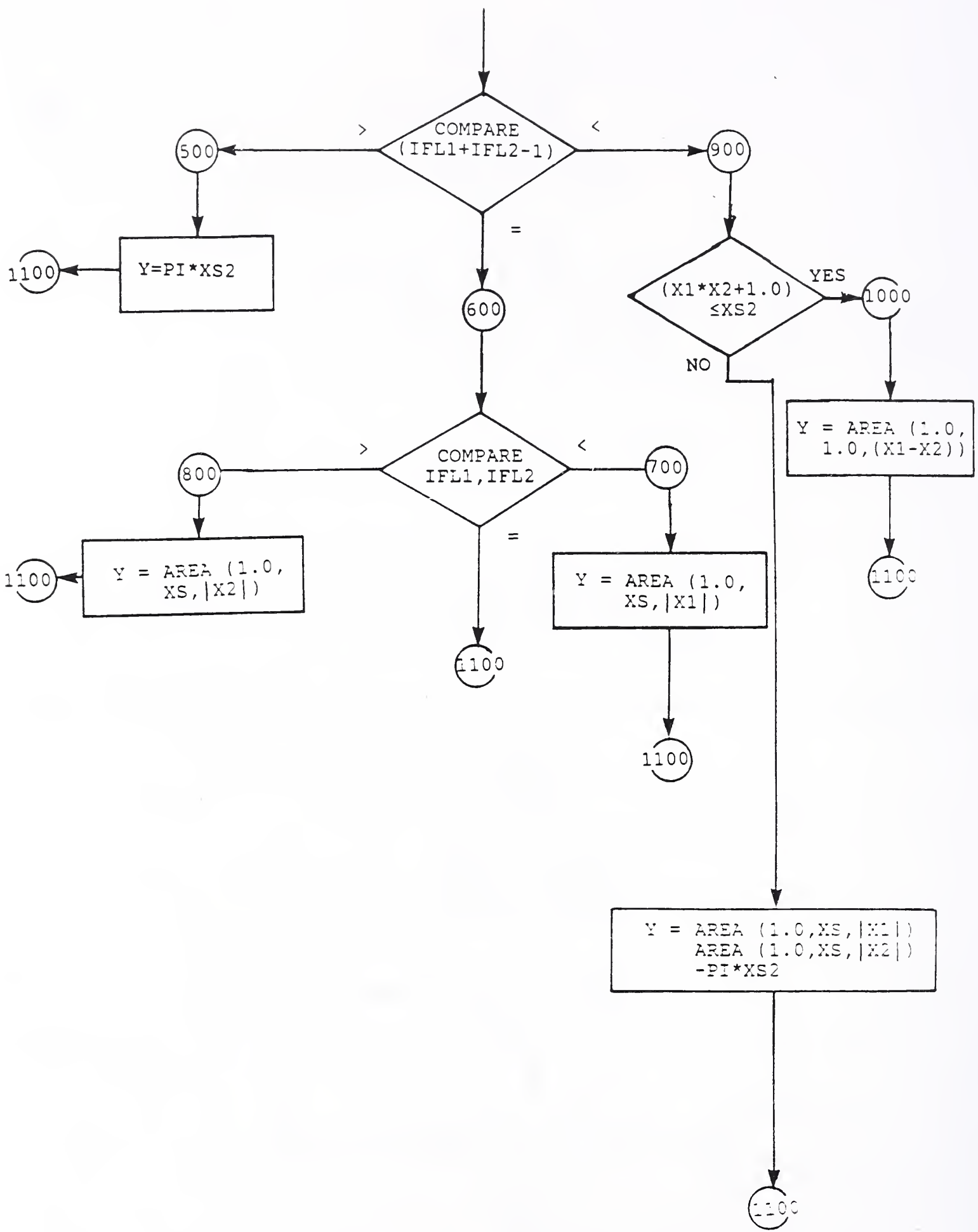


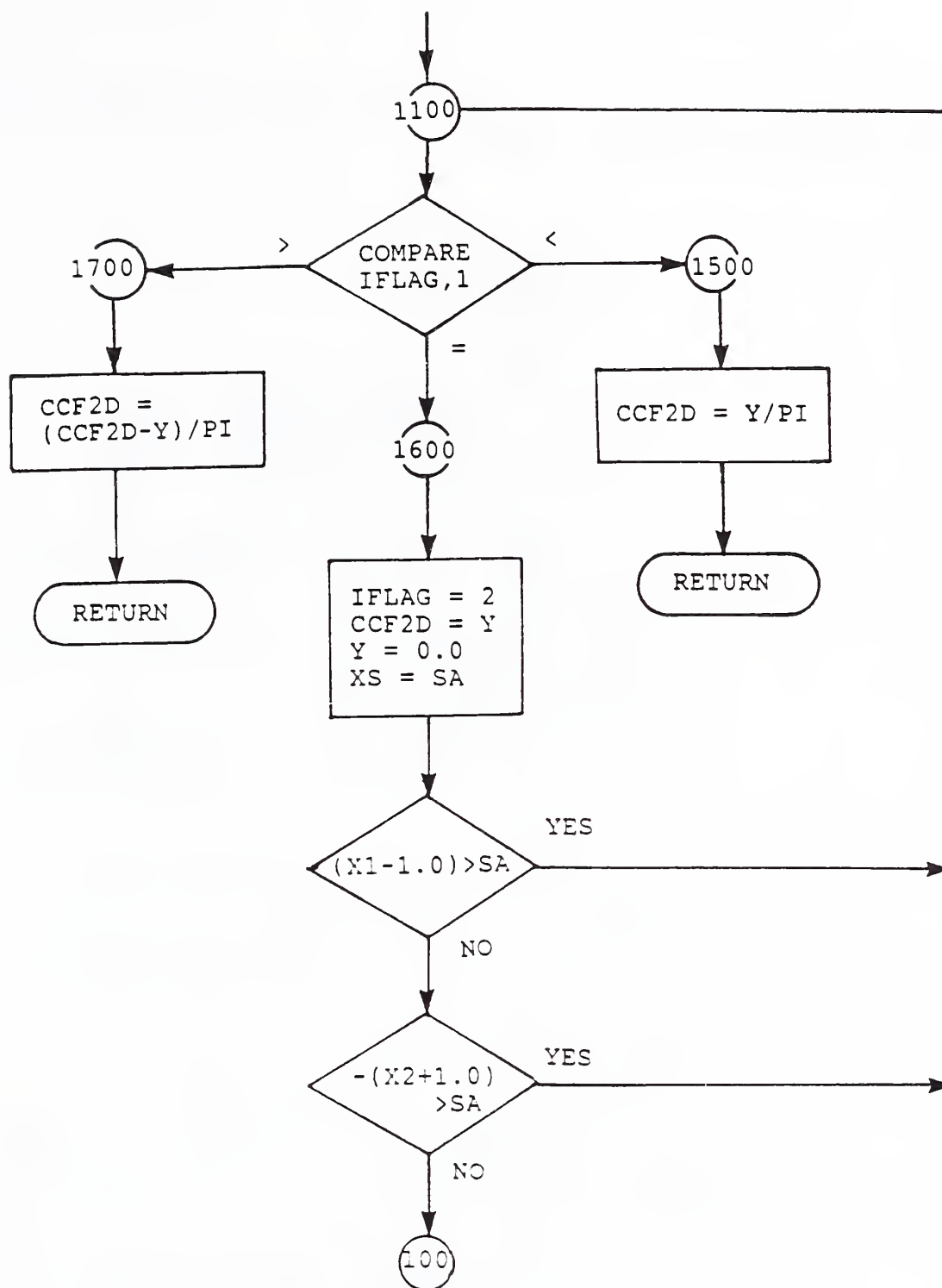
8. FLOW DIAGRAM OF THE FUNCTION 'CCF2D'



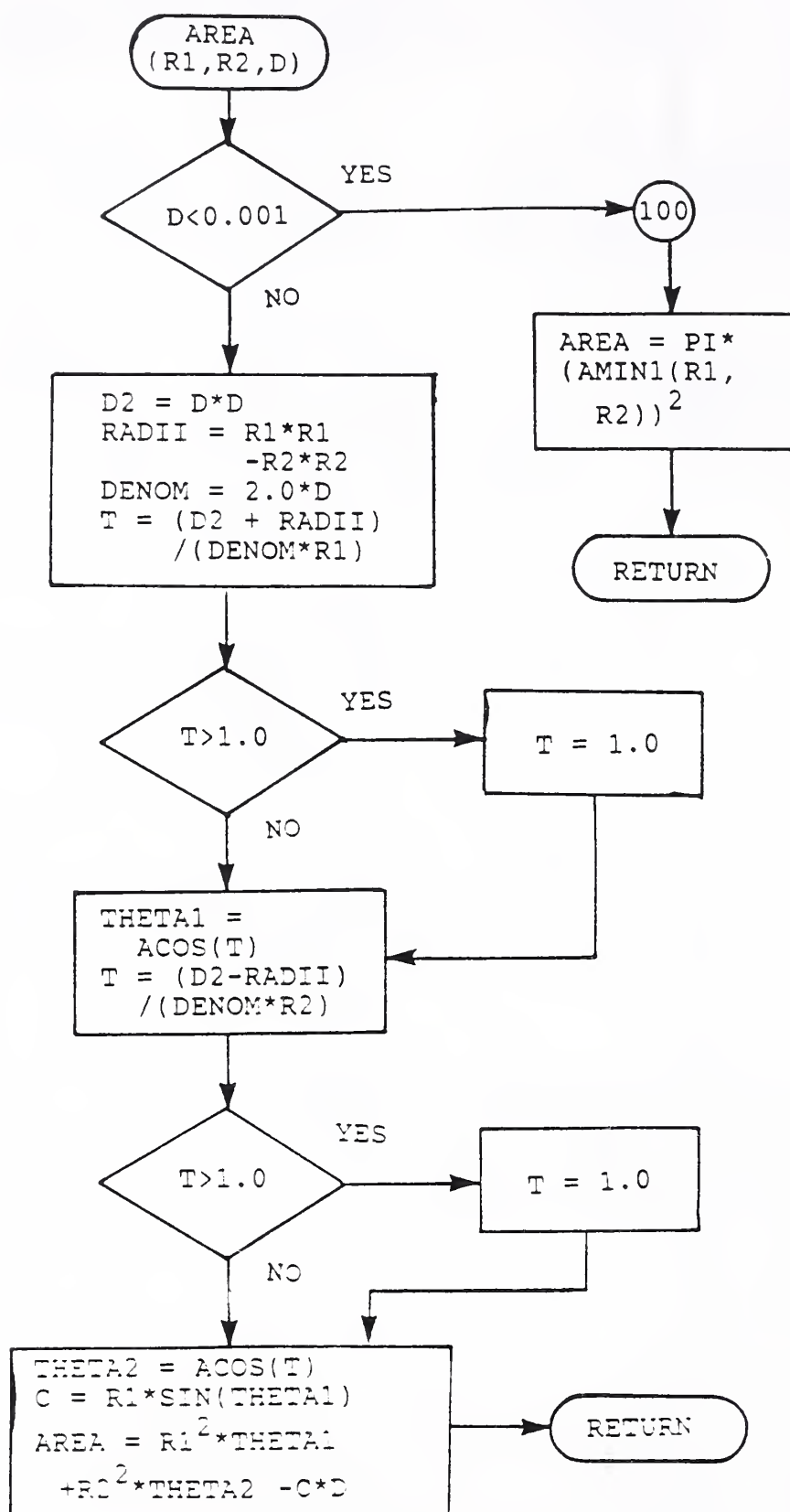




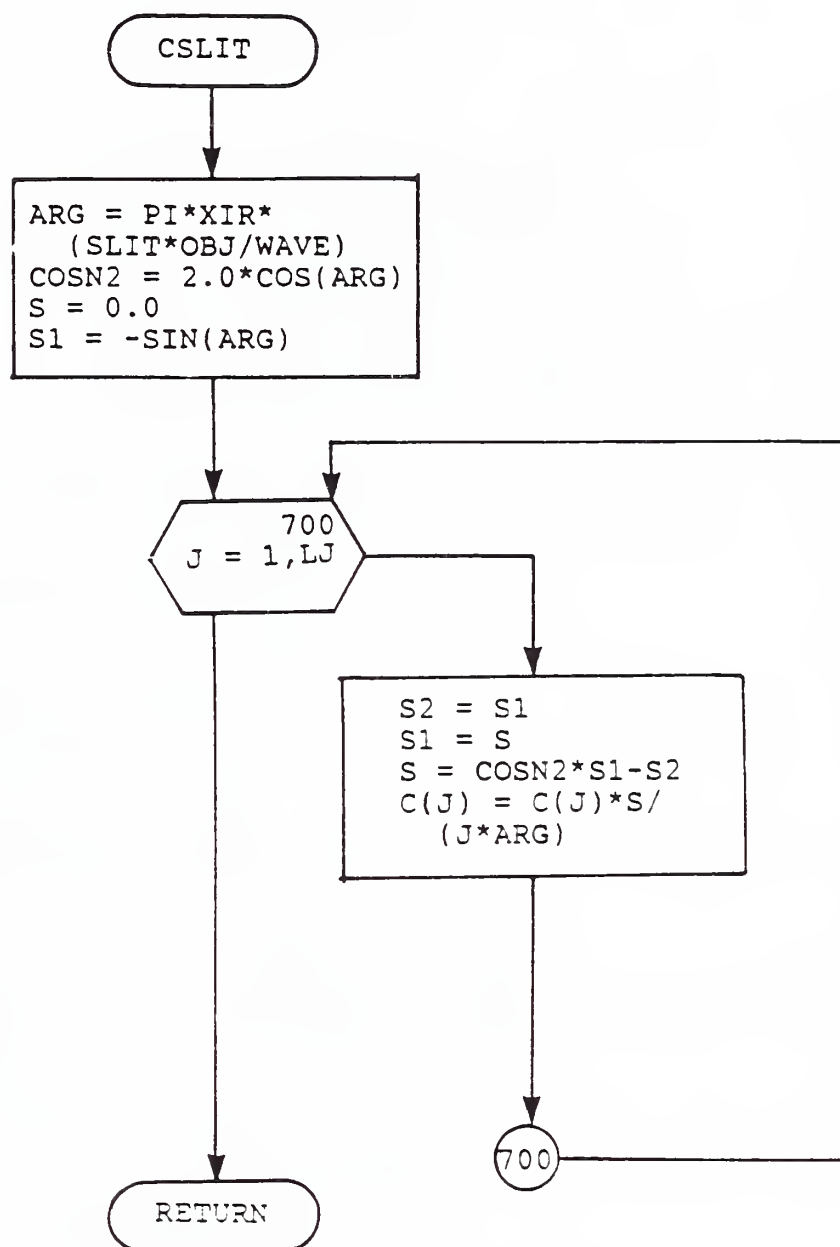




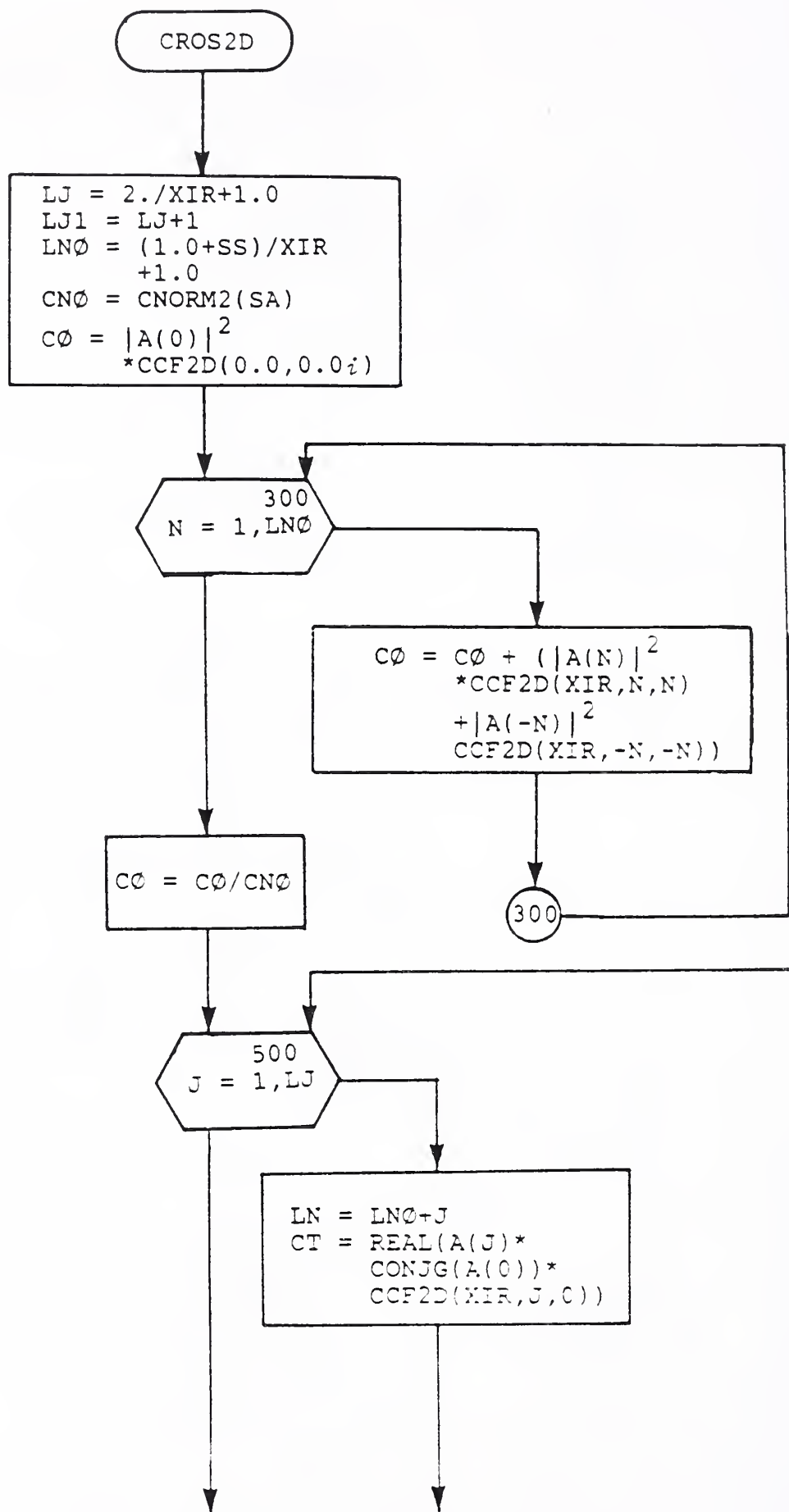
9. FLOW DIAGRAM FOR FUNCTION 'AREA'

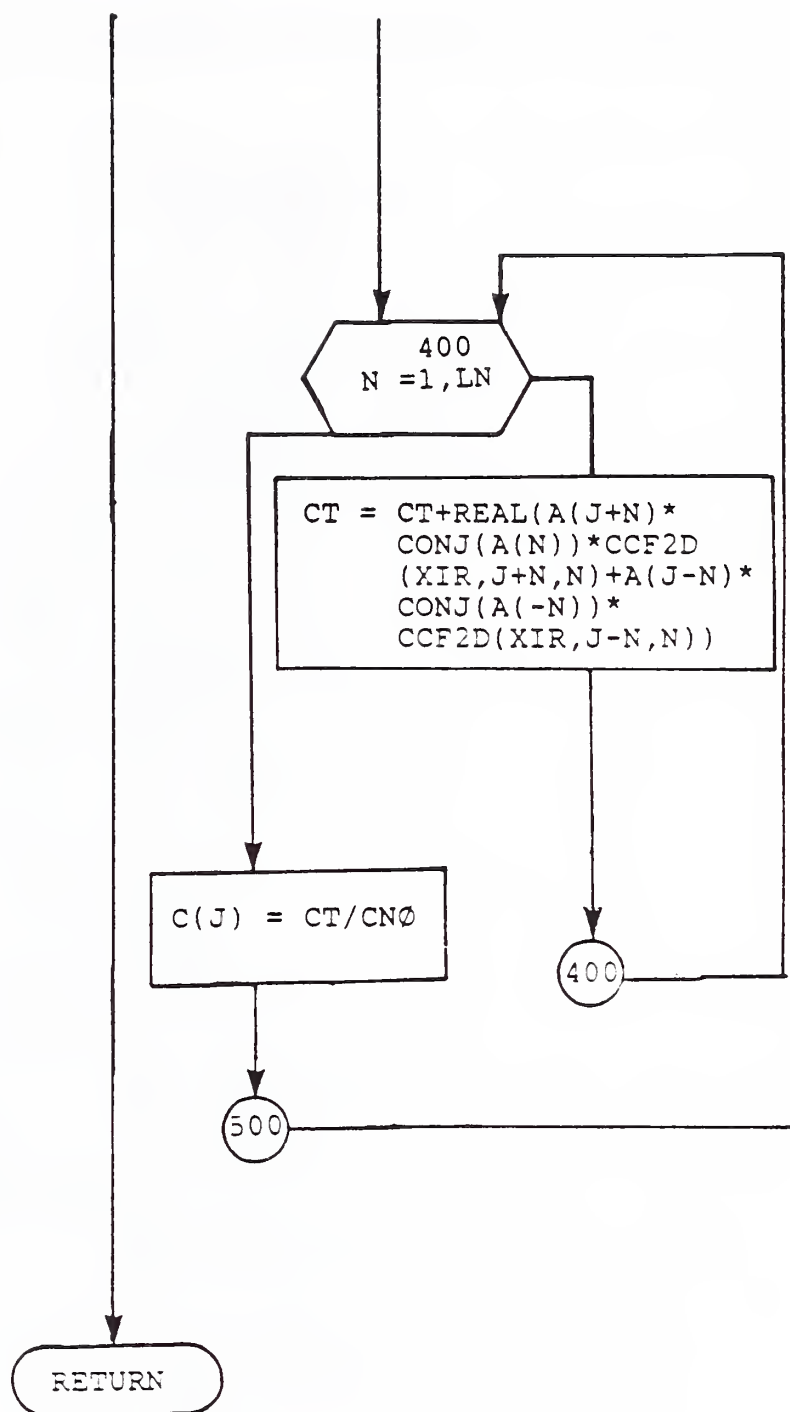


10. FLOW DIAGRAM FOR SUBROUTINE 'CSLIT'

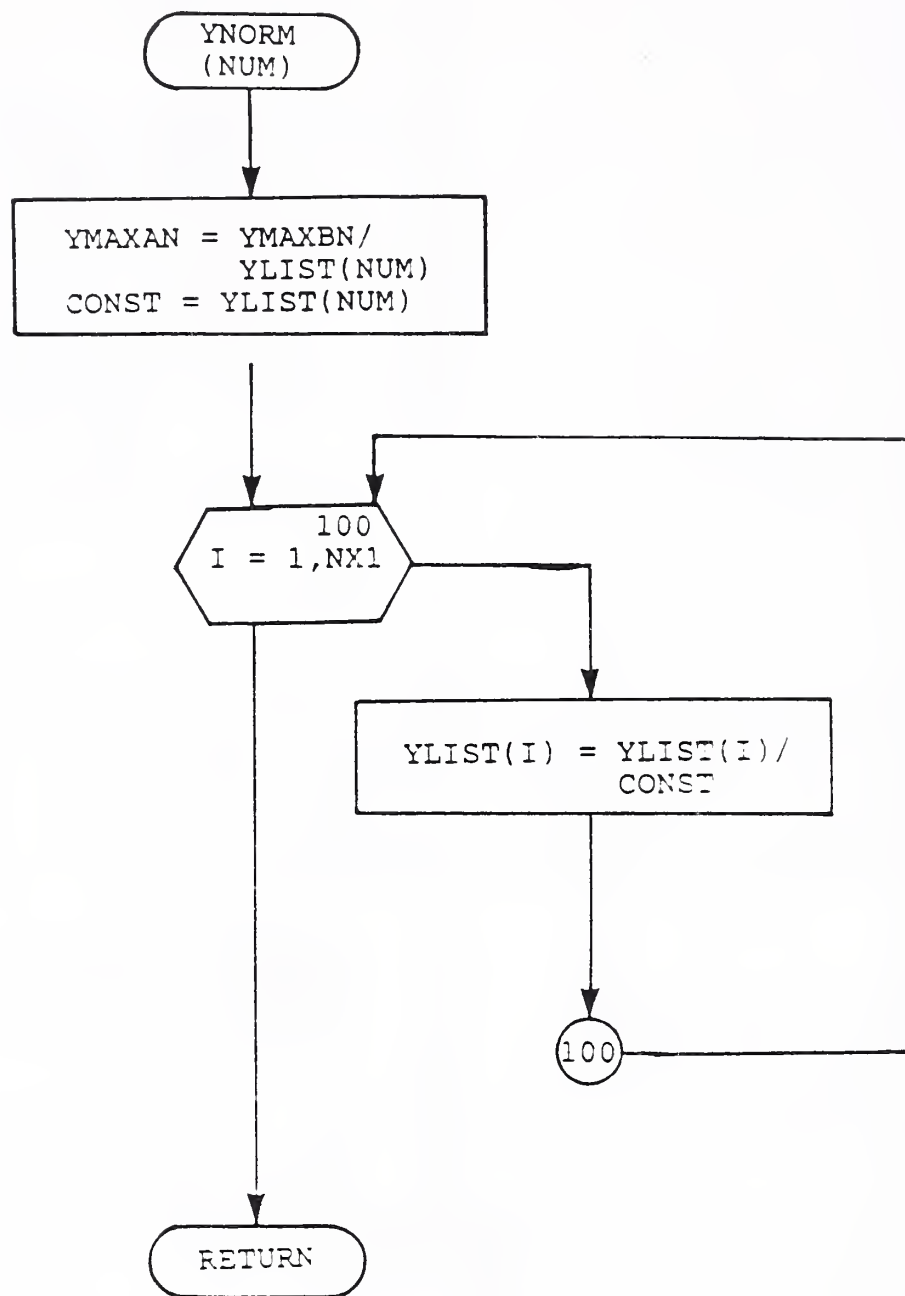


11. FLOW DIAGRAM FOR SUBROUTINE 'CROS2D'

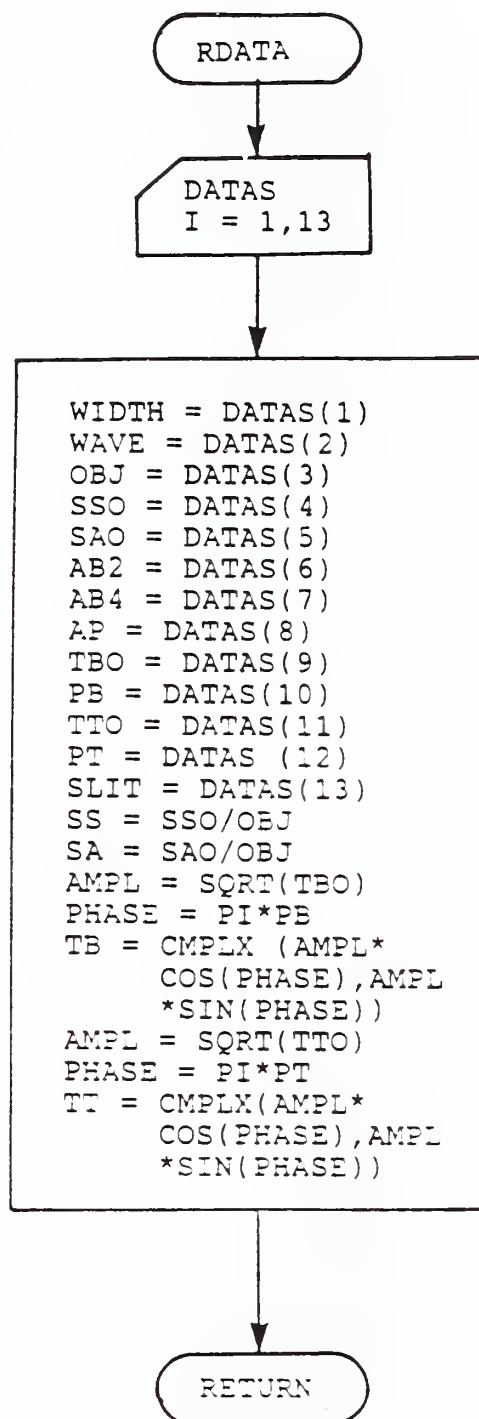




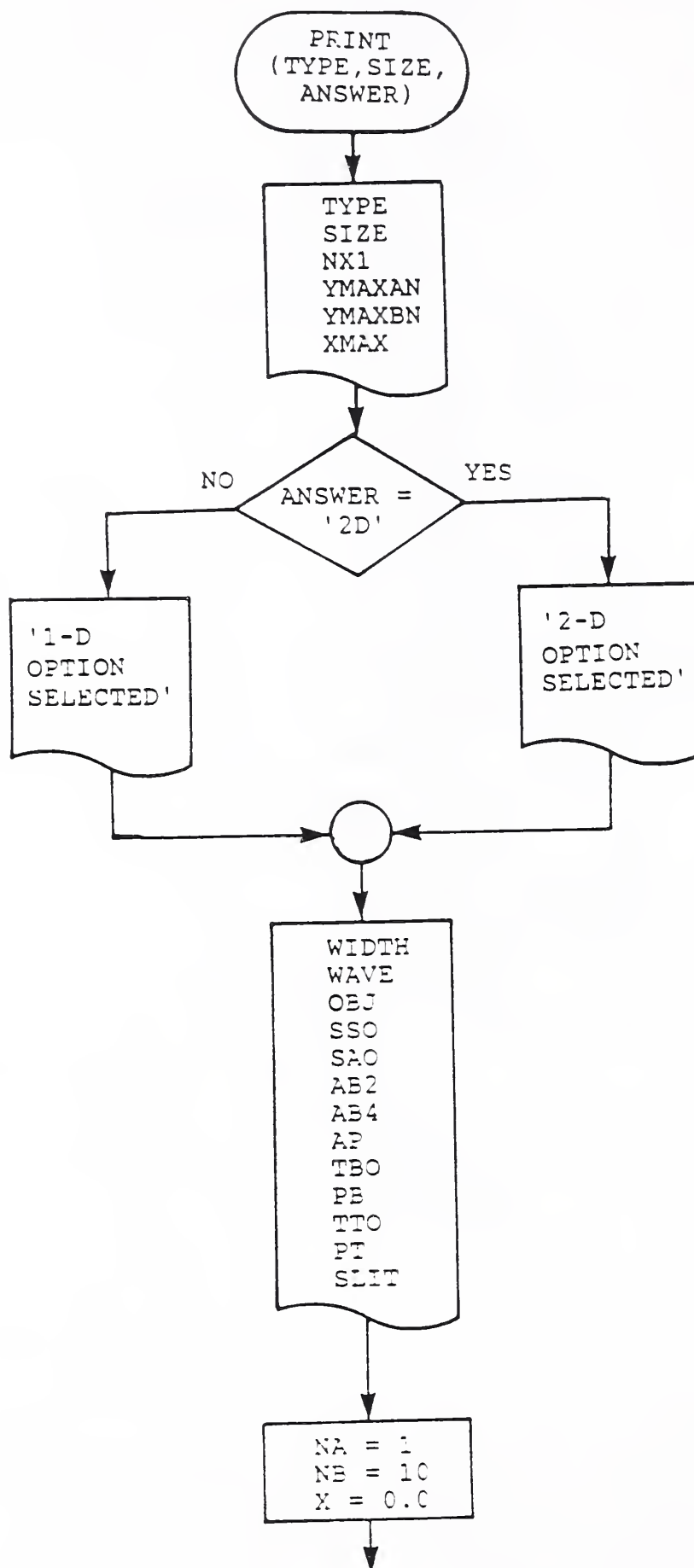
12. FLOW DIAGRAM FOR THE SUBROUTINE 'YNORM'

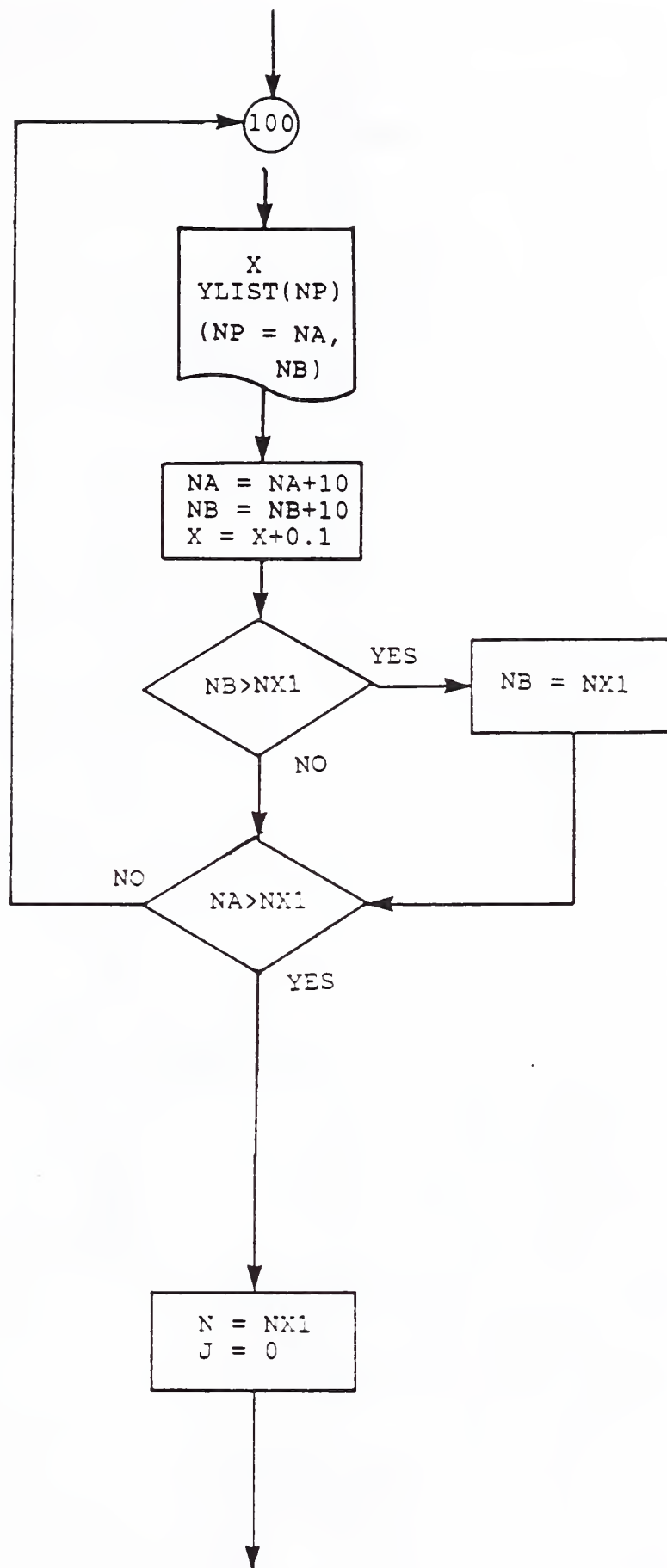


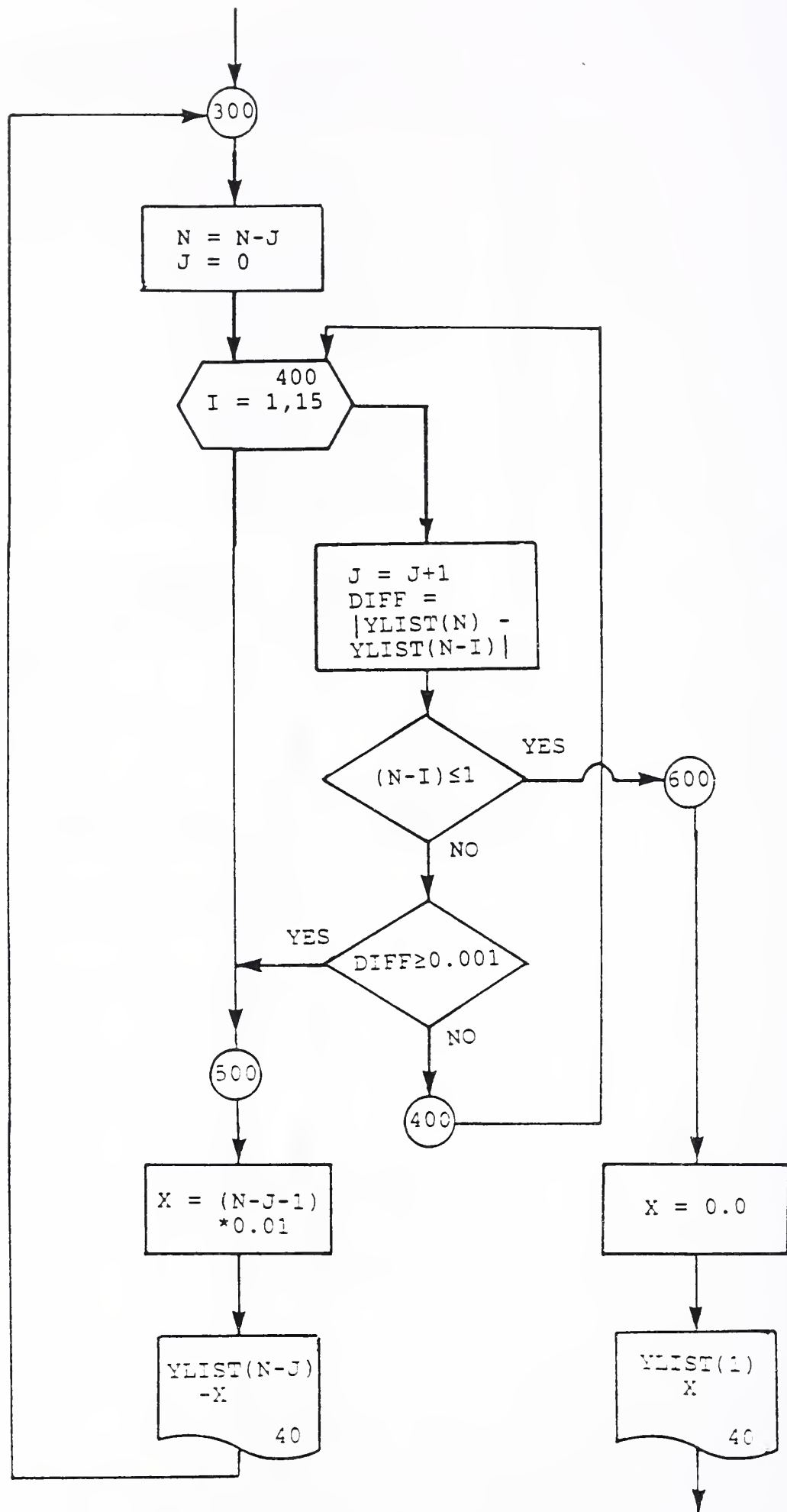
13. FLOW DIAGRAM FOR THE SUBROUTINE 'RDATA'



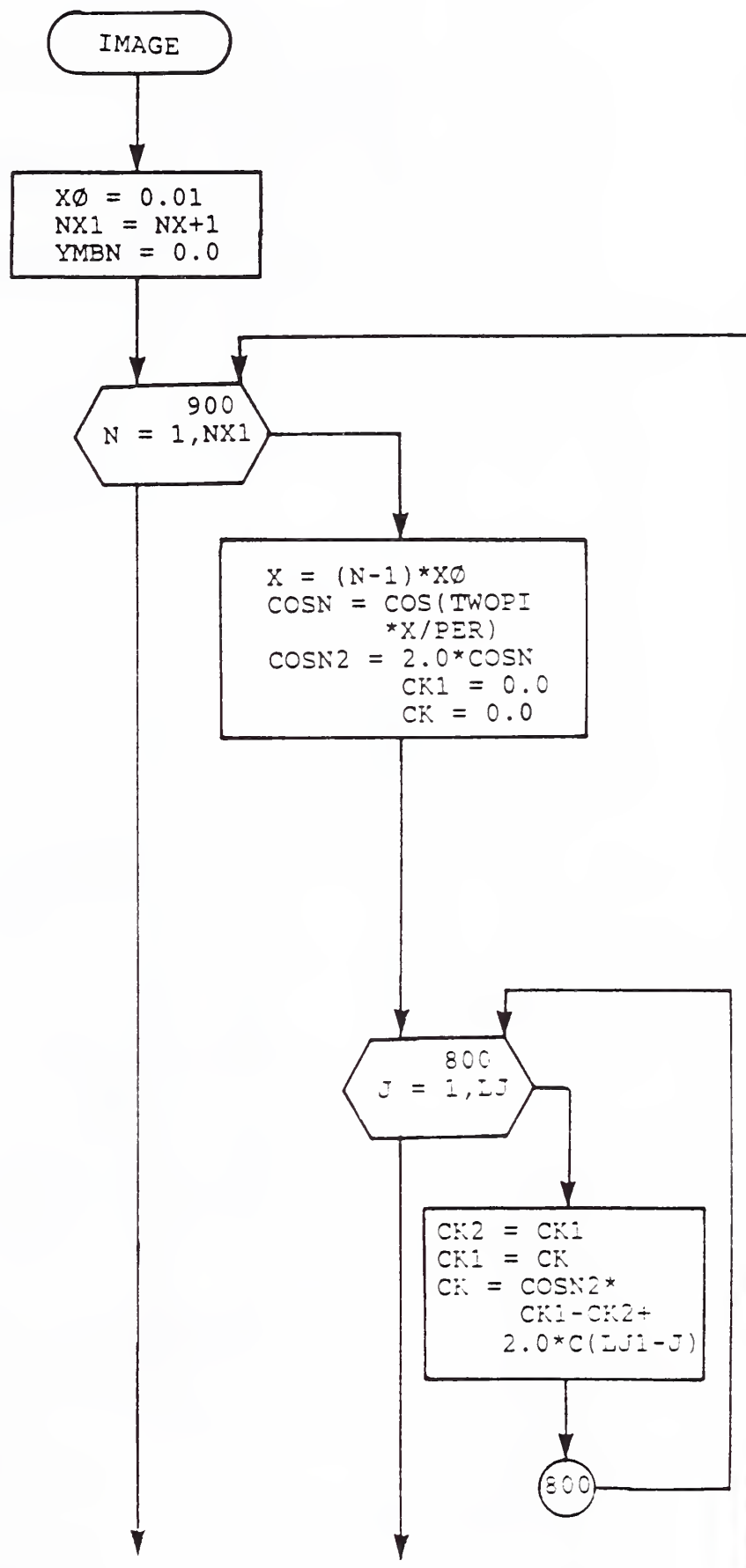
14. FLOW DIAGRAM FOR THE SUBROUTINE 'PRINT'

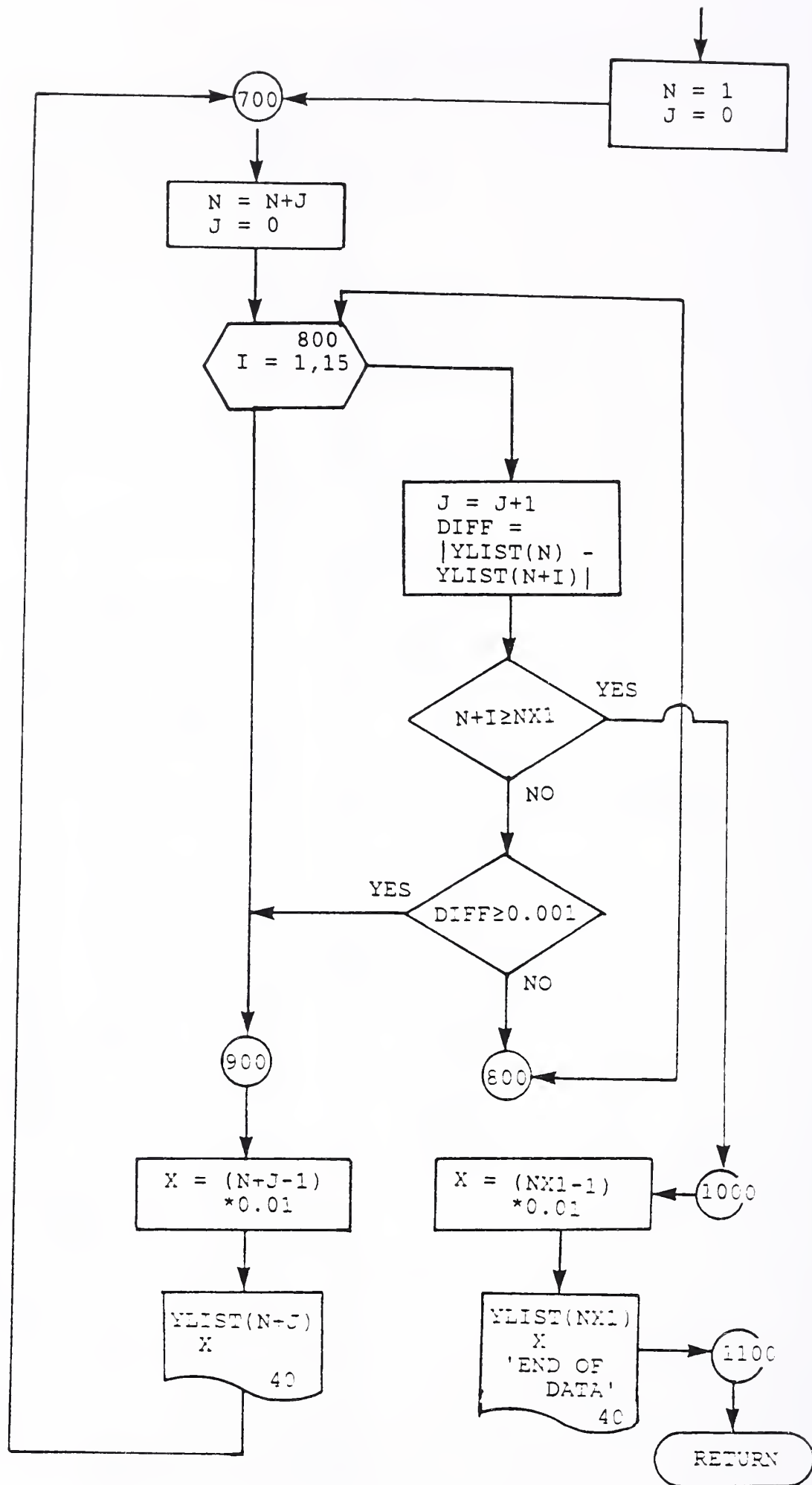


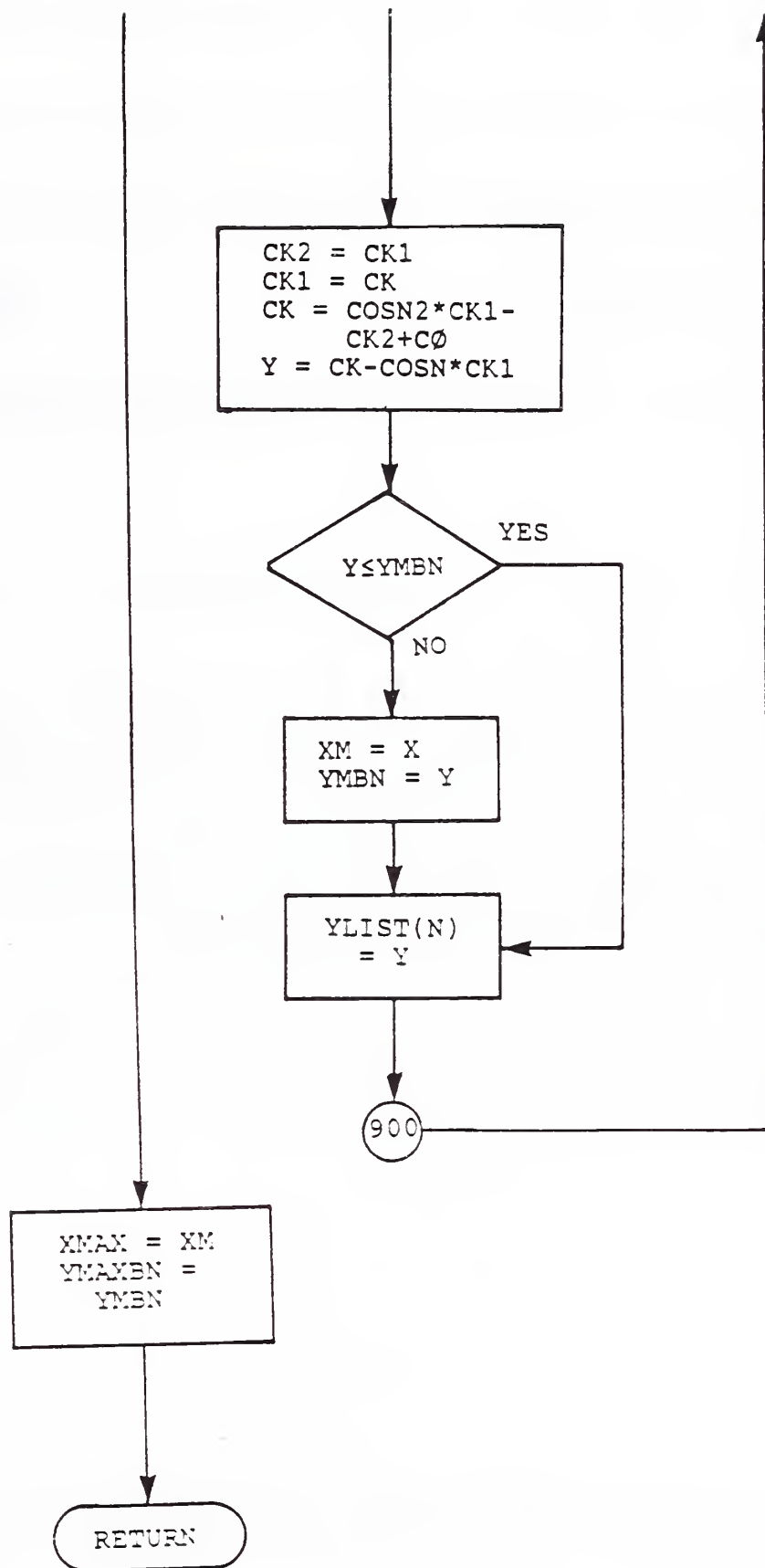




15. FLOW DIAGRAM FOR SUBROUTINE 'IMAGE'







Acknowledgments

Support for documentation and publication of this software was provided by VLSI Standards, Inc. under an NBS Research Associate Agreement. A PASCAL version of this software has also been developed. In addition, the assistance of Ruth N. Varner and Carmelo Montanez in converting this software for use on the CYBER 855 is gratefully acknowledged.

U.S. DEPT. OF COMM. BIBLIOGRAPHIC DATA SHEET (See instructions)	1. PUBLICATION OR REPORT NO. NISTIR 88-3808	2. Performing Organ. Report No.	3. Publication Date APRIL 1989
4. TITLE AND SUBTITLE Narrow-Angle Laser Scanning Microscope System for Linewidth Measurement on Wafers			
5. AUTHOR(S) D. Nyyssonen			
6. PERFORMING ORGANIZATION (If joint or other than NBS, see instructions) NATIONAL BUREAU OF STANDARDS U.S. DEPARTMENT OF COMMERCE GAITHERSBURG, MD 20899			7. Contract/Grant No. 8. Type of Report & Period Covered
9. SPONSORING ORGANIZATION NAME AND COMPLETE ADDRESS (Street, City, State, ZIP)			
10. SUPPLEMENTARY NOTES <input type="checkbox"/> Document describes a computer program; SF-185, FIPS Software Summary, is attached.			
11. ABSTRACT (A 200-word or less factual summary of most significant information. If document includes a significant bibliography or literature survey, mention it here) The integrated-circuit industry in its push to finer and finer line geometries approaching submicrometer dimensions has created a need for ever more accurate and precise feature-size measurements to establish tighter control of fabrication processes. In conjunction with the NBS Semiconductor Linewidth Metrology Program, a unique narrow-angle laser measurement system was developed. This report describes the theory, optical design, and operation of this system and includes computer software useful for characterizing the pertinent optical parameters and images for patterned thin layers. For thick layers, the physics in more detail the reader is referred to several related reports listed in the references.			
12. KEY WORDS (Six to twelve entries; alphabetical order; capitalize only proper names; and separate key words by semicolons) coherence; critical dimensions; linewidth measurements; metrology; micrometrology; scanning microscopy			
13. AVAILABILITY <input checked="" type="checkbox"/> Unlimited <input type="checkbox"/> For Official Distribution. Do Not Release to NTIS <input type="checkbox"/> Order From Superintendent of Documents, U.S. Government Printing Office, Washington, D.C. 20402. <input checked="" type="checkbox"/> Order From National Technical Information Service (NTIS), Springfield, VA. 22161			14. NO. OF PRINTED PAGES 110 15. Price \$19.95

